AD_____

Award Number: DAMD17-98-1-8121

TITLE: Ultrasonic Stimulated Acoustic Emission for Detection of Breast Microcalcifications

PRINCIPAL INVESTIGATOR: Mostafa Fatemi, Ph.D.

CONTRACTING ORGANIZATION: Mayo Foundation
Rochester, Minnesota 55905

REPORT DATE: May 2002

TYPE OF REPORT: Final

PREPARED FOR: U.S. Army Medical Research and Materiel Command
Fort Detrick, Maryland 21702-5012

Mayo Foundation
200 First Street SW
Rochester, Minnesota 55905
507-284-2511

Department of Physiology & Biophysics

May 31, 2002

Commander
U.S. Army Medical Research and Materiel Command
ATTN: MCMR-RMI-S
504 Scott Street
Fort Detrick, MD 21701-5012

RE: Final Report for DAMD17-98-1-8121

Dear Commander:

This report contains no proprietary or unpublished data. There are no limitations of the report.

Sincerely,

Mostafa Fatemi

Mostafa Fatemi, Ph.D.
Associate Consultant

MF:ecq

PHONE: 507 284-0608 FAX: 507 266-0361 E-MAIL: FATEMI.MOSTAFA@MAYO.EDU

REPORT DOCUMENTATION PAGE

Form Approved
OMB No. 074-0188

1. AGENCY USE ONLY (Leave blank)	2. REPORT DATE	3. REPORT TYPE AND DATES COVERED
	May 2002	Final (15 Apr 98 - 14 Apr 02)

4. TITLE AND SUBTITLE
Ultrasonic Stimulated Acoustic Emission for Detection of Breast Microcalcifications

5. FUNDING NUMBERS
DAMD17-98-1-8121

6. AUTHOR(S)
Mostafa Fatemi, Ph.D.

7. PERFORMING ORGANIZATION NAME(S) AND ADDRESS(ES)
Mayo Foundation
Rochester, Minnesota 55905

E-Mail: Fatemi.Mostafa@mayo.edu

8. PERFORMING ORGANIZATION REPORT NUMBER

9. SPONSORING / MONITORING AGENCY NAME(S) AND ADDRESS(ES)
U.S. Army Medical Research and Materiel Command
Fort Detrick, Maryland 21702-5012

10. SPONSORING / MONITORING AGENCY REPORT NUMBER

11. SUPPLEMENTARY NOTES
Report contains color.

12a. DISTRIBUTION / AVAILABILITY STATEMENT
Approved for Public Release; Distribution Unlimited.

12b. DISTRIBUTION CODE

13. ABSTRACT *(Maximum 200 Words)*

The purpose of this research is to develop an experimental imaging system based on Ultrasound Stimulated Acoustic Emission (USAE) for detecting microcalcifications in human breast tissue specimens. The scope of this research is to develop the theory, improve the experimental USAE system, and perform USAE imaging on human breast tissue samples. The first task of this research is focused on system development and optimization for detection of beast microcalcifications. The second task is centered on imaging breast tissues using USAE method for detection of microcalcifications. This report covers the entire project period including the results of Tasks 1 and 2. Results show that USAE can detect microcalcifications and calcified vessels. Results are verified using x-ray mammography. In addition to detection of microcalcifications, it is shown that USAE has may be used to determine the mechanical properties of the medium surrounding a small inclusion.

14. SUBJECT TERMS
Breast Cancer, Microcalcifications, Ultrasound, Acoustic Emission

15. NUMBER OF PAGES
124

16. PRICE CODE

17. SECURITY CLASSIFICATION OF REPORT	18. SECURITY CLASSIFICATION OF THIS PAGE	19. SECURITY CLASSIFICATION OF ABSTRACT	20. LIMITATION OF ABSTRACT
Unclassified	Unclassified	Unclassified	Unlimited

FOREWORD

Opinions, interpretations, conclusions and recommendations are those of the author and are not necessarily endorsed by the U.S. Army.

____ Where copyrighted material is quoted, permission has been obtained to use such material.

____ Where material from documents designated for limited distribution is quoted, permission has been obtained to use the material.

MF Citations of commercial organizations and trade names in this report do not constitute an official Department of Army endorsement or approval of the products or services of these organizations.

____ In conducting research using animals, the investigator(s) adhered to the "Guide for the Care and Use of Laboratory Animals," prepared by the Committee on Care and use of Laboratory Animals of the Institute of Laboratory Resources, national Research Council (NIH Publication No. 86-23, Revised 1985).

____ For the protection of human subjects, the investigator(s) adhered to policies of applicable Federal Law 45 CFR 46.

____ In conducting research utilizing recombinant DNA technology, the investigator(s) adhered to current guidelines promulgated by the National Institutes of Health.

____ In the conduct of research utilizing recombinant DNA, the investigator(s) adhered to the NIH Guidelines for Research Involving Recombinant DNA Molecules.

____ In the conduct of research involving hazardous organisms, the investigator(s) adhered to the CDC-NIH Guide for Biosafety in Microbiological and Biomedical Laboratories.

Mostafa Tatemi 6/24/02

PI - Signature Date

Table of Contents

Appendix 6: Fatemi, M., and Greenleaf, J. F.: Imaging the viscoelastic properties of tissue. In: M. Fink, J-P. Montagner, A. Tourin: *Topics in Applied Physics*. Springer, Heidelberg, Berlin 2002, vol 84, pp 257-275 (book chapter).

Appendix 7: Fatemi, M., Wold, L. E., Morton, M. J., and Greenleaf, J. F.: Imaging Breast microcalcifications by vibro-acoustography. J Ultrasound Med 20(3):S25-26, 2001

Appendix 8: Fatemi, M., and Greenleaf, J. F.: Probing the dynamics of tissue at low frequencies with the radiation force of ultrasound. Phys Med Biol 45(6):1449-1464, 2000.

Appendix 9: Chen, S.: Shear property characterization of viscoelastic media using vibrations induced by ultrasound radiation force. Ph.D. dissertation, Mayo Graduate School, Rochester, MN, 2002 (Table of contents and Introduction).

Appendix 10: Chen, S., Fatemi, M., and Greenleaf, J. F.: Vibro-acoustography of small spheres. J Acoust Soc Am 108(5 pt. 2):2505, Nov 2000.

Appendix 11: Chen, S., Fatemi, M., and Greenleaf, J. F.: Remote measurement of material properties from radiation force induced vibration of an embedded sphere. J Acoust Soc Am 2002 (submitted).

1. INTRODUCTION

The ultimate goal of this research is to develop a new non-invasive imaging modality for breast imaging that is capable of detecting small microcalcifications. Our present goal is to further develop an experimental system based on Ultrasound Stimulated Acoustic Emission (USAE) for in vitro imaging of breast tissue specimens and test its performance in detecting microcalcifications. The general theory of USAE, later named *vibro-acoustography*, is described in [1-4], and some of its applications are explained in [5-7]. This research includes two tasks. The first task of this research is focused on the development of the theory, system development, and optimization of the method for detection of beast microcalcifications. The second task is centered on experiments and breast tissue imaging. This final report addresses the activities related to both tasks.

2. BODY

This research includes two main tasks: (1) System development, including theoretical developments, system design and optimizations. (2) Detection of microcalcifications in breast tissue samples (experiments). Here we report activities on these two tasks.

2.1. System and Theory Developments:

In this section, we report activities relating to the first task of this project. These activities include theoretical developments, experimental system development and optimization.

2.1.1. Development of the vibro-acoustography imaging theory:

We reported the principles and theory of USAE (or vibro-acoustography) in [1-4]. This theory includes modeling USAE imaging in four parts:

1. Generation of localized radiation force (vibrating force) by means of two ultrasound beams
2. A model for object vibration in response to the radiation force
3. A model for the acoustic emission field in the surrounding medium due to object vibration
4. A model for image formation and system point spread function (PSF).

Based on this theory, a USAE (vibro-acoustography) system was designed for imaging tissue samples [7]. We have refined this theory in several aspects during the past 3 years. Because the theory plays a central role in understanding USAE, here we present a summary of the revised version of USAE theory.

Radiation force is generated by a change in the energy density of an incident acoustic field. Consider a collimated ultrasound beam interacting with an object. The radiation force arising from this interaction has a component, F, in the beam direction. This component is proportional to the time average energy density of the incident wave $\langle E \rangle$ and the projected area of the object, S, as:

$$F = d_r S < E > \qquad (1)$$

where d_r is the drag coefficient (or the radiation force function), and is a function of the scattered and absorbed power by the object [1,2]. For the simple case of a reflecting plane target, d_r is proportional to the power reflection coefficient. In vibro-acoustography [1, 2], this force is used for imaging. This is accomplished by probing the object point-by-point. This technique ideally requires the stress field to be confined to a point, while its amplitude oscillates at selected frequencies. To generate a localized oscillatory stress field, two intersecting CW focused ultrasound beams of different frequencies are used. It is only in the intersection region that the ultrasound field energy density is sinusoidally modulated, and hence, the field can generate an oscillatory radiation force by interacting with the object. For this purpose, we use a two-element focused annular array, consisting of a ring and a concentric disc element, both focused at the same focal point. We refer to this arrangement as "confocal" beams.

We consider a two-element spherically focused annular array, consisting of a central disc with the radius of a_1, and an outer ring with the inner radius of a_2' and the outer radius of a_2. The common focal length of the elements is z_0. We also assume that the elements are excited by two CW signals at frequencies ω_1 and $\omega_2 = \omega_1 + \Delta\omega$. Let us assume that the beams are propagating in the z direction with the joint focal point at $z=0$. The resultant field at a point defined by vector $\bar{r}$ on the $z=0$ plane may be written as:

$$p(\bar{r},t) = P_1(\bar{r})\cos[\omega_1 t + \psi_1(\bar{r})] + P_2(\bar{r})\cos[\omega_2 t + \psi_2(\bar{r})] \qquad (2)$$

where $P_1(\bar{r})$ and $P_2(\bar{r})$ are the pressure field radial profiles across the focal plane with $\psi_1(\bar{r})$ and $\psi_2(\bar{r})$ being the associated phase functions. It is noted from the diffraction theory that $P_1(\bar{r})$ and $P_2(\bar{r})$ are determined by the two-dimensional (2D) Fourier transforms of the corresponding transducer aperture [2, 3]. For the confocal transducer described above, these amplitude functions can be written as [2]:

$$P_1(\bar{r}) = \rho c U_{01} \frac{\pi a_1^2}{\lambda_1 z_0} \mathrm{jinc}\left(\frac{r a_1}{\lambda_1 z_0}\right) \qquad (3)$$

and

$$P_2(\bar{r}) = \rho c U_{02} \frac{\pi}{\lambda_2 z_0}\left[a_2^2 \,\mathrm{jinc}\left(\frac{r a_1}{\lambda_1 z_0}\right) - a_2'^2 \,\mathrm{jinc}\left(\frac{r a_2'}{\lambda_2 z_0}\right)\right] \qquad (4)$$

where $\lambda_i = 2\pi/\omega_i$ for $i=1, 2$, are ultrasound wavelengths at the *i-th* transducer element, U_{0i}, $i=1, 2$, is the velocity amplitude at the corresponding element, and $r = |\bar{r}|$.

Also, $\mathrm{jinc}(X) = J_1(X)/\pi X$, where $J_1(X)$ is the first order Bessel function of the first kind. For well-focused beams, $P_1(\bar{r})$ and $P_2(\bar{r})$ diminish quickly away from the origin. The phase functions, $\psi_i(\bar{r}) = -\pi r^2 / \lambda_i z_0$, for $i=1, 2$, are conveniently set to be zero at the origin.

It can be shown that the short time average of the acoustic energy density in the intersection region has slow variations at frequency $\Delta\omega$ about its long time average (mean). Denoting this low frequency component by $e_{\Delta\omega}(\bar{r},t)$, we can write:

$$e_{\Delta\omega}(\bar{r},t) = \frac{P_1(\bar{r})P_2(\bar{r})}{\rho c^2}\cos[\Delta\omega t + \Delta\psi(\bar{r})] \qquad (5)$$

where ρ is the density, c is the sound speed, and

$$\Delta\psi = \psi_2(\bar{r}) - \psi_1(\bar{r}) = -r^2\Delta\omega / 2cz_0 \qquad (6)$$

Now, consider a planar target on the focal plane. Referring to (1) and considering that the average energy density is position and time dependent in this case we may replace <E> with $e_{\Delta\omega}(\bar{r},t)$. The normal component of the time varying force on a unit area element $dS=1$ at $\bar{r}$ with a unit local drag coefficient $d_r(r_0)=1$ is:

$$f_{\Delta\omega}(\bar{r},t) = \frac{P_1(\bar{r})P_2(\bar{r})}{\rho c^2}\cos[\Delta\omega t + \Delta\psi(\bar{r})] \qquad (7)$$

This function also represents the distribution of force, or the stress field, on the focal plane. It is convenient to define the complex amplitude of the stress field as:

$$F_{\Delta\omega}(\bar{r}) = \frac{P_1(\bar{r})P_2(\bar{r})}{\rho c^2}\exp[j\Delta\psi(\bar{r})] \qquad (8)$$

When an oscillating force is applied to the object, the object vibrates at the frequency of the stress field. Let us assume an object on the focal plane. (To simplify the solution, here we consider only two-dimensional flat objects. In reality, the stress field may be exerted on a volume of the object.) The radiation force on an area element dS of this object at point $\bar{r}$ is given by $F_{\Delta\omega}(\bar{r})d_r(\bar{r})dS$.

Object vibration due to this excitation is a function of object size, shape, and mechanical impedance. The relationship between the applied force and object motion may be defined in terms of a function called the acoustic outflow, which describes the volume of the surrounding fluid displaced per unit time because of object vibrations. An example of the acoustic outflow function for a circular disc object is given in [2]. Here we denote the acoustic outflow of the object due to a force at frequency $\Delta\omega$ applied on an area element dS at $\bar{r}$ by $Q_{\Delta\omega}(\bar{r})$.

Vibration of the particles in the surrounding medium produces an acoustic field called the "acoustic emission." The characteristic of the acoustic emission field is partly a function of the mechanical properties of the vibrating object and partly a function of the propagation medium. We may write the incremental acoustic emission pressure field observed at a point located at $\bar{l}$ in the surrounding medium as:

$$dP_{\Delta\omega} = \rho c^2 M_{\Delta\omega}(\bar{l})Q_{\Delta\omega}(\bar{r})d_r(\bar{r})F_{\Delta\omega}(\bar{r})dS \qquad (9)$$

where $M(\bar{l})$ is the transfer function of the medium, describing the effect of medium on acoustic wave propagating from the object to the observation point $\bar{l}$. The subscript $\Delta\omega$ indicates the frequency of the acoustic emission field.

To calculate the total acoustic emission filed, we must integrate $dP_{\Delta\omega}$ over S. Before integrating the acoustic emission field, we may take a few steps to simplify our treatment of the problem.

In many practical cases, the wavelength of this acoustic field, $\Delta\lambda = 2\pi c / \Delta\omega$, is much larger than the effective dimension of the vibrating part of the object. Hence, the object approximately acts as a dipole or an almost omni-directional source, and thus $M_{\Delta\omega}(\bar{l})$ may be considered independent of the object.

We also note that the only terms in (9) that depend on the object are $d_r(\bar{r})$ and $Q_{\Delta\omega}(\bar{r})$. Hence, we may define the object function as

$$G_{\Delta\omega}(\bar{r}) = Q_{\Delta\omega}(\bar{r}) d_r(\bar{r}) \qquad (10)$$

This function defines object characteristics at frequency $\Delta\omega$.
Now, to generalize the problem, we may assume that the focus of the ultrasound beam is moved from the origin to an arbitrary location $\bar{r}$ on the focal plane (the beam axis still being parallel to the z-axis). To find the complex amplitude of the total acoustic emission field, we now integrate $dP_{\Delta\omega}$ over the object:

$$P_{\Delta\omega}(\bar{r}) = \rho c^2 M_{\Delta\omega}(\bar{l}) \int_S G_{\Delta\omega}(\bar{r}') F_{\Delta\omega}(\bar{r}' - \bar{r}) dS \qquad (11)$$

where $\bar{r}'$ is the integration variable. The integral in the above equation constitutes a two-dimensional convolution of the object function and the stress field, and may be summarized as:

$$P_{\Delta\omega}(\bar{r}) = \rho c^2 M_{\Delta\omega}(\bar{l}) G_{\Delta\omega}(\bar{r}) * F_{\Delta\omega}(\bar{r}) \qquad (12)$$

where $*$ represents the convolution operation.

To produce an image, we move (scan) the focal point of the ultrasound beam across the object on the focal plane and record the amplitude of the acoustic emission field at each beam position. The image is formed by modulating the brightness of each point on the image plane proportional to $P_{\Delta\omega}(\bar{r})$ (or its magnitude) recorded from the corresponding point on the object.

Commonly, an imaging system is characterized by its point-spread-function (PSF), which is defined as the image of a point object. To determine the PSF of the system, we consider a point object defined as:

$$G_{\Delta\omega}(\bar{r}) = \delta(\bar{r}) \qquad (13)$$

The resulting image according to (12) is $P_{\Delta\omega p}(\bar{r}) = \rho c^2 M_{\Delta\omega}(\bar{l}) F_{\Delta\omega}(\bar{r})$, where the subscript p is added to indicate the point object. It is convenient to define the normalized PSF of the system as:

$$\begin{aligned} H_{\Delta\omega}(\bar{r}) &= P_{\Delta\omega p}(\bar{r}) / P_{\Delta\omega p}(0) \\ &= F_{\Delta\omega}(\bar{r}) / F_{\Delta\omega}(0) \end{aligned} \qquad (14)$$

Referring to (3 and 4) we can write:

$$H_{\Delta\omega}(\bar{r}) = \frac{1}{a_2^2 - a_2'^2} \operatorname{jinc}\left(\frac{r a_1}{\lambda_1 z_0}\right) \left[a_2^2 \operatorname{jinc}\left(\frac{r a_2}{\lambda_2 z_0}\right) - a_2'^2 \operatorname{jinc}\left(\frac{r a_2'}{\lambda_2 z_0}\right) \right] \exp[j\Delta\psi(\bar{r})] \qquad (15)$$

The above equation indicates that the PSF is a complex function. However, for a reasonably focused transducer, $|H_{\Delta\omega}(\bar{r})|$ is significant only within a small radius. Within this radius and for $\Delta\omega \ll \omega_i$, $i=1,2$, we may assume $\Delta\psi(\bar{r}) \approx 0$ as one may conclude from (6). Thus, the PSF may be considered as a real function for practical purposes. For a given object $G_{\Delta\omega}(\bar{r})$, the image may be written as:

$$P_{\Delta\omega}(\bar{r}) = K G_{\Delta\omega}(\bar{r}) * H_{\Delta\omega}(\bar{r}) \qquad (16)$$

where K is a constant multiplier.

Application of the theory to microcalcification imaging:

Breast microcalcifications are normally in sub millimeter ranges, and they are often smaller than the ultrasound beam width. Hence we may consider them as "point objects". Therefore, mathematically we may model a microcalcification as:

$$G_{\Delta\omega}(\bar{r}) \approx A\delta(\bar{r}) \qquad (17)$$

Were A is a constant multiplier. Referring to Eq. (16) the image of a small microcalcification may be written as:

$$P_{\Delta\omega}(\bar{r}) \approx AKH_{\Delta\omega}(\bar{r}) \quad (19)$$

Therefore, image of small microcalcifications would be displayed as the PSF of the system. Typical PSF image of a USAE system is presented in [2,3].

2.1.2. Method of vibrating spheres:

In an effort for better understanding of the dynamic behavior of microcalcifications in response to the radiation force of ultrasound, we have modeled microcalcification as an elastic sphere in a fluid medium. The sphere is exposed to two plane ultrasound waves at slightly different frequencies. The vibration velocity of the sphere and the acoustic emission field has been calculated in terms of sphere size and elastic properties [8-11]. An interesting result of this theory is that under some conditions, the vibrating sphere exhibits a resonance effect. The resonance frequency of the sphere is a function of the sphere parameters, such as its size and elasticity, as well as the mechanical properties of the surround medium. In particular, it can be shown that knowing the sphere parameters, the sheer modulus of the surrounding medium can be evaluated from the frequency response of the vibrating sphere. This phenomenon is illustrated in Figure 1 (see appendix 1). This figure shows that the frequency response of the sphere exhibits a clear peak, and the resonance frequency of the sphere increases as the sheer elasticity of the surrounding medium (gel) increases.

To validate this finding, experiments were conducted on steel spheres embedded in gel medium, and the velocity of the spheres was measured directly by a laser interferometer system (vibrometer). We also measured the acoustic emission field by a calibrated hydrophone. This arrangement is used to model vibration of a microcalcification in breast tissue. The experimental result was used to calculate the sheer modulus of the gel. The resulting values of the sheer modulus were then validated by comparing with independently measured values. For more detail, refer to reference [8-11].

The above method is significant in quantitative analysis of microcalcifications using USAE in the following two ways:

1. Knowing the parameters of the soft tissue, one can use this method to evaluate the size of the microcalcification.
2. Knowing the parameters of the microcalcification, sheer elasticity of the surrounding tissue can be remotely evaluated. This information is especially important in tissue characterization and diagnosing lesions in breast.

The above results have opened a new way for breast tissue characterization.

2.1.3. System Improvements:

Noise Reduction:

The acoustic emission from microcalcifications is normally very small and often comparable to the noise level. To improve the signal quality, we reduced system noise by various means. These methods include:

1. Quite room: This room is designed with walls and ceiling covered by sound absorbing material to reduce the ambient noise. We used this room to conduct our tissue experiments.
2. Air table: To reduce transmission of structural vibrations to the experiment setup, we started to use an air table to support the water tank. This air table provides vertical isolation efficiency 90-99% at 10Hz. It has improved the signal-to-noise ratio significantly.
3. Modified water tank design: To reduce multipath and reverberation effects we designed a new tank. The walls of the new tank is covered with sound absorbing layers, and the bottom is covered by a sound absorbing layer positioned at 15 degree angle to reduce reverberation. We also added sound absorbing wedges in the tank to reduce the possibility of tank resonance.
4. To reduce the noise from the scanning motors, we used a customized scanning system based on analog servomotors instead of previous digital step motors. The new analog motors produce much less noise.

High-speed Scanning:

In order to speed up the scanning process, we must scan the object in a continuous motion while the data are collected. The problem in this method is that the audio noise generated by the scanning motors interferes with the acoustic emission signal from the object, which dramatically reduces signal quality. Therefore, one must use a method that stops the noise from the scanning motors while they are running. One way to do this is by increasing the acoustic emission frequency beyond the spectral bandwidth of the scanner-generated noise, such that the noise can be filtered out without losing the acoustic emission signal.

Based on this strategy, we have performed high speed scanning at 30—60 kHz. A programmable filter was used to remove the scanner noise. The noise bandwidth in our system is about 20 kHz. In this method, the transmitting transducer continuously transmits the ultrasound while the scanner scans the object without stopping, and at the same time, the hydrophone continuously receives the resulting acoustic emission signal. Using this method an object can be scanned in a fraction of the time that would be required for scanning by the conventional point-by-point scanning. The resulting images have high signal-to-noise ratio. The only drawback of this method is that it cannot be used at acoustic emission frequencies lower than 20 kHz.

Tone Burst Scanning:

Tone burst scanning is a method we have used to avoid the ultrasound standing wave effect and acoustic emission multipath effect in the water tank. Ultrasound standing wave effect is caused by multiple reflection of the sound between a highly reflective object and the transducer. Acoustic emission multipath effect is caused by multiple reflection of the acoustic emission by the walls or other reflectors within the tank. Both these phenomena reduce the quality of the final image and can introduce false patterns on the image. In this method, we excite each transducer element with tone bursts of continuous waves. The length of the bursts is chosen to be at least several times the acoustic emission period, but short enough to avoid any overlapping with its multiple reflections from the nearby structures such as the tank walls.

There are two major drawbacks for this method. The first problem is limitation on acoustic emission frequency. To satisfy the above conditions we often have to use a high acoustic emission frequency. In our experimental setup, the acoustic emission frequency needs to be about 40 kHz or more. The second problem is production of unwanted acoustic noise. Applying a sudden burst of energy to a transducer usually produces a transient vibration of the transducer case. This vibration introduces a wideband noise in the entire experimental setup. To reduce this effect, we can use a gradual ascending and descending tone burst, which is described in the next section.

Gating Tone Bursts:

A "Soft Gate" was constructed using a raised cosine shaping circuit to
Reduce rise time and fall time of tone burst edges. This approach greatly reduces the shock and the acoustic noise from transducer element, thus improving the detection threshold of the system. To test this method, we scanned the RTV glass-bead phantom with and without the soft gate. Without this gate, the noise from the transducer shock overwhelmed the weak acoustic emission from the bead. The image quality was greatly improved and the bead became readily detectable after using the soft gate. Experiments on the RTV phantom with holes also showed the same improvement.

Receiver Lock-in Amplifier:

Our previous receiver included a per-amplifier followed by a narrow-band programmable filter. This configuration operates well as long as the signal level at the hydrophone is high enough for subsequent amplification and detection. However, when imaging small microcalcifications, the signal level can be very low in comparison to the ambient noise within the pass-band of the narrow-band filter. There are several sources of noise in the system, including airborne noise in the room, structural vibrations, acoustic noise from the scanning motors, and the noise from equipment fans. There is also some electrical noise in the system.

To improve the signal-to-noise ratio, we modified the receiver by replacing the preamplifier and the programmable filter with a lock-in amplifier (EG&G Instruments, Model 7264 DSP). The lock-in amplifier uses a reference signal to set the lock frequency.

The frequency of the reference signal must be exactly equal to the frequency of the input signal to the amplifier (hydrophone output). This system locks to the frequency of the reference signal ($\Delta\omega$) and tracks the input signal by an active phase-lock loop. In effect, the lock-in amplifier acts as a very narrow band filter with a pass band of only a few Hz centered at the difference frequency $\Delta\omega$. This system allows the acoustic emission signal to pass and rejects the noise outside the pass band. The reference signal (at $\Delta\omega$) is provided by down-mixing the signals from the two RF generators driving the two elements of the transducer.

Improved System Control:

To improve the scanning process a GPIB control card has been added to the scanner workstation (Sun Sparc Station 5). This card allows all sub-systems, such as RF generators, lock-in amplifier, digitizer, and the new scanner system with servomotors, to be controlled by software. This system operates under LabView software.

Direct Displacement Measurement by Laser Vibrometer:

We started using a laser vibrometer for direct measurement of velocity and displacement in the order of nano-meters at frequencies up to 250 kHz range. This system allows us to directly measure the vibration that we introduce in an object by the radiation force of ultrasound. Hence, we can validate our acoustic measurements by direct optical measurement.

Direct Displacement Measurement by Scanning Vibrometer

The main function of USAE is to vibrate the object by the radiation force of ultrasound. It is therefore a fundamental issue to understand object vibration and its role in generating the acoustic emission field. In order to analyze object vibration and verify our acoustic measurements we need to measure such vibrations directly. For this purpose we have acquired a scanning vibrometer (Polytec VibraScan PSV-300F) that enables us to measure object vibrations in two dimensions, in Angstrom range, and produce an image (or a movie) that shows displacement (or particle velocity) at every point on the objet. (This instrument is in addition to the laser vibrometer mentioned above, which measures vibration at only one point at a time.) This tool will help us to further develop USAE for breast imaging. The funds or this instrument is provided by a Major Research Instrumentation grant from the National Science Foundation.

Anechoic Chamber:

Because USAE experiments are performed at low acoustic intensities, it is essential to keep the environmental noise and structural vibration as low as possible. For this purpose, we have designed a 12'x10'x7' anechoic chamber with a 150 Hz cutoff frequency. This room includes acoustically insulated walls and floor, with the interior covered with absorbing wedges. This room significantly reduces the noise level and improve the quality of data in our experiments. Funding for the anechoic chamber is provided by a Major Research Instrumentation grant from the National Science Foundation. Mayo Clinic provides the space for this room.

Software Development:

1. **Data Acquisition**: The software for controlling the new scanning system and the data acquisition system was developed.
2. **Interactive Imaging and Object Analysis**: New software has been developed for interactive scanning and data collection. An important feature of the new software is its capability to produce the image of the object as it is scanned, and allows the user to select a point on the image and reposition the transducer beam to the selected points in the object. Once at the new position, the system can collect the acoustic emission signal from that particular point of the object. Another important feature of this software is its capability in measuring the frequency response of a selected point in the object. This feature allows the user to point the ultrasound beam at a selected point in the object and sweep the vibration frequency $\Delta\omega$ while the system records the acoustic emission signal. By employing a built-in fast Fourier transform algorithm, this system then calculates and displays the frequency response (spectrum) of the object. This feature is particularly useful in imaging and analyzing the frequency response of microcalcifications. Employing the method of vibrating spheres described earlier, we may be able to use the frequency domain signatures of microcalcifications to characterize the soft tissue or microcalcifications in breast. This would open the way for using USAE as a "non-invasive biopsy" tool.

2.2. Tissue Experiments

The hypothesis is that ultrasound stimulated acoustic emission can be used to image tissue and detect microcalcifications. To test this hypothesis, we scanned 75 excised human breast tissue and compared the results with the x-ray mammography and histology.

2.2.1. Procedure

Experiments were conducted on human breast tissue samples in the following manner:

(a) Initial tissue selection

(b) Initial tissue preparation

(c) Screening mammography

(d) Reading mammography

(e) Final tissue selection

(f) Mounting on Scanning Bracket

(g) Base Mammography

(h) USAE Scanning

(i) Image evaluation (USAE vs. x-ray)

(j) Histological study

2.2.2. Results:

Experiments were conducted on breast tissue samples collected from 94 patients. We mounted 219 tissue samples in total. From this collection, 207 tissue samples were x-rayed using high-resolution mammography. 12 tissue samples were excluded from the study because they were not usable (lost their water content or became too old for imaging). Based on the x-ray images, we found microcalcifications in 75 from 207 tissue samples, and another 22 samples were suspicious of having some microcalcifications. We conducted USAE (vibro-acoustography) imaging of those tissue samples that were microcalcifications positive in their x-rays. Out of the 75 sample, one was excluded from the study because of the tissue was damaged in the process of mounting. In the USAE images, we found 44 samples to be microcalcification positive (a ratio of 0.6), out of which 42 were also histologically positive. Microcalcifications as small as 110 μm in diameter could be identified in USAE images. We also studied appearance of soft tissue in USAE images. Tissue structure appearance in the USAE images were rated perfect or fair, as compared to the x-ray. We found 49 perfect and 25 fair tissue structures in the total 74 samples imaged. More details on experiments can be found in [5-7].

Discussion:

The theory presented here clarifies the fundamental relationships between the object parameters and its USAE image. This theory indicates that the acoustic emission from an object is related to its mechanical admittance and the size of the object.

In the case of small microcalcifications, detection of the acoustic emission is often a challenge. To improve the detectability by USAE, the acoustic noise in the medium must be minimized. The acoustic noise includes the ambient noise, noise from the scanner, vibrations produced by the transducer body, etc. The improvements that we have made in the laboratory setup, including using the quiet room, airtable, absorbing material, soft gate, etc., have enabled us to considerably increase the signal-to-noise ratio of our data. Now, with our low-noise setup, we can detect smaller glass beads in our control test phantoms. Using the tone burst method has enabled us to eliminate the standing wave problem at the expense of working at a higher acoustic emission frequency.

Driving a particle at its resonance could provide useful information about the particle and its surrounding medium. In addition, it can enhance the detectability and selectivity. That is because at resonance particle motion is at its maximum, hence produces a stronger acoustic emission. Also, because the resonance frequency of a particle depends on its size and mass, this method can be used to selectively detect particles of particular size or mass. Based on this concept we developed the theory of vibrating spheres in a viscoelastic medium. An interesting result of this method is that by measuring the resonance frequency of such sphere it is possible to calculate the sheer elasticity of the medium.

Experimental USAE images presented in this report demonstrate two important facts: (1) USAE imaging method is capable of detecting small microcalcifications, as well as calcifications in vessels, in breast tissue; (2) Microcalcifications can be delineated form other tissue structures. The results shown here also indicate that such images have high spatial resolution, good contrast, and high signal to noise ratio. Microcalcifications shown in our results are only a few hundred microns in diameter, and the calcifications in the vessel wall were not more than 100 microns thick.

A comparison between the USAE image (Figure 4 of reference [7]) and the corresponding mammography reveals an interesting capability of USAE method. High tissue density in the region surrounding the microcalcification absorbs a great deal of x-ray energy, hence the x-ray image shows very low contrast within this region, and as a result, microcalcifications are barely visible. However, the USAE image delineates these calcifications with high contrast. This is because the acoustic emission is sensitive to the elastic properties of the object.

The histology of the tissue samples indicates that USAE can image breast microcalcifications in a wide range of pathological conditions (refer to 2001 Annual Report). This improves our prospects for future use of USAE for in-vivo breast imaging. In most cases, tissue inhomogenieties seem not to interfere with detection of microcalcifications.

Acoustic images reported here were obtained at relatively high vibration frequencies (20--40 kHz). At these frequencies we are able to acquire the data at much higher speed, reducing the acquisition time to a few minutes per image (for more details, refer to the Annual Report 2000). This is because at these frequencies the noise level from the scanner mechanism is negligible; hence, we can keep the scanning motor running while collecting the data. Scanning speed is an important factor in our experiments and eventually in application of USAE on humans.

3. Key Research Accomplishments

- Development of the theoretical model describing the relation between the acoustic emission field and the mechanical parameters of the object and the surrounding medium.
- Development the theory describing the point spread function of the imaging system.
- Improvement of the sensitivity of the system to be able to detect small particles in a viscoelastic medium.
- Identifying causes of image artifacts, such as ultrasound standing wave, multipath, and reverberation of acoustic emission.
- Developing methods for reducing or eliminating acoustic emission multipath and reverberation problems.

- Developing methods for reducing acoustic and vibrational noise in the system
- Demonstrated that small microcalcification (as small as 110 microns in diameter) and vessel calcifications can be detected by USAE imaging method.
- Demonstrated that in USAE images microcalcification can be delineated from other tissue structures.
- Demonstrated that microcalcification can be imaged at high vibrational frequencies.
- Demonstrated that USAE can detect microcalcifications in various pathological conditions.
- Developed the theory of vibrating sphere in a viscoelastic medium
- Demonstrated that a small sphere in a viscoelastic medium can exhibit a resonance. The resonance frequency depends on the parameters of the sphere and the mechanical properties of the medium.
- Demonstrated that sheer elasticity of the medium can be evaluated based on the resonance of the sphere. This method provides the possibility of characterizing the soft tissue surround the microcalcification.

4. Reportable Outcomes

1. Fatemi M, and Greenleaf, J. F., "Vibro-acoustography. An imaging modality based on ultrasound stimulated acoustic emission," Proc. Nat. Acad. Sci. USA., vol. 96, pp. 6603-6608, June 1999.
2. Greenleaf, J. F. and Fatemi, M.: Ultrasound-stimulated vibro-acoustic imaging in vivo. 1998 IEEE Ultrasonics Symposium Proceedings 2(2):1635-1638, 1998 (invited).
3. Fatemi, M., and J. F. Greenleaf: Beam forming for ultrasound-stimulated vibro-acoustography. ICTCA'99 Fourth International Conference on Theoretical and Computational Acoustics, Trieste, Italy, May 10--14, 1999 (Key note Abstract).
4. Fatemi, M., and J. F. Greenleaf: Point response of vibro-acoustography system. 1999 IEEE Ultrasonics Symposium, Lake Tahoe, NV, October 18--21, 1999.
5. Fatemi, M., and J. F. Greenleaf: Remote measurement of shear viscosity with ultrasound-stimulated vibro-acoustic spectrography. Acta Physica Sinica 8:S27-S32, August 1999.
6. Fatemi, M., and J. F. Greenleaf: Imaging and evaluating the elastic properties of biological tissues. The British Medical Ultrasound Society Bulletin, 8(4):16-18, November 2000.
7. Fatemi, M and Greenleaf, JF, New trends in ultrasonic imaging, 2000 IEEE Solid-State Circuits and Technology Committee Workshop on Biomedical Electronics (B. Ziaie and J. Von Arx), Oct. 2000 (Invited presentation).

8. Fatemi, M., and Greenleaf, J. F.: Probing the dynamics of tissue at low frequencies with the radiation force of ultrasound. Physics in Medicine and Biology, 45 (6): 1449 - 1464, 2000.
9. Fatemi, M., and J. F. Greenleaf: Vibro-acoustography system modeling. Era of Hope Meeting, DoD Breast Cancer Research Program, Department of Defense, U. S. Army Medical Research and Materiel Command, Atlanta, GA, June 8-12, 2000.
10. S. Chen, M. Fatemi, and J.F. Greenleaf: Vibro-acoustography of small spheres. Journal of Acoustical Society of America 108(5): 2505, 2000.
11. Fatemi, M, Wold, LE, Morton, MJ, and Greenleaf, JF, Imaging Breast microcalcifications by vibro-acoustography. J Ultrasound Med. 20(3): S25-26, 2001.
12. Fatemi, M., L. E. Wold, A. Alizad, K. Kazunori, and J. F. Greenleaf: Detection of breast microcalcifications by vibro-acoustography: advantages and limitations, Proceedings of the 17th International Congress on Acoustics, 2001 (in press).
13. Fatemi, M., L. E. Wold, A. Alizad, M. J. Morton, and J. F. Greenleaf: Application of vibro-acoustography in breast imaging, Mayo Research Forum 2001, Rochester, MN Sept. 21-22.
14. Fatemi, M., and J. F. Greenleaf: Imaging the viscoelastic properties of tissue. In: M. Fink, J-P. Montagner, A. Tourin: *Topics in Applied Physics*. Springer, Heidelberg, Berlin 2002, volume 84, pp 257-275. (Book chapter).
15. Fatemi, M., L. E. Wold, A. Alizad, and J. F. Greenleaf: Vibro-acoustic tissue mammography. IEEE Transactions on Medical Imaging, 21(1):1-8, 2002.
16. Alizad, A., M. Fatemi, R. A. Nishimura, and J. F. Greenleaf: Detection of calcium deposits on heart valve leaflets by vibro-acoustography: an in vitro study. Journal of the American Society of Echocardiography (accepted).
17. Alizad, A., M. Fatemi, and J. F. Greenleaf, Manifestation of solid masses in vibro-acoustography, Proc. of the Ninth Int. Cong. on Sound and Vibration, 2002 (in press).
18. Chen, S., M. Fatemi, and J.F. Greenleaf: Remote measurement of material properties from radiation force induced vibration of an embedded sphere. Submitted to Journal of Acoustical Society of America.
19. Chen, S., M. Fatemi, and J.F. Greenleaf: Shear property characterization of viscoelastic media using vibrations induced by ultrasound radiation force. Submitted to IEEE International Ultrasonics Symposium, Munich, Germany, 2002.
20. Chen, S.: Shear property characterization of viscoelastic media using vibrations induced by ultrasound radiation force. Ph.D. dissertation, Mayo Graduate School, Rochester, MN, 2002.

Research Grants:

21. (Research grant awarded) In-vivo Breast Imaging by Vibro-acoustography, The Susan G Komen Cancer Foundation (PI: M Fatemi) 2001-2003.
22. (Research grant awarded) Vibro-acoustography System with Contact Array Probe, National Institute of Health R21/R33 (PI:M. Fatemi), 2002-2005.

5. Conclusions

Small microcalcifications (as small as 110 microns in diameter) and vessel calcifications in breast tissue can be detected by USAE imaging method. In the images microcalcifications appear with high contrast with respect to the soft tissue, hence can be delineated from other tissue structures. Image quality and system sensitivity is improved by using various noise reduction methods. It is also shown that USAE may be used to determine the mechanical properties of the medium surrounding a small sphere. This finding opens the way for characterization of the lesion surrounding a breast microcalcification.

5.1. So What?

The body of knowledge collected in this research may be used to development of a new class of non-invasive imaging tool for breast imaging and visualization of breast microcalcifications. The results of the present research on breast tissue samples warrant further research to explore the utility of USAE in detection of microcalcifications and lesions in human breast. This research will be continued at a more advanced level within the framework of two funded research grants. The first grant on in-vivo breast vibro-acoustography (USAE) is funded by Komen Breast Cancer Foundation.

The second grant, which is funded by NIH, is focused on development of a vibro-acoustography system that will be designed for in vivo applications.

6. References

1. Fatemi, M., and Greenleaf, J. F.: Ultrasound-stimulated vibro-acoustic spectrography. Science 280:82--85, April 3, 1998.
2. Fatemi M, and Greenleaf, J. F., "Vibro-acoustography. An imaging modality based on ultrasound stimulated acoustic emission," Proc. Nat. Acad. Sci. USA., vol. 96, pp. 6603-6608, June 1999.
3. Fatemi, M, and Greenleaf, JF, "Probing the dynamics of tissue at low frequencies with the radiation force of ultrasound," Phys. Med. Biol., vol. 45, pp.1449-1464, 2000.
4. Fatemi, M., and J. F. Greenleaf: Imaging the viscoelastic properties of tissue. In: M. Fink, J-P. Montagner, A. Tourin: *Topics in Applied Physics*. Springer, Heidelberg, Berlin 2002, volume 84, pp 257-275. (Book chapter).
5. Fatemi, M, and Greenleaf JF, Imaging and evaluating the elastic properties of biological tissues. British Medical Ultrasound (BMUS) Bulletin, 8(4):16-18, Nov. 2000.
6. Fatemi, M. Wold, LE, Morton, MJ, and Greenleaf, JF, Imaging Breast microcalcifications by vibro-acoustography. J Ultrasound Med. 20(3): S25-26, 2001.
7. Fatemi, M., L. E. Wold, A. Alizad, and J. F. Greenleaf: Vibro-acoustic tissue mammography. IEEE Transactions on Medical Imaging, 21(1):1-8, 2002.
8. Chen, S., M. Fatemi, and J.F. Greenleaf: Vibro-acoustography of small spheres. Journal of Acoustical Society of America 108(5): 2505, 2000.

9. Chen, S.: Shear property characterization of viscoelastic media using vibrations induced by ultrasound radiation force. Ph.D. dissertation, Mayo Graduate School, Rochester, MN, 2002.
10. Chen, S., M. Fatemi, and J.F. Greenleaf: Remote measurement of material properties from radiation force induced vibration of an embedded sphere. Submitted to Journal of Acoustical Society of America, 2002.
11. Chen, S., M. Fatemi, and J.F. Greenleaf: Shear property characterization of viscoelastic media using vibrations induced by ultrasound radiation force. Submitted to IEEE International Ultrasonics Symposium, Munich, Germany, 2002.

7. Bibliography

1. Fatemi M, and Greenleaf, JF, "Vibro-acoustography. An imaging modality based on ultrasound stimulated acoustic emission," Proc. Nat. Acad. Sci. USA., vol. 96, pp. 6603-6608, June 1999.
2. Greenleaf, J. F. and Fatemi, M.: Ultrasound-stimulated vibro-acoustic imaging in vivo. 1998 IEEE Ultrasonics Symposium Proceedings 2(2):1635-1638, 1998 (invited).
3. Fatemi, M., and J. F. Greenleaf: Beam forming for ultrasound-stimulated vibro-acoustography. ICTCA'99 Fourth International Conference on Theoretical and Computational Acoustics, Trieste, Italy, May 10--14, 1999 (Key note Abstract).
4. Fatemi, M., and J. F. Greenleaf: Point response of vibro-acoustography system. 1999 IEEE Ultrasonics Symposium, Lake Tahoe, NV, October 18--21, 1999.
5. Fatemi, M., and J. F. Greenleaf: Remote measurement of shear viscosity with ultrasound-stimulated vibro-acoustic spectrography. Acta Physica Sinica 8:S27-S32, August 1999.
6. Fatemi, M., and J. F. Greenleaf: Imaging and evaluating the elastic properties of biological tissues. The British Medical Ultrasound Society Bulletin, 8(4):16-18, November 2000.
7. Fatemi, M and Greenleaf, JF, New trends in ultrasonic imaging, 2000 IEEE Solid-State Circuits and Technology Committee Workshop on Biomedical Electronics (B. Ziaie and J. Von Arx), Oct. 2000 (Invited presentation).
8. Fatemi, M., and Greenleaf, J. F.: Probing the dynamics of tissue at low frequencies with the radiation force of ultrasound. Physics in Medicine and Biology, 45 (6): 1449 - 1464, 2000.
9. Fatemi, M., and J. F. Greenleaf: Vibro-acoustography system modeling. Era of Hope Meeting, DoD Breast Cancer Research Program, Department of Defense, U. S. Army Medical Research and Materiel Command, Atlanta, GA, June 8-12, 2000.
10. S. Chen, M. Fatemi, and J.F. Greenleaf: Vibro-acoustography of small spheres. Journal of Acoustical Society of America 108(5): 2505, 2000.
11. Fatemi, M, Wold, LE, Morton, MJ, and Greenleaf, JF, Imaging Breast microcalcifications by vibro-acoustography. J Ultrasound Med. 20(3): S25-26, 2001.
12. Fatemi, M., L. E. Wold, A. Alizad, K. Kazunori, and J. F. Greenleaf: Detection of breast microcalcifications by vibro-acoustography: advantages and limitations, Proceedings of the 17th International Congress on Acoustics, 2001 (in press).
13. Fatemi, M., L. E. Wold, A. Alizad, M. J. Morton, and J. F. Greenleaf: Application of vibro-acoustography in breast imaging, Mayo Research Forum 2001, Rochester, MN Sept. 21-22.
14. Fatemi, M., and J. F. Greenleaf: Imaging the viscoelastic properties of tissue. In: M. Fink, J-P. Montagner, A. Tourin: *Topics in Applied Physics*. Springer, Heidelberg, Berlin 2002, volume 84, pp 257-275. (Book chapter).

15. Fatemi, M., L. E. Wold, A. Alizad, and J. F. Greenleaf: Vibro-acoustic tissue mammography. IEEE Transactions on Medical Imaging, 21(1):1-8, 2002.
16. Alizad, A., M. Fatemi, R. A. Nishimura, and J. F. Greenleaf: Detection of calcium deposits on heart valve leaflets by vibro-acoustography: an in vitro study. Journal of the American Society of Echocardiography (accepted).
17. Alizad, A., M. Fatemi, and J. F. Greenleaf, Manifestation of solid masses in vibro-acoustography, Proc. of the Ninth Int. Cong. on Sound and Vibration, 2002 (in press).
18. Chen, S., M. Fatemi, and J.F. Greenleaf: Remote measurement of material properties from radiation force induced vibration of an embedded sphere. Submitted to Journal of Acoustical Society of America, 2002.
19. Chen, S, M. Fatemi, and J.F. Greenleaf: Shear property characterization of viscoelastic media using vibrations induced by ultrasound radiation force. Submitted to IEEE International Ultrasonics Symposium, Munich, Germany, 2002.
20. Chen, S.: Shear property characterization of viscoelastic media using vibrations induced by ultrasound radiation force. Ph.D. dissertation, Mayo Graduate School, Rochester, MN, 2002.

8. List of Personnel:

Mostafa Fatemi, PhD
James F Greenleaf, PhD
Azra Alizad, MD
Randall R Kinnick
Thomas M Kinter
Elaine C Quarve

9. Appendices

Appendix 1: Figure 1 and legend.

Appendix 2: Fatemi, M., Wold, L. E., Alizad, A., and Greenleaf, J. F.: Vibro-acoustic tissue mammography. IEEE Trans on Med Imag 21(1):1-8, 2002.

Appendix 3: Fatemi, M., and Greenleaf, J. F.: Vibro-acoustography. An imaging modality based on ultrasound stimulated acoustic emission. Proc Nat Acad Sci USA 96:6603-6608, June 1999.

Appendix 4: Fatemi, M., and Greenleaf, J. F.: Ultrasound-stimulated vibro-acoustic spectrography. Science 280:82-85, April 3, 1998.

Appendix 5: Fatemi, M., and Greenleaf J. F.: Imaging and evaluating the elastic properties of biological tissues. BMUS Bulletin 8(4):16-18, Nov 2000.

Appendix 6: Fatemi, M., and Greenleaf, J. F.: Imaging the viscoelastic properties of tissue. In: M. Fink, J-P. Montagner, A. Tourin: *Topics in Applied Physics*. Springer, Heidelberg, Berlin 2002, vol 84, pp 257-275 (book chapter).

Appendix 7: Fatemi, M., Wold, L. E., Morton, M. J., and Greenleaf, J. F.: Imaging Breast microcalcifications by vibro-acoustography. J Ultrasound Med 20(3):S25-26, 2001

Appendix 8: Fatemi, M., and Greenleaf, J. F.: Probing the dynamics of tissue at low frequencies with the radiation force of ultrasound. Phys Med Biol 45(6):1449-1464, 2000.

Appendix 9: Chen, S.: Shear property characterization of viscoelastic media using vibrations induced by ultrasound radiation force. Ph.D. dissertation, Mayo Graduate School, Rochester, MN, 2002 (Table of contents and Introduction).

Appendix 10: Chen, S., Fatemi, M., and Greenleaf, J. F.: Vibro-acoustography of small spheres. J Acoust Soc Am 108(5 pt. 2):2505, Nov 2000.

Appendix 11: Chen, S., Fatemi, M., and Greenleaf, J. F.: Remote measurement of material properties from radiation force induced vibration of an embedded sphere. J Acoust Soc Am 2002 (submitted).

Appendix 1 (Figure 1)

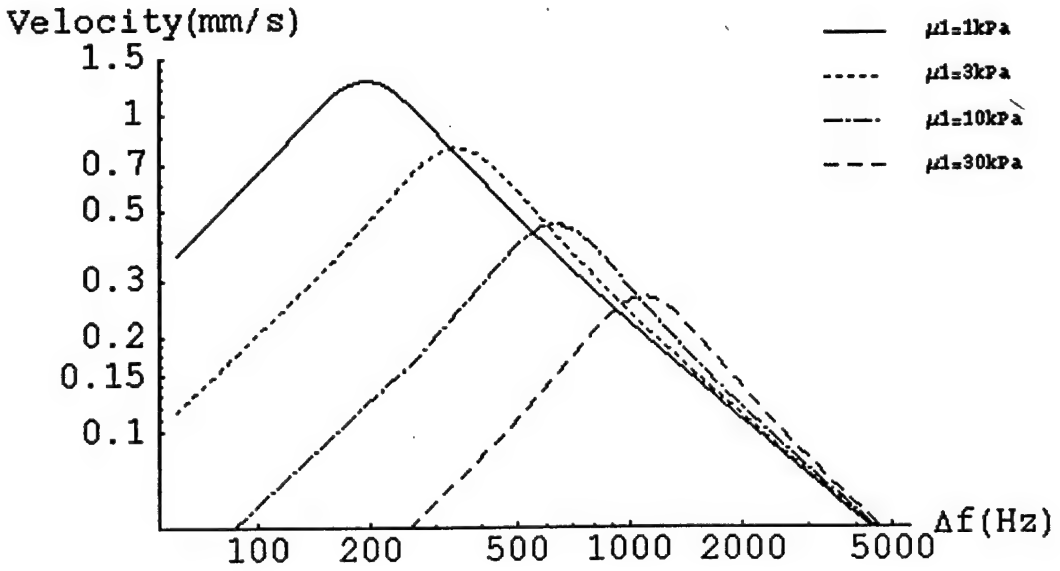

FIG. 1. Simulation of a sphere vibrated in gel. Parameters for the sphere: radius=0.59 mm, density= $7667 kg/m^3$. The gel has a shear viscosity of 0.1 $Pa \cdot s$, and shear elasticity of 1, 3, 10, and 30 kPa, respectively.

IEEE TRANSACTIONS ON MEDICAL IMAGING, VOL. 21, NO. 1, JANUARY 2002

Vibro-Acoustic Tissue Mammography

Mostafa Fatemi*, *Member, IEEE*, Lester E. Wold, Azra Alizad, and James F. Greenleaf, *Fellow, IEEE*

***Abstract*—A novel method for detection and imaging of microcalcifications in breast tissue is presented. The method, called vibro-acoustography, uses the radiation force of ultrasound to vibrate tissue at low (kHz) frequency and utilizes the resulting response to produce images that are related to the hardness of the tissue. The method is tested on human breast tissues. The resulting vibro-acoustographic images are in agreement with corresponding X-ray mammography images of the specimens. The existence of microcalcifications in locations indicated by vibro-acoustography is confirmed by histology. Microcalcifications as small as 110 μm in diameter are detected by this method. Resulting vibro-acoustographic images show microcalcifications with high contrast with respect to the background soft tissue. Structures such as dense sclerotic tissue do not seem to interfere with detection of microcalcifications.**

***Index Terms*—Breast, mammography, microcalcifications, ultrasound, vibro-acoustography.**

I. Introduction

X-RAY mammography is currently the only imaging modality clinically used for detection of breast microcalcifications. The widespread use of screening mammography has resulted in the increased detection of microcalcifications [1]. A wide spectrum of breast lesions is associated with microcalcifications, ranging from benign (fibrocystic changes, vascular changes, fat necrosis) to malignant [2]. The mammographic detection of microcalcifications frequently results in additional diagnostic studies, including: spot magnification mammographic views, stereotaxic biopsy and wire-localized biopsies. Follow-up of microcalcifications that are not biopsied, or that are benign by stereotaxic biopsy, may require additional mammograms, e.g., at six-month intervals. This results in significant additional costs, discomfort, anxiety, and some increase in X-ray exposure [1]. Recent changes in American Cancer Society (ACS) and National Cancer Institute (NCI) screening guidelines for women in their forties will increase both the number of mammograms and the number of detected microcalcifications, with resultant increased costs and morbidity. The ACS recommends annual mammography for women beginning at age 40. In women at "high" risk for breast cancer surveillance may begin at age 35 [3].

There exist subsets of women for whom mammographic screening and follow-up is limited by reduced mammographic sensitivity. Fibrocystic change is the most common benign condition of the breast, with the greatest incidence in women 30–50 years old [4]. The ACS estimates that about half of all women in America have fibrocystic breasts and many of them have very radiologically dense breast tissue. For this group, the failure rate to detect cancer on their mammogram may be as high as 15%–25% [5], [6]. Mammography is more effective in detecting occult malignancy as age increases and the breast becomes more fatty. It is the density of the breast on film screen mammography that most directly affects the risk for false-negative and false-positive interpretation [7], [8]. Several factors affect breast density. Age is the most significant factor, with more premenopausal women, especially in the 40- to 49-year age group, having breasts that are denser. For premenopausal women mammographic sensitivity may be increased by scheduling evaluation the first two weeks of their cycle corresponding with the follicular phase [9], [10]. Pregnant or lactating women may have extremely dense breast tissue, which may affect the sensitivity of mammography; also these conditions are a relative contraindication for X-ray mammography and, thus, limit its usefulness. Some studies have shown hormone replacement therapy, commonly used in postmenopausal patients, reduces the sensitivity of mammographic screening [11]–[13]. The sensitivity or accuracy of film screen mammography is also influenced by the experience of the radiologist, with experienced radiologists having the highest sensitivity in diagnosing breast cancer [14]. Finally, the ionizing nature of the X-ray mammography limits its frequent use.

To overcome some of these problems associated with mammography, a number of new technologies are currently being explored. Investigators have utilized alternative breast imaging methods, such as magnetic resonance imaging (MRI) and conventional ultrasound for imaging breast microcalcifications. Scintimammography and contrast-enhanced MRI are not sufficiently sensitive to detect clinically significant microcalcifications [15]. Similarly, conventional medical ultrasound imaging is not currently considered sufficiently reliable to visualize breast microcalcifications [16]–[18]. Microcalcification visualization by ultrasound is limited by a number of factors specific to this technique, such as speckle noise [18]. Although ultrasound can be used as an effective adjunct to mammography in detecting breast cancer [19], this technique will miss occult cancers where microcalcification may be the only sign of malignancy [20]. Thus, a sensitivity of only 63% was found in a study by Kasumi [21]. However, Yang, *et al.*

Manuscript received April 30, 2001; revised November 20, 2001. This work was supported by the Army Medical Research and Material Command under Grant DAMD 17-98-1-8121. The Associate Editor responsible for coordinating the review of this paper and recommending its publication was M. Insana. *Asterisk indicates corresponding author.*

*M. Fatemi is with the Basic Ultrasound Research Laboratory, Department of Physiology and Biophysics, Mayo Clinic and Mayo Foundation, Rochester, MN 55905 USA (e-mail: fatemi.mostafa@mayo.edu).

L. E. Wold is with the Laboratory of Medicine and Biology, Mayo Clinic and Mayo Foundation, Rochester, MN 55905 USA.

A. Alizad and J. F. Greenleaf are with the Basic Ultrasound Research Laboratory, Department of Physiology and Biophysics, Mayo Clinic and Mayo Foundation, Rochester, MN 55905 USA.

Publisher Item Identifier S 0278-0062(02)01043-1.

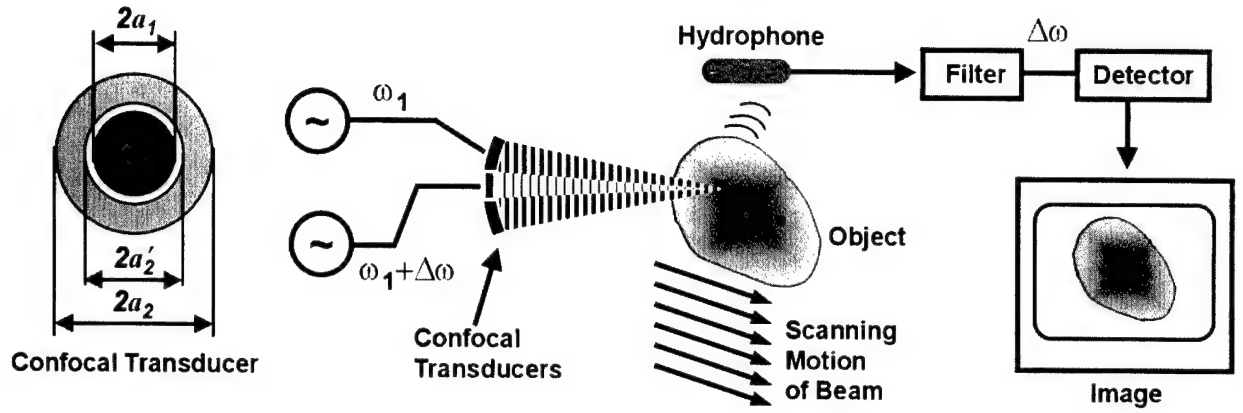

Fig. 1. Vibro-acoustography system diagram. The system includes a focused confocal transducer, (details shown on the left) consisting of a center disk and an outer ring. Two continuous wave generators drive these elements at slightly different frequencies. The transducer is focused on the object, with the beams interacting at the joint focal point to produce an oscillating radiation force on the object at the difference frequency. This force causes the object to vibrate and as a result an acoustic emission field is produced in the surrounding medium. This field is detected by the hydrophone and filtered by a bandpass filter centered at the difference frequency. The amplitude of the resulting signal, detected by the detector, is used to modulate the intensity of the image at a point corresponding to the position of the beam on the object. The image is formed by raster scanning of the object. The experiments take place in a water tank (not shown) containing the transducer, hydrophone and the object. The object, such as a tissue specimen, is secured on a latex sheet attached to a bracket for the scanning process.

[22] reported that using high-resolution ultrasound and X-ray mammography as the gold standard resulted in a sensitivity of 95% and specificity of 87% and accuracy of 91% in the detection of microcalcifications when these calcifications are within a mass lesion [22]. It should be noted that the presence of a mass lesion and its appearance in the ultrasound image could have been instrumental in the localization and identification of microcalcifications in such studies.

Microcalcifications are mainly composed of hydroxyapatite [18], [23], which is a very hard material compared with breast tissues. Therefore, an imaging modality that is sensitive to the elastic properties of tissues would likely be suitable for detection of microcalcifications. This group of imaging techniques is called elasticity imaging [24]–[37].

The general approach in elasticity imaging is to measure the response of tissue to an excitation force. An interesting strategy for producing the necessary excitation is to use the radiation force of ultrasound. This approach allows one to generate the force directly inside an organ. Several researchers have previously investigated the use of ultrasound radiation pressure for tissue characterization purposes. Sugimoto *et al.* [38] presented a method to measure tissue hardness by using the radiation force of a single ultrasound beam. In this method, the impulsive radiation force was used to generate localized deformation of tissue. Resulting transient deformation was measured as a function of time by the ultrasound Doppler method. Nightingale *et al.* [39] have studied the radiation force of ultrasound in a method named "remote palpation" to evaluate lesions in breast. They also used the ultrasound pulse-echo technique to detect tissue displacement. None of the above methods [38], [39] are specifically applied to the detection of breast microcalcifications. Walker [40] evaluated the deformation of soft tissues, including breast, by the radiation force of ultrasound. It should be noted that motion detection by ultrasound techniques (at diagnostic frequencies) becomes technically difficult if the motion is less than 1 μm. Walker predicted that the displacement produced by absorption of a continuous wave ultrasound beam of moderate intensity (1 W/ cm^2) in breast tissue is too small (less than 0.01 μm) for consistent ultrasound detection.

Vibro-acoustography is a new imaging method based on the radiation force of ultrasound [41], [42]. This method is particularly useful in detecting hard inclusions in soft material. For example, vibro-acoustography has been used to image calcifications in human arteries [43]–[45]. A comparative study of vibro-acoustography with other radiation force methods for tissue elasticity imaging is presented in [46]. The spatial resolution of vibro-acoustography is in the submillimeter range, which makes the technique suitable for imaging microcalcifications [47], [48].

In this paper, we present an application of vibro-acoustography for detection of breast microcalcifications. We may call the new method vibro-acoustic tissue mammography. We compare images of human breast tissue specimens obtained by vibro-acoustography with high-resolution X-ray tissue mammography and validate the presence and position of calcifications in the tissue histologically.

II. Methods and Materials

A. Theory of Radiation Force

Radiation force is generated by a change in the energy density of an incident acoustic field. Consider a collimated ultrasound beam interacting with an object. The radiation force arising from this interaction has a component, F, in the beam direction. This component is proportional to the time average energy density of the incident wave $\langle E \rangle$ and the projected area of the object, S, as

$$F = d_r S \langle E \rangle \tag{1}$$

where d_r is the drag coefficient and is a function of the scattered and absorbed power by the object. For the simple case of a reflecting plane target, d_r is proportional to the power reflection coefficient. In vibro-acoustography [17], this force is used for imaging. This is accomplished by probing the object

point-by-point. This technique ideally requires the stress field to be confined to a point, while its amplitude oscillates at selected frequencies.

To generate a localized oscillatory stress field, two intersecting continuous-wave focused ultrasound beams of different frequencies are used. It is only in the intersection region that the ultrasound field energy density is sinusoidally modulated and hence, the field can generate an oscillatory radiation force by interacting with the object.

The ultrasound beams can be shaped in a variety of ways for this purpose. An interesting configuration that results in a radially symmetric modulated field is obtained when two coaxial, confocal transducer elements are used (Fig. 1). In this case, we consider a two-element spherically focused annular array, consisting of a central disc with the radius of a_1 and an outer ring with the inner radius of a_2' and the outer radius of a_2. The common focal length of the elements is z_0. We also assume that the elements are excited by two CW signals at frequencies ω_1 and $\omega_2 = \omega_1 + \Delta\omega$. Let us assume that the beams are propagating in the z direction with the joint focal point at $z = 0$. The resultant field on the $z = 0$ plane may be written as

$$p(t) = P_1(r)\cos[\omega_1 t + \psi_1(r)] + P_2(r)\cos[\omega_2 t + \psi_2(r)] \quad (2)$$

where $P_1(r)$ and $P_2(r)$ are the pressure radial profiles in r direction with $\psi_1(r)$ and $\psi_2(r)$ being the associated phase functions across the focal plane. For the transducer described above, these amplitude functions can be written as [31]

$$P_1(r) = \rho c U_{01} \frac{\pi a_1^2}{\lambda_1 z_0} \text{jinc}\left(\frac{r a_1}{\lambda_1 z_0}\right) \quad (3)$$

and

$$P_2(r) = \rho c U_{02} \frac{\pi}{\lambda_2 z_0} \times \left[a_2^2 \text{jinc}\left(\frac{r a_1}{\lambda_1 z_0}\right) - a_2'^2 \text{jinc}\left(\frac{r a_2'}{\lambda_2 z_0}\right)\right] \quad (4)$$

where $\lambda_i = 2\pi/\omega_i$ for $i = 1, 2$, are ultrasound wavelengths at the ith transducer element U_{0i}, $i = 1, 2$, is the velocity amplitude at the corresponding element. Also, $\text{jinc}(X) = J_1(X)/\pi X$, where $J_1(X)$ is the first-order Bessel function of the first kind. For well-focused beams, $P_1(r)$ and $P_2(r)$ diminish quickly away from the origin.

It can be shown that the short time average of the acoustic energy density in the intersection region has slow variations at frequency $\Delta\omega$ about its long time average (mean). Denoting this low-frequency component by $e_{\Delta\omega}(t)$, we can write

$$e_{\Delta\omega}(t) = \frac{P_1(r_0)P_2(r_0)}{\rho c^2}\cos[\Delta\omega t + \Delta\psi(r_0)] \quad (5)$$

where ρ is the density, c is the sound speed and $\Delta\psi = \psi_2(r) - \psi_1(r)$. Now, consider a planar target on the focal plane. Referring to (1) and considering that the average energy density is position and time dependent in this case, the normal component of the time-varying force on an area element dS at $r = r_0$ with a local drag coefficient $d_r(r_0)$ is

$$f_{\Delta\omega}(r_0, t) = \frac{P_1(r_0)P_2(r_0)}{\rho c^2}\cos[\Delta\omega t + \Delta\psi(r_0)]d_r(r_0)dS. \quad (6)$$

This function also represents the distribution of force, or the stress field, on the focal plane. The total force on the object can be found by integrating the above incremental force over the projection area S on the focal plane

$$\bar{f}_{\Delta\omega}(r_0, t) = \left|\bar{F}_{\Delta\omega}\right|\cos(\Delta\omega t + \Delta\bar{\psi}) \quad (7)$$

where $\bar{F}_{\Delta\omega}$ is the complex amplitude of the total force and $\Delta\bar{\psi}$ is the associated phase. For a well-focused beam S is very small and hence, the force can be thought of as an oscillating point-like force applied to the object at the origin.

B. Vibro-Acoustography System

To explain the imaging method, we consider an oscillating point force, $\bar{F}_{\Delta\omega}$, applied to a point in the object. This force vibrates the object. Object vibrations result in the emission of an acoustic field in the surround energy that can be detected by a microphone (or hydrophone in water). The system diagram is shown in Fig. 1. The complex amplitude of acoustic emission pressure field, $P_{\Delta\omega}$, can be written as [17]

$$P_{\Delta\omega} = \rho c^2 H_{\Delta\omega}(l) Q_{\Delta\omega} \bar{F}_{\Delta\omega} \quad (8)$$

where $Q_{\Delta\omega}$ is a complex function representing the mechanical frequency response of the object at this point $H_{\Delta\omega}(l)$ represents the combined frequency response of the propagation medium and the microphone located at distance l from the object. It is assumed that $H_{\Delta\omega}(l)$ is unchanged for any target point in the object. Now, by scanning the object at a fixed-frequency $\Delta\omega$ and recording the acoustic emission signal, one can obtain the spatial distribution of $Q_{\Delta\omega}F_{\Delta\omega}$ (within a constant multiplier) which can be mapped into an image, displaying object morphology.

The point-spread-function (PSF) of this system is defined as the image of a point target located on the focal plane [17]. This function is proportional to the radiation stress field on the focal plane. This function can be found in an analytical form by combining (3), (4), and (6). The amplitude of this function can be written as [17]

$$h(r) = \frac{1}{a_2^2 - a_2'^2}\text{jinc}\left(\frac{r a_1}{\lambda_1 z_0}\right) \times \left[a_2^2 \text{jinc}\left(\frac{r a_2}{\lambda_2 z_0}\right) - a_2'^2 \text{jinc}\left(\frac{r a_2'}{\lambda_2 z_0}\right)\right] \exp(j\Delta\bar{\psi}). \quad (9)$$

Assuming a 3-MHz-transducer with the outer diameter of 45 mm, inner disk diameter of 29.6 mm, and a gap of 2 mm between the inner disk and the outer ring and a focal length of 70 mm, the amplitude of the resulting PSF function for $\Delta f = \Delta\omega/2\pi = 7.3$ kHz is shown in Fig. 2. The spatial resolution of the system, defined by the diameter of the central lobe, is about 0.7 mm. The depth resolution (or the focal depth) of this transducer was experimentally determined. For this purpose, a small glass bead was scanned at different depths. The depth resolution, defined as the -6-dB width of the response in the axial direction, was

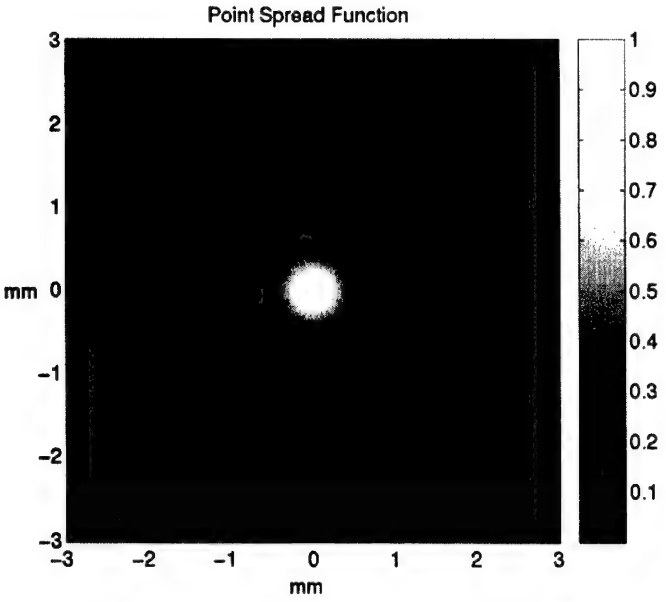

Fig. 2. Theoretical point spread function of the vibro-acoustography system.

found to be about 9 mm. The peak response occurred when the bead was located at the focal distance from the transducer.

C. Experimental Setup

The experimental setup is shown in Fig. 1. The experiments were conducted in a water tank. (In a system designed for *in vivo* imaging the transducers can be placed in contact with the skin instead of using water. The hydrophone would also be placed in contact with the skin. Because at low frequencies the sound wave propagates almost uniformly in all directions, hydrophone position is not critical, as long as it is relatively close to the exposure site but not in the ultrasound path.) A two-element confocal ultrasound transducer array was positioned such that the beams meet the object at their joint focal point. Transducer specifications are as those in the previous section. The elements were driven by two stable radio-frequency (RF) synthesizers (HP 33 120A) at frequencies of 3 MHz and 3 MHz $+ \Delta f$ Sound produced by the object vibration was detected by a submerged hydrophone (ITC model 680) placed within the water tank. The received signal was filtered and amplified by a programmable filter (Stanford Research Systems, SR650) to reject the noise, then digitized by a 12-bits/sample digitizer (National Instruments VXI-1000) at a rate sufficiently higher than the Nyquist rate. Data are recorded on a computer disc.

D. Experiment Procedure

To evaluate the capability of the system for imaging small particles about the size of a common breast microcalcification, we constructed a test object comprised of four small glass beads, ranging from 260 μm to 400 μm in diameter imbedded in a block of tissue- mimicking gel. The resulting vibro-acoustography image is shown in Fig. 3, demonstrating the capability of the system in detecting and imaging beads that are at least 260 μm in diameter.

Tissue experiments were conducted on excised human breast tissue samples. These tissues were obtained postsurgically and

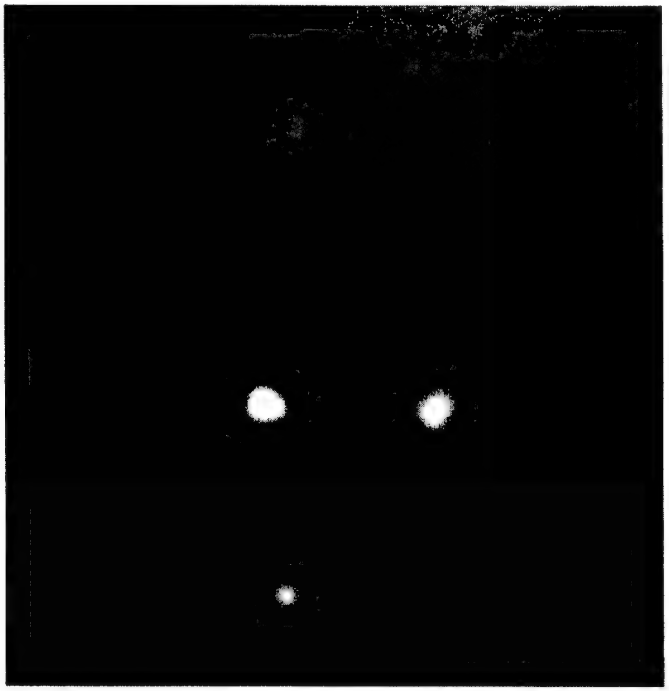

Fig. 3. Image of glass beads in gel. This image is obtained by scanning the gel phantom. This image covers an area of 20 mm by 20 mm, scanned at 0.2 mm/pixel. The beads are located about 10 mm deep inside the gel. The diameter of the top bead is about 260 μm and the diameter of the largest bead is about 400 μm. The vibration frequency was set at 53.5 kHz.

were fixed in formaldehyde for at least three days and not more than six months at the time of experiments. It is known that formaldehyde tends to harden soft tissue and, thus, may introduce an additional variable in the experiments. However, because our main target (microcalcifications) is much harder than the fixed tissue, we did not consider tissue-hardening phenomenon as a major problem in our experiments. Patients' records were reviewed to identify tissues with high probability of having microcalcifications. Selected tissues were cut into (approximately) 3×3 cm and 3- to 5-mm-thick pieces and imaged using a high-resolution X-ray mammography machine. Therefore microcalcifications were at most 5 mm from the front surface of the sample. The X-ray mammograms were then read to identify presence of microcalcifications. Tissue pieces identified with microcalcification were each mounted flat with a few droplets of glue on a latex sheet and secured in a scanning bracket. This bracket is designed to hold the tissue piece in the water for acoustic scanning. Glue drops were carefully placed on areas away from the region with microcalcifications. Small pieces of suture were sewed to the tissue and used as identification marks. For this purpose, small knots are placed at different positions on the tissue away from microcalcifications. These markers could be seen in vibro-acoustography, X-ray (often very dim) and photographic images.

Specimen X-ray mammographic images were obtained from each mounted sample. Each X-ray image was used as a reference for comparison with the corresponding vibro-acoustography image. The system illustrated in Fig. 1 was used to obtain vibro-acoustography images of tissue samples. The scanning process was performed by a raster motion of the specimen, the ultrasound beam being perpendicular to the large flat surface

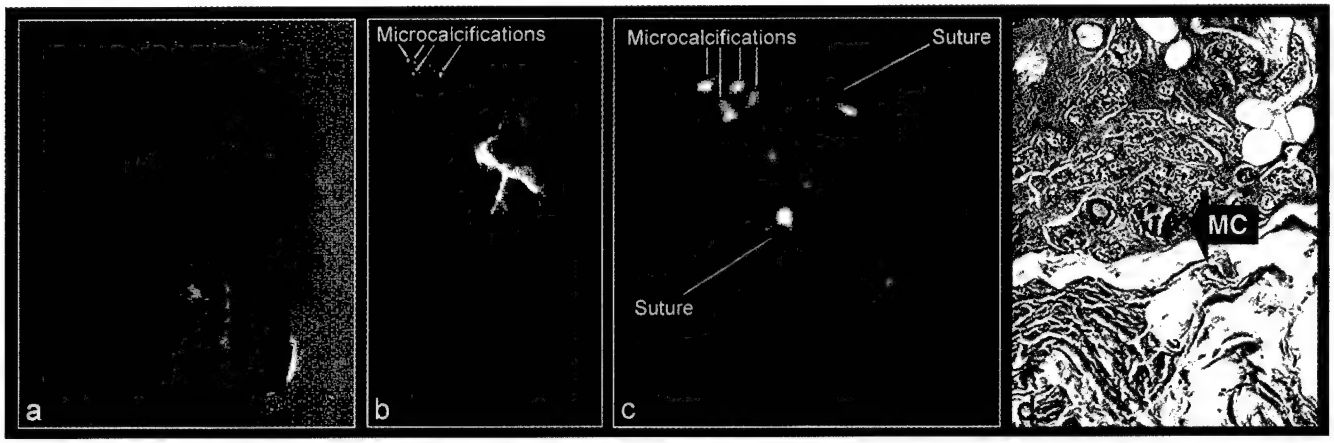

Fig. 4. Vibro-acoustography of the first specimen. (a) Photograph of a breast specimen mounted on the scanning bracket, (b) The X-ray mammogram of the selected tissue pieces mounted on the scanning bracket. Microcalcifications can be seen on the top left of this X-ray, (c) Vibro-acoustography image of the tissue at 25 kHz. Microcalcifications can be seen in this image as bright spots on the top left and (d) Histology of the tissue specimen around the region with some microcalcifications.

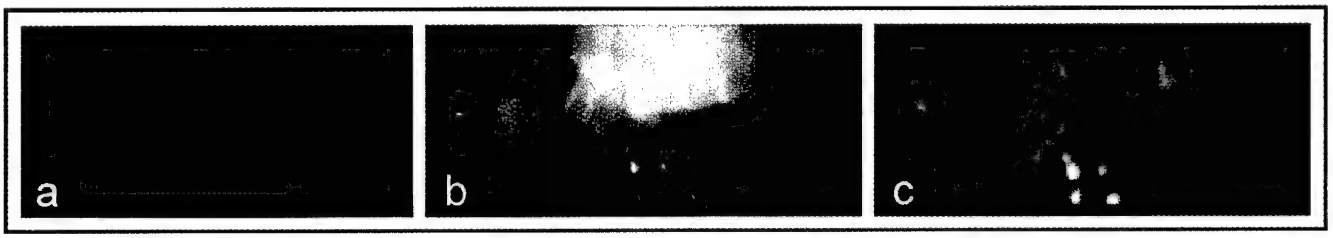

Fig. 5. Vibro-acoustography of the second specimen. (a) Photograph of the tissue specimen mounted on the scanning bracket. (b) X-ray mammogram of (a) showing some microcalcifications at the center of the image. (c) Vibro-acoustography of (a). Microcalcifications can be seen as bright spots at same location as in the X-ray.

of the tissue layer and passing through the 3- to 5-mm-thickness of the tissue. The specimen was placed on the focal plane, such that its entire thickness was within the focal depth of the transducer. Experiments were conducted in a water tank at room temperature (about 21 °C). Sections of the tissue identified with microcalcification were then cut for histologic study to identify microcalcifications and validate the imaging results.

III. Results

Fig. 4(a) shows the photograph of a breast specimen mounted on the scanning bracket. Sutures are knotted on the tissue for identification purpose. Fig. 4(b) shows the X-ray mammogram of the selected tissue pieces mounted on the scanning bracket. The sutures are barely visible. Microcalcifications can be seen on the top left of this X-ray in a high-density sclerotic region. This sample was then scanned in the water tank. The vibro-acoustography image of the tissue, at $\Delta f = 25$ kHz, is shown in Fig. 4(c). Microcalcifications can be seen in this image as bright spots. Note that the number of microcalcifications matches with the corresponding spots in the X-ray mammography. Also noticeable is that dense sclerotic tissue appears dim and does not interfere with identification of calcification in the vibro-acoustic image. Microcalcifications identified by vibro-acoustography were verified histologically. Fig. 4(d) shows the histology of the region around the calcifications. The breast parenchyma shows atypical lobular hyperplasia and microcalcifications in the lobules. We measured the size of the microcalcification at the lower left, by measuring the spot size in the X-ray mammogram and found to be approximately 110 μm in diameter.

Fig. 5(a) shows the photograph of the second breast tissue specimen mounted on the scanning bracket. Fig. 5(b) is the X-ray mammogram of this tissue and shows the microcalcifications at the center of the image. Fig. 5(c) shows the vibro-acoustic image of this tissue at 22 kHz. Microcalcifications can be seen as bright spots at the same location as in the X-ray. The breast parenchyma histologically showed comedo type ductal carcinoma *in situ*, with calcifications in regions of comedo necrosis.

Fig. 6(a) shows the X-ray mammogram of another breast tissue specimen with a large microcalcification. Fig. 6(b) shows the corresponding vibro-acoustic image, with the microcalcification shown as a bright spot within the relatively dark background of soft tissue.

IV. Discussion

Experimental vibro-acoustography images presented in this report demonstrate two important facts: 1) The vibro-acoustography imaging method is capable of detecting small microcalcifications in breast tissue; 2) Microcalcifications can be delineated from within dense and sclerotic tissues. Results shown here also indicate that such images have high spatial resolution (700 μm), the capability of detecting small (about 110 μm in diameter and above) microcalcifications, no speckles, good contrast and high signal to noise ratio.

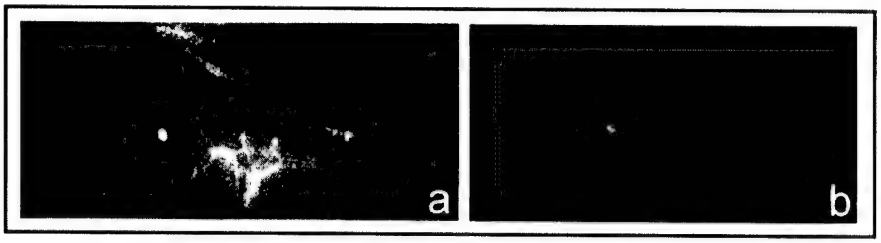

Fig. 6. Vibro-acoustography of the third specimen. (a) X-ray mammogram of the tissue sample showing a large microcalcification and (b) Vibro-acoustography image of (a).

A comparison between the vibro-acoustography image [Fig. 4(b)] and the corresponding X-ray mammography [Fig. 4(c)], reveals an interesting capability of vibro-acoustography method. High-density sclerotic tissue in the region surrounding the microcalcification absorbs a great deal of X-ray energy; hence, the X-ray image shows very low contrast within this region and as a result microcalcifications are barely visible. However, the vibro-acoustography image delineates these calcifications with high contrast. This demonstrates that some tissues that are radiologically opaque may be transparent in vibro-acoustography images giving the potential to detect calcification in radiologically dense breasts.

The halo seen around the images of each microcalcification is an artifact of the vibro-acoustography system. This effect is seen more clearly in the PSF image shown in Fig. 2. Multiple rings around the center spot are due to the sidelobes of the Bessel functions that appear in the PSF function (9) as discussed in the previous section.

Another artifact is due to the glue used to bond the tissue specimens to the latex sheet. We used small droplets of instant glue (Krazy Glue brand, Elmers Products, Inc. Columbus, OH) for this purpose. This type of glue produces a relatively strong acoustic emission making it visible in vibro-acoustography images. Fig. 7 shows a vibro-acoustography image of three droplets of this glue on a latex sheet, resembling images of breast microcalcification. To avoid mistaking glue droplets for microcalcifications, we marked the glued region of tissue and took extra precautions to locate these regions on the vibro-acoustography images.

The choice of vibration frequency Δf used in each experiment was, to some extent, determined by the resonance frequencies of the water tank. The acoustic emission field resulting from vibrations of microcalcifications is very small. To facilitate the detection process, we often chose the vibration frequency to correspond to one of the resonance frequencies of the water tank. This way, the water tank acts as an amplifier to improve the signal-to-noise ratio (SNR). Because the human body does not have a regular geometric shape with parallel walls, such resonance phenomenon is not likely to take place. Therefore, the choice of Δf may no longer be based on the resonance effect.

Ultrasound standing waves between the transducer and the object may cause artifacts in the image. This may happen if the object reflects a significant portion of the incident beam back to the transducer. The transducer surface can then act as a mirror to re-reflect the reflected field toward the object. This process may occur more than once. The resulting field at the object is the sum of the incident and all the reflected fields. Depending on the distance between the transducer and the object and the ultrasound- wavelength, those components may interact constructively or destructively. Hence, the field intensity and the resulting image can, therefore, become excessively sensitive to the transducer-to-object distance. The effect of standing wave phenomena on the image diminishes as the ultrasound bath loss increases. Therefore, it is expected that standing wave artifacts would be less of a problem in clinical applications of vibro-acoustography for *in vivo* breast imaging.

Fig. 7. Vibro-acoustography of the instant glue drops. The glue drops (about 1 mm in diameter) are placed on a latex sheet.

In the present study, we imaged tissue samples only in two dimensions (i.e., a single slice). However, the ultrasound beam used here produces a stress field that is confined in three dimensions. Therefore, it is possible, in principle, to selectively scan several slices of the object at different depths to produce a three-dimensional (volume) image of the object.

Application of the vibro-acoustography for breast imaging is both promising and challenging. An expected difficulty in using vibro-acoustography on patients is achieving a high SNR. Several factors that can reduce the SNR below what we have in the experimental system. These factors include limitation on the ultrasound intensity, body attenuation of the ultrasound beam, defocusing of the ultrasound beam due to phase aberrations, and the biological noise generated by the body. Imaging speed is

another concern in *in vivo* vibro-acoustography. The scanning mechanism used in the experiment presented in this paper scan the object one point at a time, making the data collection a relatively lengthy process (up to a few minutes per image). A long imaging time is not desirable for breast imaging because body motions within this period can introduce "motion artifact " in the images.

There are several benefits in using vibro-acoustography for *in vivo* breast imaging as an alternative, or in parallel, to X-ray mammography. One advantage of vibro-acoustography stems from the fact that it uses ultrasound energy, which can easily penetrate in dense tissues. Such tissues are normally radio-opaque and difficult to image with X-ray. Additionally, the present method is relatively safe and hence, may be useful in applications where the use of X-ray is limited to its ionizing effects. Vibro-acoustic detection and follow-up of microcalcifications has several clinical potentials, including the following.

- Detection of microcalcifications in the breast of women who are younger and/or have radiologically very dense breast. We showed that ultrasound can penetrate radiologically dense tissue and detect calcification.
- Detection of microcalcification in pregnant or lactating women.
- Detection of microcalcifications in women with radio-opaque breast implants.

V. Summary

In this paper, we present a noninvasive imaging method for detecting microcalcifications in breast tissue. This method uses ultrasound in a fundamentally new way to image the tissue at low (kHz range) frequencies, producing high signal-to-noise and speckle-free images.

The spatial resolution of vibro-acoustic images is determined by the focal beamwidth of the two-element transducer, which was in the order of 0.7 mm for the transducer used here. Experiments were conducted on human breast tissue specimens. X-ray tissue mammography images were used for initial identification of microcalcifications and also as reference images for comparison with the corresponding vibro-acoustography images. Tissue histology was also used to validate presence of microcalcification.

Results indicate that microcalcifications associated with a variety of breast pathology, including those located in high-density or sclerotic regions of tissue, can be detected by vibro-acoustography. Microcalcifications as small as 110 μm in diameter were detected by vibro-acoustic tissue mammography.

Further development of vibro-acoustic tissue mammography may lead to a novel imaging tool for applications. This method can be considered as a nonionizing alternative to conventional X-ray mammography and may be useful for such cases as pregnant patients, where the use of ionizing radiation is not allowed. Also, vibro-acoustography is potentially useful for imaging dense breast where the use of conventional X-ray mammography may be limited.

Acknowledgment

The authors are grateful to the following individuals for their valuable work during the course of this study: Dr. R. E. Johnson for valuable comments on the clinical aspects of microcalcification in breast, T. Distad for providing postsurgical tissue specimens, M. Siewert for providing tissue X-rays, Dr. M. Morton for reading X-ray mammograms, R. Kinnick for laboratory support and scanning tissues, D. Cook for scanning some of the tissues, Dr. K. Kanehira for histologic evaluation of tissues, J. Patterson for graphic support and E. Quarve for secretarial assistance.

References

[1] M. D. Abeloff, A. S. Lichter, J. E. Niederhuber, L. J. Pierce, and R. R. Love, "Breast," in *Clinical Oncology*, 2nd ed, M. D. Pierce, Ed. New York: Churchill Livingstone, 2000, ch. 75, pp. 2051–2138.

[2] S. C. Lester and R. S. Cortan, "The breast," in *Robins Pathologic Basis of Diseases*, 6th ed, V. Kumar, T. Collins, and T. Collins, Eds. Philadelphia, PA: Saunders, 1999, pp. 1093–1117.

[3] G. D. Dodd, "American cancer society guidelines on screening for breast cancer," *Cancer*, vol. 69, no. 7, pp. 1885–1887, 1992.

[4] J. V. Fioricia, "The breast," in *Danforth Obstetrics and Gynecology*, 8th ed, J. R. Scott, P. J. Di Saia, C. B. Hammond, and W. M. Spellacy, Eds. Philadelphia, PA: Lippincott Williams and Williams, 1999, ch. 40.

[5] "Screening recommendations of the forum panel," *J. Gerontol.*, no. 5, p. 47, Nov. 1992.

[6] S. W. Fletcher, W. Black, and R. Harris *et al.*, "Report of the international workshop on screening for breast cancer," *J. Nat. Cancer Inst.*, vol. 85, no. 30, pp. 1644–1656, 1993.

[7] K. Kerlikowske, "Effect of age, breast density and family history on the sensitivity of first screen mammography," *JAMA*, vol. 276, no. 1, pp. 33–37, July 1996.

[8] C. D. Lehman, E. White, S. Peacock, and M. J. Drucker, "Urban N. effect of age and breast density on screening mammograms with false-positive findings," *Amer. J. Roentgenol.*, vol. 173, no. 6, pp. 1651–1655, Dec. 1999.

[9] C. J. Baines, M. Vidmar, G. McKeown-Eyssen, and R. Tibshirani, "Impact of menstrual phase on false-negative mammograms in the canadian national breast screening study," *Cancer*, vol. 80, no. 4, pp. 720–724, August 1997.

[10] E. White, P. Velentgas, and M. T. Mandelson *et al.*, "Variation in mammographic breast density by time in menstrual cycle among women aged 40 to 49 years," *J. Nat. Cancer Inst.*, vol. 90, no. 12, pp. 906–910, June 1998.

[11] M. B. Laya, D. B. Larson, S. H. Taplin, and E. White, "Effect of estrogen replacement therapy on the specificity and sensitivity of screening mammography," *J. Nat. Cancer Inst.*, vol. 88, no. 10, pp. 643–649, 1996.

[12] J. C. Litherland, S. Scotland, D. Hole, and C. Cordiner, "The effect of hormone replacement therapy on the sensitivity of screening mammograms," *Clin. Radiol.*, vol. 54, no. 5, pp. 285–288, May 1999.

[13] A. M. Kavanagh, H. Mitchel, and G. G. Giles, "Hormone replacement therapy and accuracy of mammographic screening," *Lancet*, vol. 355, no. 9200, pp. 270–274, Jan. 2000.

[14] L. Liberman, A. F. Abramson, and F. B. Squires *et al.*, "The breast imaging reporting and data system-positive predictive value of mammographic features and final assessment categories," *Amer. J. Roentgenol.*, vol. 171, no. 1, pp. 35–40, July 1998.

[15] R. R. Tiling, I. Khalkhali, H. Sommer, R. Link, R. Moser, F. Willemen, T. Pfluger, K. Tats, and K. Hahn, "Limited value of scintimammography and contrast-enhanced MRI in the evaluation of microcalcification detected by mammography," *Nucl. Med. Common*, vol. 19, no. 1, pp. 55–62, Jan. 1998.

[16] A. J. Potterton, D. J. Peakman, and J. R. Young, "Ultrasound demonstration of small breast cancers detected by mammographic screening," *Clin. Radiol.*, vol. 49, pp. 808–813, Nov. 1994.

[17] P. B. Guyer, K. C. Dewbury, D. Warwick D, J. Smallwood, and I. Taylor, "Direct contact B-scan clinical ultrasound in the diagnosis of solid breast masses," *Clin. Radiol.*, vol. 37, no. 5, pp. 451–458, Sept. 1986.

[18] M. E. Anderson, M. S. Soo, R. C. Bentley, and G. E. Trahey, "The detection of breast microcalcifications with medical ultrasound," *J. Acoust. Soc. Amer.*, vol. 101, no. 1, pp. 29–39, Jan. 1997.

[19] H. M. Zonderland, E. G. Cokerkamp, J. Hemans, M. J. van de Vijver, and A. E. Van Voorthuisen, "Diagnosis of breast cancer: Contribution of US as an adjunct to mammography," *Radiol.*, vol. 213, no. 2, pp. 413–422, Nov. 1999.

[20] E. A. Sickles, "Sonographically detectability of breast calcifications," *Proc. SPIE*, vol. 419, pp. 51–52, 1983.

[21] F. Kasumi, "Can microcalcifications located within breast carcinomas be detected by ultrasound imaging?," *Ultrasound Med. Biol.*, vol. 14, no. 1, pp. 175–82, 1988.

[22] W. T. Yang, M. Suen, A. Ahuja, and C. Meterweli, "*In vivo* demonstration of microcalcification in breast cancer using high resolution ultrasound," *Br. J. Radiol*, vol. 70, pp. 685–690, July 1997.

[23] D. E. Grenoble, J. L. Katz, K. L. Dunn, K. L. Murty, and R. S. Gilmore, "The elastic properties of hard tissues and apatites," *J. Biomed. Mater. Res.*, vol. 6, no. 3, pp. 221–233, May 1972.

[24] M. O'Donnell, A. R. Skovoroda, B. M. Shapo, and S. Y. Emelianov, "Internal displacement and strain imaging using ultrasonic speckle tracking," *IEEE Trans. Ultrason. Ferroelect. Freq. Contr.*, vol. 1, pp. 314–325, May 1994.

[25] J. Ophir, I. Cespedes, H. Ponnekanti, Y. Yazdi, and X. Li, "Elastography: A quantitative method for imaging the elasticity of biological tissues," *Ultrason. Imag.*, vol. 13, no. 2, pp. 111–134, April 1991.

[26] Y. Yamakoshi, J. Sato, and T. Sato, "Ultrasonic imaging of internal vibration of soft tissue under forced vibration," *IEEE Trans. Ultrason. Ferroelect. Freq. Contr.*, vol. 37, pp. 45–53, Mar. 1990.

[27] T. A. Krouskop, D. R. Dougherty, and F. S. Vinson, "A pulsed doppler ultrasonic system for making noninvasive measurements of the mechanical properties of soft tissue," *J. Rehab. Res. Dev.*, vol. 24, no. 2, pp. 1–8, 1987.

[28] R. M. Lerner, S. R. Huang, and K. J. Parker, "Sonoelasticity images derived from ultrasound signals in mechanically vibrated tissues," *Ultrasound Med. Biol.*, vol. 16, no. 3, pp. 231–239, 1990.

[29] S. K. Alam, D. W. Richards, and K. J. Parker, "Detection of intraocular pressure change in the eye using sonoelastic doppler ultrasound," *Ultrasound Med. Biol.*, vol. 20, no. 8, pp. 751–758, 1994.

[30] L. Gao, K. J. Parker, R. M. Lerner, and S. F. Levinson, "Imaging of the elastic properties of tissue—A review," *Ultrasound Med. Biol.*, vol. 22, no. 8, pp. 959–977, 1996.

[31] R. Muthupillai, D. J. Lomas, P. J. Rossman, J. F. Greenleaf, A. Manduca, and R. L. Ehman, "Magnetic resonance elastography by direct visualization of propagating acoustic strain waves," *Science*, vol. 269, no. 5232, pp. 1854–1857, Sept. 1995.

[32] J. Ophir, S. K. Alam, B. Garra, F. Kallel, E. Konofagou, T. Krouskop, and T. Varghese, "Elastography: Ultrasonic estimation and imaging of the elastic properties of tissues," *Proc. Inst. Mech. Eng. [H]—J Eng. Med.*, vol. 213, no. 3, pp. 203–233, 1999.

[33] D. Fu, S. F. Levinson, S. M. Gracewski, and K. J. Parker, "Non-invasive quantitative reconstruction of tissue elasticity using an iterative forward approach," *Phys. Med. Biol.*, vol. 45, no. 6, pp. 1495–509, June 2000.

[34] L. S. Taylor, B. C. Porter, D. J. Rubens, and K. J. Parker, "Three-dimensional sonoelastography: Principles and practices," *Phys. Med. Biol.*, vol. 45, no. 6, pp. 1477–1494, June 2000.

[35] K. J. Parker, D. Fu, S. M. Graceswki, F. Yeung, and S. F. Levinson, "Vibration sonoelastography and the detectability of lesions," *Ultrasound Med. Biol.*, vol. 24, no. 9, pp. 1437–1447, November 1998.

[36] D. D. Steele, T. L. Chenevert, A. R. Skovoroda, and S. Y. Emelianov, "Three-dimensional static displacement, stimulated echo NMR elasticity imaging," *Phys. Med. Biol.*, vol. 45, no. 6, pp. 1633–1648, June 2000.

[37] T. L. Chenevert, A. R. Skovoroda, M. O'Donnell, and S. Y. Emelianov, "Elasticity reconstructive imaging by means of stimulated echo MRI," *Magn. Reson. Med.*, vol. 39, no. 3, pp. 482–490, Mar. 1998.

[38] S. Sugimoto, S. Ueha, and K. Itoh, "Tissue hardness measurement using the radiation force of focused ultrasound," in *IEEE Ultrason. Symp. Proc.*, 1990, pp. 1377–1380.

[39] K. R. Nightingale, R. W. Nightingale, M. T. Palmeri, and G. E. Trahey, "A finite element model of remote palpation of breast lesions using radiation force: Factors affecting tissue displacement," *Ultrason. Imag.*, vol. 22, no. 1, pp. 35–54, Jan. 2000.

[40] W. F. Walker, "Internal deformation of a uniform elastic solid by acoustic radiation force," *J. Acoust. Soc. Amer.*, vol. 105, no. 4, pp. 2508–2558, Apr. 1999.

[41] M. Fatemi and J. F. Greenleaf, "Ultrasound stimulated vibro-acoustic spectroscopy," *Science*, vol. 280, pp. 82–85, Apr. 1998.

[42] ——, "Vibro-acoustography: An imaging modality based on ultrasound stimulated acoustic emission," in *Proc. Nat. Acad. Sci. USA*, vol. 96, June 1999, pp. 6603–6608.

[43] J. F. Greenleaf, R. L. Ehman, M. Fatemi, and R. Muthupillai, "Imaging elastic properties of tissue," in *Ultrasound in Medicine*, F. A. Duck, A. C. Baker, and H. C. Starritt, Eds. Philadelphia, PA: Inst. Phys., 1998, ch. 14.

[44] M. Fatemi and J. F. Greenleaf, "Probing the dynamics of tissue at low frequencies with the radiation force of ultrasound," *Phys. Med. Biol.*, vol. 45, pp. 1449–1464, 2000.

[45] ——, "Imaging the viscoelastic properties of tissue," in Topics in Applied Physics, M. Fink, J.-P. Montagner, and A. Tourin, Eds. Berlin, Germany: Springer-Verlag, 2001, vol. 82, to be published.

[46] ——, "Imaging and evaluating the elastic properties of biological tissues," *BMUS Bulletin*, vol. 8, no. 4, pp. 16–18, Nov. 2000.

[47] ——, "Vibro-acoustography system modeling," in *Era of Hope Proc.*, vol. I, June 2000, p. 192.

[48] P. M. Morse and K. U. Ingard, *Theoretical Acoustics*. New York: McGraw-Hill, 1968, p. 192.

Proc. Natl. Acad. Sci. USA
Vol. 96, pp. 6603–6608, June 1999
Engineering

Vibro-acoustography: An imaging modality based on ultrasound-stimulated acoustic emission

MOSTAFA FATEMI* AND JAMES F. GREENLEAF

Ultrasound Research, Department of Physiology and Biophysics, Mayo Clinic and Foundation, 200 First Street SW, Rochester, MN 55905

Communicated by Floyd Dunn, Professor Emeritus, University of Illinois, Urbana, IL, March 11, 1999 (received for review August 11, 1998)

ABSTRACT **We describe theoretical principles of an imaging modality that uses the acoustic response of an object to a highly localized dynamic radiation force of an ultrasound field. In this method, named ultrasound-stimulated vibro-acoustography (USVA), ultrasound is used to exert a low-frequency (in kHz range) force on the object. In response, a portion of the object vibrates sinusoidally in a pattern determined by its viscoelastic properties. The acoustic emission field resulting from object vibration is detected and used to form an image that represents both the ultrasonic and low-frequency (kHz range) mechanical characteristics of the object. We report the relation between the emitted acoustic field and the incident ultrasonic pressure field in terms of object parameters. Also, we present the point-spread function of the imaging system. The experimental images in this report have a resolution of about 700 μm, high contrast, and high signal-to-noise ratio. USVA is sensitive enough to detect object motions on the order of nanometers. Possible applications include medical imaging and material evaluation.**

The study of objects in terms of their mechanical response to external forces is of considerable interest in material science and medical diagnosis. Elastic constants are closely connected to the thermodynamic properties of materials and can be related to a wide range of physical parameters. Elastic constants can be determined by measuring deformation in response to an applied force. Although a static force can be used for this purpose, using a dynamic force is preferred if one is interested in measuring the dynamic characteristics of the material (1).

Changes in elasticity of soft tissues are often related to pathology. Palpation is a traditional example of estimating mechanical parameters for tissue characterization, where a static force is applied and a crude estimation of the tissue elasticity is obtained through the sense of touch. In palpation, force is exerted on the body surface, and the result is an accumulative response of all the tissues below. Physicians can sense abnormalities if the response to palpation of the suspicious tissue is sufficiently different from that of normal tissue. However, if the abnormality lies deep in the body, or if it is too small to be resolved by touch, then the palpation method fails.

Elasticity imaging, a subject extensively investigated in recent years, is a quantitative method that measures the mechanical properties of tissue. The general approach is to measure tissue motion caused by an external (or, in some methods, internal) force/displacement and use it to reconstruct the elastic parameters of the tissue. Some investigators have used static force to compress the tissue and measured the resulting strain by ultrasound (2, 3). Others have used external mechanical vibrators to vibrate the tissue and detected the resulting displacement in tissue by Doppler ultrasound (4–7). For a review of elasticity imaging methods, refer to ref. 8. A recently developed method uses an actuator to vibrate the body surface and then measures the strain waves with phase-sensitive MRI (9).

Most of the elasticity imaging methods are based on an external source of force resulting in a spatially wide stress-field distribution. This requires the stress field to pass through the superficial portion of an object before reaching the interior part. Analysis of the object response can be complicated because the stress-field pattern changes, often unpredictably, at different depths before it reaches the region of interest within the object. An alternative strategy is to apply a localized stress directly in the region of interest. One way to accomplish this is to use the radiation pressure of an ultrasound source(s). Based on this strategy, Sugimoto *et al.* (10) presented a method to measure tissue hardness by using the radiation force of a single focused ultrasound beam. In this method, impulsive radiation force was used to generate localized deformation of the tissue. Resulting transient deformation was measured as a function of time by an ultrasound Doppler method. Radiation force has also been used to generate shear elastic waves in tissues (11).

In this paper, we describe the principles of an imaging technique that produces a map of the mechanical response of an object to a force applied at each point. The method uses ultrasound radiation force to remotely exert a localized oscillating stress field at a desired frequency within (or on the surface of) an object. In response to this force, a part of the object vibrates. The size of this part and the motion pattern depend on object viscoelastic characteristics. The acoustic field resulting from object vibration, which we refer to as "acoustic emissions,"† is detected by a sensitive hydrophone and used to form the image of the object. This method benefits from the high spatial definition of ultrasound radiation force and high motion-detection sensitivity offered by the hydrophone. We call this technique ultrasound-stimulated vibro-acoustography (USVA). Some general aspects of this method, including some experimental results, have been outlined by the authors in ref. 12. Here we present the theoretical foundations of USVA.

METHODS

Our aim is to image an object based on its mechanical characteristics. This is achieved by vibrating the object by applying a highly localized oscillating force to each point of the object. The localized force is produced by modulating the intensity, and thereby the radiation force, of the ultrasound at low frequencies (normally in kHz range). The resulting sound emitted by the object is a function of object mechanical

The publication costs of this article were defrayed in part by page charge payment. This article must therefore be hereby marked "*advertisement*" in accordance with 18 U.S.C. §1734 solely to indicate this fact.

PNAS is available online at www.pnas.org.

Abbreviations: USVA, ultrasound-stimulated vibro-acoustography; PSF, point spread function; CW, continuous wave.

*To whom reprint requests should be addressed at: Ultrasound Research, Mayo Clinic. e-mail: fatemi.mostafa@mayo.edu.

†The term "acoustic emission" is used to describe the acoustic field in response to a cyclic vibration of the object. Similar terminology is also used in the field of nondestructive testing of materials and in optoacoustic imaging to describe a different phenomenon, usually the acoustic field resulting from structural deformation.

characteristics and the location of the excitation point. The image is produced by mapping the amplitude or phase of this sound, which is detected by a sensitive hydrophone, vs. position. Fig. 1 illustrates this method. In the following section, we describe the relationship between the USVA image and the properties of the object.

THEORY

Generation of a Dynamic Radiation Force on a Target. The acoustic radiation force is the time-average force exerted by an acoustic field on an object. This force is an example of a universal phenomenon in any wave motion that introduces some type of unidirectional force on absorbing or reflecting targets in the wave path. Radiation force is produced by a change in the energy density of an incident acoustic field. For a review of this phenomenon, refer to ref. 13. Consider a plane ultrasound beam interacting with a planar object of zero thickness and arbitrary shape and boundary impedance that scatters and absorbs. The radiation force vector, **F**, arising from this interaction has a component in the beam direction and another transverse to it. The magnitude of this force is proportional to the average energy density of the incident wave $\langle E \rangle$ at the object, where $\langle\ \rangle$ represents the time average and S, the projected area of the object (14)

$$\mathbf{F} = \mathbf{d}_r S \langle E \rangle, \qquad [1]$$

where $\mathbf{d}_r$ is the vector drag coefficient with a component in the incident beam direction and another transverse to it. The coefficient $\mathbf{d}_r$ is defined per unit incident energy density and unit projected area. For a planar object, $\mathbf{d}_r$ is numerically equal to the force on the object. Physically, $\mathbf{d}_r$ represents the scattering and absorbing properties of the object and is given by (14)

$$\mathbf{d}_r = \hat{\mathbf{p}} S^{-1} (\Pi_a + \Pi_s - \int \gamma \cos\alpha_s dS) + \hat{\mathbf{q}} S^{-1} \int \gamma \sin \alpha_s dS, \qquad [2]$$

where $\hat{\mathbf{p}}$ and $\hat{\mathbf{q}}$ are the unit vectors in the beam direction and normal to it, respectively. The quantities Π_a and Π_s are the total absorbed and scattered powers, respectively, and γ is the scattered intensity, all expressed per unit incident intensity. Also, α_s is the angle between the incident and the scattered intensity, and dS is the area element. The drag coefficient can also be interpreted as the ratio of the radiation force magnitude on a given object to the corresponding value if the object were replaced by a totally absorbing object of similar size. This is because $|\mathbf{d}_r| = 1$ for a totally absorbing object. This coefficient can be determined for objects of different shapes and sizes. For simplicity, we assume a planar object normal to the beam axis. In this case, the transverse component vanishes, thus the drag coefficient (force) will have only a component normal to the target surface, which we denote by scalar d_r (F). Values of d_r for spheres, in terms of the diameter and the wavelength, are given in ref. 14.

To produce a dynamic radiation force, one can use an amplitude-modulated beam (15). Consider an amplitude-modulated incident (ultrasonic) pressure field, $p(t)$, as

$$p(t) = P_{\omega_0} \cos(\Delta\omega t/2) \cos\omega_0 t, \qquad [3]$$

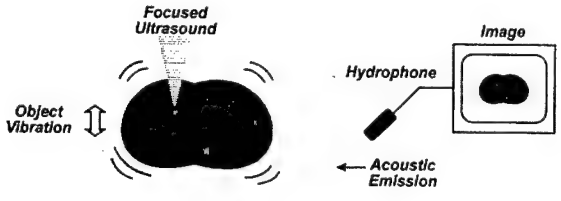

FIG. 1. Principle of ultrasound-stimulated vibro-acoustography.

where P_{ω_0}, $\Delta\omega/2$, and ω_0 are the pressure amplitude, modulating frequency, and center frequency, respectively. In our analysis and experiments, we assume that the condition $\Delta\omega \ll \omega_0$ holds. In such a case, the energy density of the incident field has slow variations in time. To discriminate the slow time variations of a function, let us define the *short-term time average* of an arbitrary function $\xi(t)$ over the interval of T seconds at time instance t, as $\langle \xi(t) \rangle_T = 1/T \int_{t-T/2}^{t+T/2} \xi(\tau) d\tau$, which is a function of t. The long-term time average (or simply the time average) is obtained by setting $T \to \infty$. To compute the short-term time average of the acoustic-energy density relevant to field variations at $\Delta\omega/2$, we choose T longer than the ultrasound wave period but much shorter than the modulation period, that is $2\pi/\omega_0 \ll T \ll 4\pi/\Delta\omega$. Under this condition, the short-term time average of $p^2(t)$ is $\langle p^2(t) \rangle_T = (P_{\omega_0}^2/4)\ (1 + \cos\Delta\omega t)$. The energy density is given by $p^2(t)/\rho c^2$, where ρ and c are the density and propagation speed in the medium (16). We are interested in the time-varying component of the short-term time average of the energy density. Denoting this component by $e_{\Delta\omega}(t)$, we can write: $e_{\Delta\omega}(t) = (P_{\omega_0}^2/4\rho c^2) \cos\Delta\omega t$. This component of the energy density produces a time-varying radiation force on the target (Eq. **1**) at frequency $\Delta\omega$. The amplitude of this force, $F_{\Delta\omega}$, is

$$F_{\Delta\omega} = P_{\omega_0}^2 S d_r / 4\rho c^2. \qquad [4]$$

This equation states that the time-varying force amplitude is proportional to the square of incident ultrasound pressure, or equivalently, to the incident power. If the object moves in response to this force, then the high-frequency ultrasound energy would convert to low-frequency mechanical energy.

Acoustic Emission from a Target Caused by a Dynamic Force. The radiation force $F_{\Delta\omega}$ vibrates the target object at frequency $\Delta\omega$. Object vibration results in an acoustic field in the medium (acoustic emission). This field is related to object shape, size, and viscoelastic properties. To present a conclusive analysis of this relationship, we have to assume an object with specific characteristics. Here we assume that the vibrating object has a circular cross-section of radius b and uniformly vibrates back and forth like a piston. This choice allows us to illustrate the concept in a simple form. We also consider an area $S \leq \pi b^2$ of the piston surface to be projected normally by the beam. Similar solutions can be carried out for other objects.‡

The steady-state normal velocity amplitude of a piston, $U_{\Delta\omega}$, caused by a harmonic force $F_{\Delta\omega}$ at frequency $\Delta\omega$, can be described in terms of the mechanical impedance $Z_{\Delta\omega}$,

$$U_{\Delta\omega} = F_{\Delta\omega}/Z_{\Delta\omega}, \qquad [5]$$

where $Z_{\Delta\omega} = Z'_m + Z_r$ is comprised of the mechanical impedance of the object in vacuum Z'_m, and the radiation impedance of the object Z_r, all defined at $\Delta\omega$. Modeling the object as a mass-spring system, Z'_m can be written in terms of $\Delta\omega$ as (16, 17)

$$Z'_m = R'_m - j(m\Delta\omega - K'/\Delta\omega), \qquad [6]$$

where m, R'_m, and K' are the mass, mechanical resistance, and spring constants of the object, respectively. The radiation impedance of the piston can be written (17) as $Z_r = \pi b^2 (R_r - jX_r)$ **[7]**, where $R_r = \rho c[1 - (c/\Delta\omega b) J_1(c/2\Delta\omega b)]$, **[8]**, and $X_r = (4\rho c/\pi) \int_0^{\pi/2} \sin[(2b\Delta\omega/c)\cos\alpha] \sin^2\alpha d\alpha$ **[9]**, where $J_1(\cdot)$ is the first-order Bessel function of the first kind. In many applications of our interest, the wavelength is much greater than the object size, hence, $(\Delta\omega/c)b \to 0$. In such cases Z_r assumes a simpler form as $Z_r = \pi b^3 \rho \Delta\omega (b\Delta\omega/2c - j8/3\pi)$

‡The theory can be extended to include arbitrary vibrating-part shapes and nonuniform displacement of the object. Nonuniform displacement would be an important issue when the vibration wavelength in the object material is smaller than $2b$.

[10]. The mechanical impedance of the piston object can now be written as

$$Z_{\Delta\omega} = (R'_m + \pi b^2 R_r) - j(m\Delta\omega - K'/\Delta\omega + \pi b^2 X_r)$$
$$\approx (R'_m + \pi\rho b^4 \Delta\omega^2/2c) - j(m\Delta\omega - K'/\Delta\omega + 8\rho b^3\Delta\omega/3), \quad b(\Delta\omega/c) \to 0. \qquad \textbf{[11]}$$

Once we calculate $U_{\Delta\omega}$, we can calculate the pressure field it produces in the medium. We assume that the acoustic emission signal propagates in a free and homogenous medium. The farfield acoustic pressure caused by a piston source of radius b set in a planar boundary of infinite extent is given by (17),

$$P_{\Delta\omega} = -j\Delta\omega\rho \frac{\exp(j\Delta\omega l/c)}{4\pi l}\left[\frac{2J_1[(b\Delta\omega/c)\sin\vartheta]}{(b\Delta\omega/c)\sin\vartheta} \times \frac{\cos\vartheta}{\cos\vartheta + \beta_B}\right] \times (2\pi b^2 U_{\Delta\omega}), \qquad \textbf{[12]}$$

where l is the distance from the observation point to the center of the piston, ϑ is the angle between this line and the piston axis, and β_B is the specific acoustic admittance of the boundary surface.§ The factor of two comes from the presence of the boundary wall, which would be replaced by unity if the boundary wall were not present (16). The acoustic emission field resulting from object vibration can be written in terms of the incident ultrasound pressure by combining Eqs. **4**, **5**, and **12**, as

$$P_{\Delta\omega} = \left\{j\frac{\Delta\omega}{c^2} \times \frac{\exp(j\Delta\omega l/c)}{4\pi l}\left[\frac{2J_1[(b\Delta\omega/c)\sin\vartheta]}{(b\Delta\omega/c)\sin\vartheta} \times \frac{\cos\vartheta}{\cos\vartheta + \beta_B}\right]\right\} \times \{1/[(R'_m + \pi b^2 R_r) - j(m\Delta\omega - K'/\Delta\omega + \pi b^2 X_r)]\}(2\pi b^2) P^2_{\omega_0} S d_r. \qquad \textbf{[13]}$$

For wavelengths long compared to the object size, i.e., when $b\Delta\omega/c \to 0$, the term in the first brace approaches a constant, hence we may consider the contents of the first brace to be an object-independent function (the specific acoustic admittance β_B relates to the surrounding boundary surface). Under these conditions, the first brace in the above equation represents the effect of the medium on the acoustic emission field, which we may call the *medium transfer function*, and denote it by

$$H_{\Delta\omega}(l) = j\frac{\Delta\omega}{c^2} \times \frac{\exp(j\Delta\omega l/c)}{4\pi l}\left[\frac{2J_1[(b\Delta\omega/c)\sin\vartheta]}{(b\Delta\omega/c)\sin\vartheta} \times \frac{\cos\vartheta}{\cos\vartheta + \beta_B}\right]. \qquad \textbf{[14]}$$

The second brace in Eq. **13** is $1/Z_{\Delta\omega}$, or the mechanical admittance of the object at the frequency of the acoustic emission ($\Delta\omega$), and we denote it by $Y_{\Delta\omega}$. It is convenient to combine this term with the next term ($2\pi b^2$) in Eq. **13**, as $Q_{\Delta\omega} = 2\pi b^2 Y_{\Delta\omega} = 2\pi b^2/Z_{\Delta\omega}$, which is the total acoustic outflow by the object per unit force (acoustic outflow is the volume of the medium (e.g., the fluid) in front of the object surface that is displaced per unit time because of object vibration.). Function $Q_{\Delta\omega}$ represents the object characteristics at the acoustic frequency. We may thus rewrite Eq. **13** in a more compact form as

$$P_{\Delta\omega} = H_{\Delta\omega}(l) Q_{\Delta\omega} P^2_{\omega_0} S d_r. \qquad \textbf{[15]}$$

Eq. **15** indicates that the acoustic emission pressure is proportional to: (*i*) the square of ultrasound pressure P_{ω_0}; (*ii*) the ultrasound characteristics of the object, d_r, in the projected area S; (*iii*) the acoustic outflow by this object, $Q_{\Delta\omega}$, representing the object size b and its mechanical admittance at the acoustic frequency, $Y_{\Delta\omega}$; and (*iv*) the transfer function of the medium at the acoustic frequency, $H_{\Delta\omega}(l)$. The above equation illustrates the basic nonlinear relationship between the ultrasound and acoustic emission pressure amplitudes. Note that neither the medium nor the object needs to be nonlinear for this relationship to hold. It is interesting to note that the projection area S and the vibrating area πb^2 play different roles. The projection area determines the extent of the force applied to the object (Eq. **4**). The vibrating area, however, influences the total acoustic outflow in the medium caused by object vibration. The mechanism of object vibration is somewhat analogous to that of a loudspeaker, where the electromotive force is exerted at a small area of the membrane (usually at the center), causing the entire membrane surface to vibrate. In our method, the size of the vibrating area depends on the object structure. For a free suspended point object, smaller than the beam cross-section, the vibrating area would be the same as the projected area. For a large stiff plate, however, the vibrating area could be much larger than the projected area (similar to a loudspeaker). In some cases, it is more convenient to write the acoustic emission field in terms of the applied force $F_{\Delta\omega}$. Referring to Eq. **4**, we can rewrite Eq. **15** as

$$P_{\Delta\omega} = 4\rho c^2 H_{\Delta\omega}(l) Q_{\Delta\omega} F_{\Delta\omega}. \qquad \textbf{[16]}$$

Again in analogy to a loudspeaker, $F_{\Delta\omega}$, $Q_{\Delta\omega}$, and $H_{\Delta\omega}(l)$ represent the electromotive force, dynamic characteristics of the membrane, and propagation medium transfer function.

Beam Forming. To probe an object with the dynamic radiation force at high spatial resolution, it is ideal to confine the dynamic stress field to a very small region in three-dimensional space. We may define the resolution cell of the system as the volume within which the amplitude of the modulated field is high enough to produce a stress field on a target. The purpose of beam forming is to produce a resolution cell as small as possible. An amplitude modulated single-focused beam can provide a resolution cell that is small in diameter but long in depth direction. A superior strategy that can achieve a small resolution cell in all dimensions is to use two unmodulated focused beams at slightly different frequencies and allow them to cross each other at their focal regions. This is accomplished by projecting two coaxial confocal continuous-wave (CW) ultrasound beams on the object. An amplitude-modulated field is produced only at the interference region of the two unmodulated beams around their focal areas, resulting in a small resolution cell. For this purpose, elements of a two-element spherically focused annular array (consisting of a central disc with radius a_1 and an outer ring with the inner radius of a'_2 and outer radius of a_2) are excited by separate CW signals at frequencies $\omega_1 = \omega_0 - \Delta\omega/2$ and $\omega_2 = \omega_0 + \Delta\omega/2$. We assume that the beams are propagating in a lossless medium, in the $+z$ direction of a Cartesian coordinate system (x, y, z), with the joint focal point at $z = 0$. The resultant pressure field on the $z = 0$ plane may be written as

$$p(t) = P_1(r)\cos(\omega_1 t + \psi_1(r)) + P_2(r)\cos(\omega_2 t + \psi_2(r)), \qquad \textbf{[17]}$$

where $r = \sqrt{x^2+y^2}$ is the radial distance. The amplitude functions are (16, 18)

$$P_1(r) = \rho c U_{01}\,(\pi a_1^2/\lambda_1 z_0)\,\mathrm{jinc}(ra_1/\lambda_1 z_0), \qquad \textbf{[18]}$$

and

$$P_2(r) = \rho c U_{02}(\pi/\lambda_2 z_0)\,[a_2^2\,\mathrm{jinc}(ra_2/\lambda_2 z_0) - a_2'^2\,\mathrm{jinc}(ra'_2/\lambda_2 z_0)], \qquad \textbf{[19]}$$

where $\lambda_i = 2\pi/\omega_i$, $i = 1, 2$, is the ultrasound wavelength, U_{0i} is the particle velocity amplitude at the *i-th* transducer element surface, and $\mathrm{jinc}(X) = J_1(2\pi X)/\pi X$. The phase functions,

§The specific acoustic admittance is $\beta_B = \rho c/Z_B$, where Z_B, the acoustic impedance of the boundary, represents the ratio between the pressure and normal fluid velocity at a point on the surface.

$\psi_i(r) = -\pi r^2/\lambda_i z_0$, for $i = 1, 2$, are conveniently set to be zero at the origin.

Now, we define a *unit point target* at position (x_0, y_0) on the focal plane with a drag coefficient distribution as

$$d_r(x, y) = \delta(x - x_0, y - y_0), \quad [20]$$

such that $d_r(x, y)dxdy$ is unity at (x_0, y_0) and zero elsewhere. This equation is merely used as a mathematical model because d_r is physically finite. In this case, the projected area can be considered to be $S = dxdy$. We replace d_rS in Eq. **1** with $d_r(x, y)dxdy$ and follow the steps similar to those outlined in Eqs. **3** and **4** for the pressure field expressed by Eq. **17**, then the complex amplitude of the normal component of the force on the unit point target can be found as

$$F_{\Delta\omega}(x_0, y_0) = \rho U_{01} U_{02} (\pi a_1^2/4\lambda_1 z_0)\,\mathrm{jinc}(r_0 a_1/\lambda_1 z_0)[(\pi a_2^2/\lambda_2 z_0)\,\mathrm{jinc}(r_0 a_2/\lambda_2 z_0) - (\pi a_2'^2/\lambda_2 z_0)\,\mathrm{jinc}(r_0 a_2'/\lambda_2 z_0)]\exp(-jr_0^2\Delta\omega/2cz_0), \quad [21]$$

where the arguments x_0 and y_0 are added to denote the position of the point target and $r_0 = \sqrt{x_0^2 + y_0^2}$. Eq. **21** describes the spatial distribution of the force (the stress field). This equation shows that the stress field is confined to the regions near the beam axis ($r_0 = 0$) and decays as the radial distance r_0 increases. The lateral extent of the stress field, and hence the resolution cell diameter, would be smaller at higher ultrasound frequencies (smaller λ_1 and λ_2). One can calculate the total force on an arbitrary object by integrating the force over the projected area. The axial extent of the resolution cell (depth resolution or the depth of field) can be determined by calculating the force $F_{\Delta\omega}$ as a function of the depth variable, in a fashion as outlined in Eqs. **17** to **21**. For conciseness, we will present only the measured values for the depth resolution in *Results*.

Loss in the propagation path would attenuate both ultrasound beams, thus less radiation force would be generated by the remaining ultrasound energy. In the case of soft tissues, the force attenuation factor is $A(z_0) = \exp[\alpha z_0(\omega_1 + \omega_2)]$, where α is the attenuation coefficient of the tissue. Energy loss in the medium would also result in generation of a separate radiation stress on the medium along the ultrasound paths. However, because the two beams propagate along separate paths in the CW form, they exert mainly steady radiation stresses to the medium, which does not cause object or medium vibrations. Dynamic radiation force is produced only in the interference region around the focal area, which is another advantage of using two unmodulated beams over a modulated single beam.

Image Formation. To produce an image, we scan the object in a plane and record the complex amplitude of the acoustic emission, $P_{\Delta\omega}$, at different positions. In this process, we keep $\Delta\omega$ fixed. For transverse view images, the scan plane is the focal plane (x–y). Alternatively, for the parallel view the scan plane is the x–z plane. In the conventional ultrasound imaging context, these two views are called the C-scan and B-scan, respectively. Our main focus here is the transverse view imaging. In this case, the acoustic emission data obtained by vibrating the object at point (x, y) are assigned to the corresponding point (x, y) in the image.

Before defining the image, we need to define the function that represents the object. Referring to Eq. **15**, the terms that are object dependent are the drag coefficient d_r and the function $Q_{\Delta\omega}$ (assuming that $H_{\Delta\omega}(l)$ is object independent). The object function $g(x, y)$ is thus defined as the spatial distribution of these terms,

$$g(x, y) = Q_{\Delta\omega}(x, y)d_r(x, y). \quad [22]$$

Variables x and y are added to denote the dependency of d_r and $Q_{\Delta\omega}$ on position. In particular, $Q_{\Delta\omega}(x, y)$ implies the total acoustic outflow by the object when unit force is applied at point (x, y).

Commonly, an imaging system is studied through its point-spread function (PSF), which is defined as the image of a point object. To determine the PSF of our system, we consider a unit point target at the origin with unit mechanical response, $Q_{\Delta\omega}(x, y) = 1$. Hence, referring to Eqs. **20** and **22**, we can write $g(x, y) = \delta(x, y)$. To obtain the PSF, we move this point object to every possible position (x_0, y_0) on the $z = 0$ plane and form the image using the resulting acoustic emission field, $P_{\Delta\omega}(x_0, y_0)$. Because x_0 and y_0 are now being treated as variables, we may replace them by variables x and y, respectively. We define the normalized PSF of the coherent imaging system as the complex function

$$h(x, y) = P_{\Delta\omega}(x, y)/P_{\Delta\omega}(0, 0). \quad [23]$$

Division by $P_{\Delta\omega}(0, 0)$ cancels the constant multipliers. Referring to Eqs. **16** and **21**, we can write

$$h(x, y) = (a_2^2 - a_2'^2)^{-1}\,\mathrm{jinc}(ra_1/\lambda_1 z_0)[a_2^2\,\mathrm{jinc}(ra_2/\lambda_2 z_0) - a_2'^2\,\mathrm{jinc}(ra_2'/\lambda_2 z_0)]\exp(-jr^2\Delta\omega/2cz_0). \quad [24]$$

This equation illustrates that the system PSF is a circularly symmetric function with the peak at the origin and decaying amplitude with increasing the radial distance r. Amplitude decays faster for higher ultrasound frequency. This function will be discussed further in the next section.

EXPERIMENTS

The experimental setup is shown in Fig. 2. The confocal transducer is constructed by using a spherical piezoelectric cap. The two elements are constructed by dividing the back electrode of the piezoelectric wafer into a central disc and the outer ring, such that the elements have identical beam axes and focal lengths. Radii of the elements are $a_1 = 14.8$ mm, $a_2 = 22.5$ mm, and $a_2' = 16.8$ mm, and the focal distance is 70 mm. Transducer elements were driven by two stable radio frequency synthesizers [Hewlett–Packard 33120A and Analogic 2045 (Peabody, MA)] at frequencies of $f_0 - \Delta f/2$ and $f_0 + \Delta f/2$, where $f_0 = 3$ MHz, and the value of $\Delta f = \Delta\omega/2\pi$ is stated separately for each experiment. The object was placed at the focal plane of the ultrasound beams in a water tank. Sound produced by the object vibration was detected by an audio hydrophone (International Transducer, Santa Barbara, CA, model 680, sensitivity −154 dB re 1V/μPa) placed within the water tank. The received signal was filtered and amplified by a programmable filter (Stanford Research Sunnyvale, CA, SR650) to reject noise, then digitized by a 12 bits/sample digitizer (Hewlett–Packard E1429A) at a rate sufficiently higher than the Nyquist rate for the particular Δf used. Data were recorded on a computer disc. For coherent imaging, which requires the phase information, the reference signal (i.e., cos $\Delta\omega t$) was obtained by electronic downmixing of the

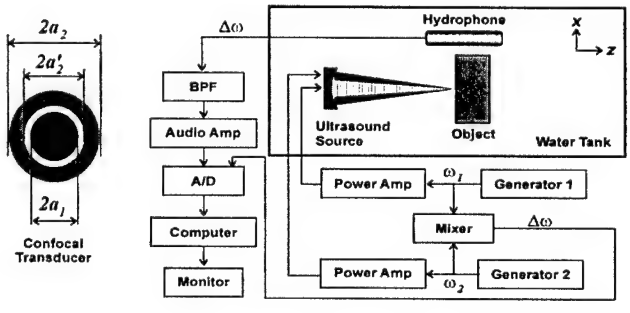

FIG. 2. Ultrasound-stimulated vibro-acoustography system. The confocal ultrasound annular array transducer with two elements is shown on the left.

two driving signals and was recorded along with the hydrophone signal. The relative phase of the acoustic emission data was then calculated at each point by discrete Hilbert transform. We conducted two experiments. The first experiment is designed to verify the relationship between the acoustic emission pressure and the ultrasound pressure (Eq. **15**), and the second is designed to experimentally measure the PSF stated in Eq. **24**. These experiments are presented to prove the principles of the method. Further experiments, illustrating applications of the method for evaluation of object mechanical properties and tissue imaging, are presented in ref. 12.

RESULTS

Acoustic Emission vs. Ultrasound Pressure. Eq. **15** states that the acoustic emission field amplitude is linearly proportional to the square of the incident ultrasound pressure, or equivalently, to the incident power. To test this hypothesis, a calibrated 1-mm-diameter ultrasound needle hydrophone, with its tip facing the ultrasound beam, was used to measure the ultrasound field at the focal point. The tip of the hydrophone also served as an object to generate the acoustic emission. Here, Δf was set at 40 kHz, and the radial distance from the tip of the needle hydrophone to the audio hydrophone was about 65 mm. The result is shown in Fig. 3. The slope of the acoustic emission intensity vs. ultrasonic intensity indicates that the intensity of the acoustic emission field is proportional to the square of the ultrasound intensity, or equivalently, the acoustic emission pressure amplitude is linearly proportional to the ultrasound power, as predicted by Eq. **15**. In another experiment, a 450-μm-diameter glass bead was used as a point object. In this case, Δf was set at either 7 or 40 kHz. The radial distance from the glass bead to the audio hydrophone was about 50 mm. Again, the data indicate a quadratic relationship between the acoustic emission and ultrasonic intensities. These glass-bead data also show that increasing the frequency increases the acoustic intensity. This can be better understood by investigating the theoretical model presented in Eq. **13**. If we assume that the mechanical admittance of the object is approximately constant at these frequencies, then the object behaves almost as a point source, and the acoustic pressure amplitude is proportional to $\Delta\omega$. Hence the acoustic emission intensities $I_{\Delta\omega_1}$ and $I_{\Delta\omega_2}$ at frequencies $\Delta\omega_1$ and $\Delta\omega_2$, respectively, are related by $I_{\Delta\omega_2}/I_{\Delta\omega_1} = (\Delta\omega_2/\Delta\omega_1)^2$. Now, letting $\Delta\omega_1$ and $\Delta\omega_2$ correspond to 7 and 40 kHz, respectively, we can write the intensity ratio as: $[I_{\Delta\omega_2}/I_{\Delta\omega_1}]_{dB} = 20 \log (\Delta\omega_2/\Delta\omega_1) = 15$ dB. The mean value of the intensity ratio calculated from the glass-bead data at 7 and 40 kHz is 16 dB, which is in close agreement with the theoretical result.

PSF Measurement. To demonstrate the image-formation process and support the theoretical derivation of the PSF (Eq. **24**), we evaluated this function experimentally. For this purpose, we used a 380-μm diameter glass bead as a model for a point and placed it on a thin latex sheet. The latex sheet produces only a small change in the incident energy, and hence does not produce significant radiation force or acoustic emission. The entire object was placed in a water tank and the latex

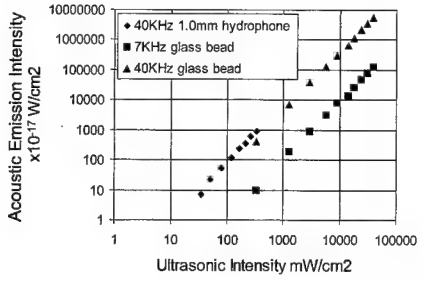

FIG. 3. Acoustic-emission field intensity vs. the combined ultrasound intensity.

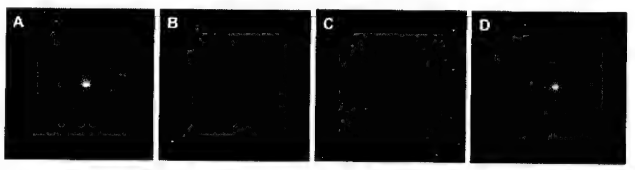

FIG. 4. USVA images of a 380-μm glass bead: (*A*) in-phase, (*B*) quadrature, (*C*) phase, and (*D*) magnitude. The phase in *C* ranges from $-\pi$ radians (black regions) to $+\pi$ radians (white regions), and was normalized to be zero at the center of the glass bead. (Modified with permission from ref. 12, copyright 1998, American Association for the Advancement of Science.)

sheet surface was scanned in a raster format at 0.2-mm increments in either direction at $\Delta f = 7.3$ kHz. The amplitude and phase of the acoustic emission signal were calculated at each point relative to the reference signal data. The phase was normalized to the phase value at the center of the bead. The resulting in-phase, quadrature, phase, and magnitude images are shown in Fig. 4A–D. Transverse image resolution, defined as the -6-dB width of the bead image, is approximately 700 μm for the in-phase image in either dimension (refer to Fig. 5). To compare the experimental results with those of the theory, we calculated the profile of the PSF for the transducer parameters used in this experiment according to Eq. **24**. Fig. 5 shows the theoretical PSF profile and the glass-bead profile obtained from the experiment (in-phase image profile, shifted to center at zero). This figure shows excellent agreement between theory and experiment for amplitudes above 20% of the peak. The experimental data show some background offset about 12% of the peak. We believe that this background offset is caused at least by the following sources: (*i*) acoustic emission by the latex sheet; (*ii*) the background acoustic noise in the experimental setup caused by equipment fans and some structural and building vibrations; (*iii*) nonlinearity of water that can produce a nonlinear mix of the two beams even in the absence of the object; and (*iv*) streaming as a result of energy absorption by water (14), which in turn can vibrate the latex sheet blocking the stream. To evaluate the depth resolution (or the slice thickness), we placed the glass bead on the beam axis and scanned it in the z-direction about the focal point. The depth resolution, defined as the distance between the points where the amplitude of the acoustic emission field drops to -6 dB of its peak, was 9 mm.

DISCUSSION

System Properties. *Spectral characteristics.* In general, USVA images represent object characteristics at two ends of the spectrum: the drag coefficient at the ultrasound frequency and the mechanical admittance at the low acoustic frequency Δf. The ultrasound frequency is usually set at a value suitable to form the beam, whereas Δf can vary in a wide range depending on the application. If the two beams are produced by similar ultrasound transducer elements, then the practical

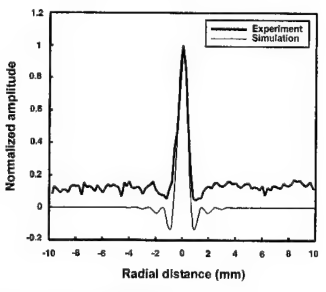

FIG. 5. The theoretical PSF profile of the USVA system according to Eq. **24** and the glass-bead in-phase image profile (Fig. 4*A*) obtained from the experiment.

upper limit for Δf is about equal to the transducer bandwidth. The lower limit of Δf is zero.

Sensitivity. System sensitivity in detecting very small displacements is an important practical issue, especially when the allowable ultrasound power is limited (for example, in medical imaging). Motion measurement with ultrasound pulse echo has been used previously to study "stiffness" of tissues (10). However, the sensitivity of ultrasound pulse echo to motion, at common medical ultrasound frequencies, is limited to several micrometers. An advantage of USVA is its high displacement sensitivity. Cyclic displacement of 100 nm at 10 kHz produces an acoustic intensity of about 3.0×10^{-3} watts/cm^2. Hydrophones similar to the one used in these experiments are sensitive to as little as 10^{-15} watts/cm^2 and therefore are capable of detecting very small cyclic displacements. For instance, the hydrophone detected an acoustic pressure of about 15×10^{-3} Pa at a distance of 5 cm from the glass bead shown in Fig. 4. Under assumptions of isotropic vibration, this pressure would be produced by a similar-sized sphere vibrating with a displacement amplitude of about 6 nm. Sensitivity increases at higher frequencies because the acoustic emission pressure is proportional to frequency for constant mechanical admittance (Eq. **13**).

Comparisons with pulse–echo systems. Some contrasting features of USVA with respect to the conventional ultrasound pulse–echo imaging (B-mode and C-mode) are: (*i*) A pulse–echo image represents object microstructure by displaying its ultrasonic reflectivity distribution. The acoustic emission signal in a USVA system is proportional to the drag coefficient $d_r(x, y)$, which is a local ultrasound parameter, and to the function $Q_{\Delta\omega}(x, y)$, which represents the bulk response of the object at acoustic frequency $\Delta\omega$. Hence, a USVA image, in general, represents both the microstructure and macrostructure of the object. (*ii*) The echo signal in a pulse–echo system is a linear function of the incident ultrasound pressure amplitude and the amplitude reflection coefficient of the object. In USVA, however, the acoustic emission signal is proportional to the ultrasound *power* and the *power* reflection coefficient of the object. (*iii*) Pulse–echo systems are not directly sensitive to medium absorption. Absorption is indicated as relative changes in the amplitude of the echoes resulting from the scatterers within the medium. In a USVA system, the acoustic emission can be produced directly as a result of energy absorption by the medium, even if the medium is homogeneous (refer to Eq. **2**). (*iv*) Pulse–echo systems are generally broadband. The USVA method presented here is basically a narrowband technique. (*v*) Pulse–echo systems achieve high depth resolution by transmitting short wideband pulses. A USVA system gains its depth resolution by tailoring beam geometry to limit the depth of the region where the two beams interfere. A USVA system does not require a wide bandwidth signal to achieve a high depth resolution. (*vi*) The data of USVA images are acquired one point at a time, which resembles the data acquisition in C-mode pulse–echo systems. B-mode pulse–echo systems, however, require much less acquisition time because the data are collected one line at a time.

Applications. USVA promises applications in two general areas: medical imaging and material evaluation.

Medical applications. USVA can be used to image tissues and evaluate their mechanical characteristics. To use USVA for *in vivo* applications, one must take into account limitations such as safe (ultrasound) power limit, tissue attenuation, body noise, and phase aberration. The ultrasound power required to generate a detectable acoustic emission depends on the object, acoustic noise, and receiver sensitivity. Experimental results shown in Fig. 3 demonstrate that ultrasound intensities as low as 30 mW/cm^2 are sufficient to detect the acoustic emission from a 1-mm-diameter object with our hydrophone in the water tank. This power value is much smaller than the FDA limit for safe diagnostic ultrasound applications. Tissue attenuation reduces the ultrasound intensity at the target, and hence the acoustic emission [by the factor $A(z_0)$]. Attenuation limits the usable ultrasound frequency, and hence, lowers the resolution. It also limits the signal-to-noise-ratio (SNR) because of the loss in the acoustic emission energy as a result of ultrasound attenuation by tissue. Direct effect of tissue attenuation on the acoustic emission signal is probably negligible because attenuation of the compressional waves at frequencies in the order of a few kHz in soft tissues is low. Sources of biological noise of the human body include cardiovascular and respiratory systems and muscle movements. Body noise is usually concentrated below 1 KHz and can be filtered out if Δf is above this value. The SNR can be improved by increasing the time duration of the signal recorded at each point (to increase the signal energy) and by using very narrowband filters (to reject the noise), while keeping the ultrasound power within the safe level. Phase aberration in tissue can reduce the sensitivity of the system by decreasing the effective ultrasound energy density at the beam interaction region. One may use known phase aberration correcting methods to reduce such an effect. The practical value of these methods for USVA remains to be studied.

Material evaluation. Another field in which USVA can be potentially useful is material characterization, including mechanical parameter evaluation, imaging, and nondestructive testing of materials. USVA can be used for detection and imaging flaws in materials. Also, one may use USVA to evaluate the mechanical frequency response of an object at low frequencies. In such case, we are interested in determining $Q_{\Delta\omega}(x, y)$ vs. frequency. We assume that the object is uniform within the projected area S. Then, the total radiation force on this object, $\bar{F}_{\Delta\omega}$, can be calculated by integrating $F_{\Delta\omega}(x, y)$ over S. Referring to Eq. **21**, one can show that for $\Delta\omega \ll \omega_0$, $\bar{F}_{\Delta\omega}$ is virtually independent of $\Delta\omega$. If $H_{\Delta\omega}(l)$ is known and nonzero, then the function $Q_{\Delta\omega}(x, y)$ can be estimated using Eq. **16** as $Q_{\Delta\omega}(x, y) = P_{\Delta\omega}(x, y)/\bar{F}_{\Delta\omega}H_{\Delta\omega}(l)$. In practice, $P_{\Delta\omega}(x, y)$ is obtained by sweeping $\Delta\omega$ in the range of interest and recording the resulting acoustic emission (12).

This work was supported in part by grant DAMD17-98-1-8121 from the Army Medical Research and Materiel Command. The authors thank R. R. Kinnick, T. Kinter, E. C. Quarve, and J. M. Patterson for their support.

1. Maynard, J. (1996) *Phys. Today* **49**(1), 26–31.
2. O'Donnell, M., Skovoroda, A. R., Shapo, B. M. & Emelianov, S. Y. (1994) *IEEE Trans. Ultrason. Ferroelectr. Freq. Contr.* **41,** 314–325.
3. Ophir, J., Cespedes, I., Ponnenkanti, H., Yazdi, Y. & Li, X. (1991) *Ultrason. Imaging* **13,** 111–134.
4. Yamakoshi, Y., Sato, J. & Sato, T. (1990) *IEEE Trans. Ultrason. Ferroelectr. Freq. Contr.* **47,** 45–53.
5. Krouskop, T. A., Dougherty, D. R. & Vinson, F. S. (1987) *J. Rehabil. Res. Dev.* **24,** 1–8.
6. Lerner, R. M., Huang, S. R. & Parker, K. J. (1990) *Ultrasound Med. Biol.* **16,** 231–239.
7. Alam, S. K., Richards, D. W. & Parker, K. J. (1994) *Ultrasound Med. Biol.* **20,** 751–758.
8. Gao, L., Parker, K. J., Lerner, R. M. & Levinson, S. F. (1996) *Ultrasound Med. Biol.* **22**(8), 959–977.
9. Muthupillai, R., Lomas, D. J., Rossman, P. J., Greenleaf, J. F., Manduca, A. & Ehman, R. L. (1995) *Science* **269,** 1854–1857.
10. Sugimoto, T., Ueha, S. & Itoh, K. (1990) *Ultrason. Symp. Proc.*, 1377–1380.
11. Sarvazyan, A. P., Rudenko, O. V., Swanson, S. D., Fowlkes, J. B. & Emelianov, S. Y. (1998) *Ultrasound Med. Biol.* **24,** 1419–1435.
12. Fatemi, M. & Greenleaf, J. F. (1998) *Science* **280,** 82–85.
13. Beyer, R. T. (1978) *J. Acoust. Soc. Am.* **63**(4), 1025–1030.
14. Westervelt, P. J. (1951) *J. Acoust. Soc. Am.* **23**(4), 312–315.
15. Greenspan, M., Breckenridge, F. R. & Tschiegg, C. E. (1978) *J. Acoust. Soc. Am.* **63**(4), 1031–1038.
16. Morse, P. M. & Ingard, K. U. (1968) *Theoretical Acoustics* (McGraw–Hill, New York).
17. Morse, P. M. (1981) *Vibration and Sound* (The Acoustical Society of America, Woodbury, NY), 3rd Ed.
18. Kino, G. S. (1987) *Acoustics Waves: Devices, Imaging, and Analog Signal Processing* (Prentice–Hall Signal Processing Series, Englewood Cliffs, NJ).

Reprint Series
3 April 1998, Volume 280, pp. 82–85

SCIENCE

Ultrasound-Stimulated Vibro-Acoustic Spectrography

Mostafa Fatemi and James F. Greenleaf

Ultrasound-Stimulated Vibro-Acoustic Spectrography

Mostafa Fatemi and James F. Greenleaf

An ultrasound method based on radiation force is presented for imaging the acoustic response of a material to mechanical excitation. Acoustic energy was emitted from solids and tissues in response to an oscillatory radiation force produced by interfering focused beams of ultrasound. Frequency spectra of ultrasound-stimulated acoustic emission exhibited object resonances. Raster-scanning the radiation force over the object and recording the amplitude and phase of the emitted sound resulted in data from which images related to the elastic compositions of the acoustically emitting objects could be computed. Acoustic emission signals distinguished tuning-fork resonances, submillimeter glass spheres, and calcification in excised arteries and detected object motions on the order of nanometers.

The mechanical response of objects to external forces is of considerable interest in medical diagnosis, nondestructive inspection of materials, and materials science. An applied force is often used to produce displacement from which elastic constants, like spring constants, can be determined. In resonant ultrasound spectroscopy, an ultrasound source and a detector are used to measure the resonance frequencies of a sample with known size and mass. The resonances are related to mechanical parameters, including the elastic constants of the material (*1*). Recently, a magnetic resonance elastography method for quantitatively measuring the displacement of tissues in response to externally applied cyclic forces was reported by Muthupillai *et al.* (*2*). The method resulted in high-resolution images of the shear modulus of normal and pathologic tissues. Others have used ultrasound to measure tissue displacement associated with externally applied compressive and cyclic forces (*3*).

We describe an imaging technique that uses acoustic emission to map the mechanical response of an object to local cyclic radiation forces produced by interfering ultrasound beams. Radiation force is generated by changes in the energy density of an acoustic field (*4*). For instance, a collimated ultrasound beam impinging normally on the surface of an object of arbitrary shape and boundary impedance will produce a radiation force. The radiation force arising from this interaction has a component $F = d_r s\langle E\rangle$ (*5*) in the beam direction. This component is proportional to the time-average energy density of the incident wave $\langle E\rangle$, the projected area of the object s, and d_r (*6*), the scattering and absorbing properties of the object.

We probe the object by arranging the intersection of two focused continuous-wave (CW) ultrasound beams of different frequencies at a selected point on the object. Interference in the intersection region of the two beams produces sinusoidal modulation of the ultrasound energy density. Modulation of the energy density creates an oscillatory force, effectively vibrating the object at the selected region. The resulting vibration of the object produces an acoustic field [acoustic emission (*7*)] that can be measured some distance away.

Ultrasound beams can be constructed in a variety of ways for this purpose (*8*). We used two coaxial, confocal transducer elements of a spherically focused annular array (consisting of a central disc and an outer annulus) driven by two CW signals at slightly different frequencies ω_1 and ω_2 (Fig. 1). The energy density at a point in this ultrasound field, say at the focus, is proportional to the square of the sum of the ultrasound fields from the two elements. Squaring the sum of two sines gives rise to sum and difference frequency terms. Thus, high-frequency and low-frequency variations in energy density result at the intersection of the two beams produced by the two elements. Ultrasound-stimulated acoustic emission results from the energy term that produces a low-frequency vibration. The low-frequency force on a target at the focal point can be computed by

$$F_l(t) = d_r \iint_S \langle E_{\text{focal}}(t,x,y)\rangle_T \, dx\,dy$$

$$= Cd_r \cos(\Delta\omega t) \qquad (1)$$

where C is a constant, $\Delta\omega = |\omega_1 - \omega_2|$, S is the area over which $E_{\text{focal}}(t,x,y)$, the total energy density in the focal plane, has significant value, and $\langle\rangle_T$ represents a short-term time average (*9*). For focused beams, the intersection region can be small enough that $F_l(t)$ can be considered to be an oscillating point force applied to the object at the focal intersection of the beams.

To produce an ultrasound-stimulated vibro-acoustic spectrogram, we vibrate a small region of the object with an oscillating radiation force of varying frequency. The complex amplitude of the resulting acoustic emission field is

$$\Phi(\Delta\omega) = Cd_r H(\Delta\omega)Q(\Delta\omega) \qquad (2)$$

where $Q(\Delta\omega)$ is a complex function representing the mechanical frequency response, or admittance, of the object at the selected point, and $H(\Delta\omega)$ represents the combined frequency response, or transfer function, of the propagation medium and receiver and is assumed to be fixed and known (*10*). Recording $\Phi(\Delta\omega)$ allows us to obtain $Q(\Delta\omega)$ for each point within a constant multiplier (*11*). We raster-scan the radiation force over the object to produce data, which can

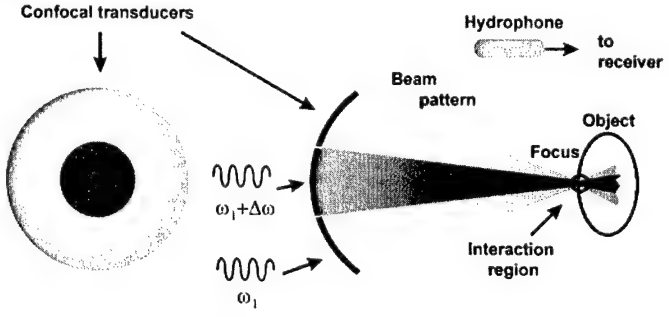

Fig. 1. Experimental system for ultrasound-stimulated vibro-acoustic spectrography: a two-element confocal ultrasound annular array transducer, consisting of a center disc and an outer ring. The elements are driven by two CW sources, at frequencies equal to ω_1 and $\omega_2 = \omega_1 + \Delta\omega$, where these frequencies are very close to the central frequency of the elements, and $\Delta\omega$ is much smaller than (<1%) the center frequency of the ultrasound transducer. The beams interact only in a small region around the joint focal point, where the amplitude of the field oscillates at the difference frequency $\Delta\omega$. The region of interest is placed at the joint focal point and is probed point-by-point by raster scanning. The sound field resulting from object vibrations at each position is received by a hydrophone and recorded. The recorded signal at one or more difference frequencies is used to form an image of the object. The experiments were conducted in a water tank. The transducer center frequency was 3 MHz; its outer diameter was 45 mm; and it was focused at 70 mm. The difference frequencies used in each experiment are mentioned in the corresponding legends.

Ultrasound Research, Department of Physiology and Biophysics, Mayo Clinic and Mayo Foundation, Rochester, MN 55905, USA.

be mapped into a pictorial format. The spatial resolution of the resulting image is determined by the region in which significant interference between the ultrasound beams occurs and is of the order of a few wavelengths at the ultrasound frequency.

Experiments were conducted in a water tank, which provided good ultrasonic and acoustic coupling to the object and freedom of movement for the prototype scanner mechanism (Fig. 1). The two-element confocal ultrasound transducer array was positioned such that the beams interfered at the selected region of the object. Sound produced by vibrations of the object is approximately omnidirectional because of the small size of the vibrating portion of the object compared with the wavelength. This sound was detected by a submerged hydrophone placed near the object within the water tank.

To test the hypothesis that ultrasound-stimulated acoustic emission is sensitive to object mechanical properties and to show how such properties can be quantitatively evaluated by this method, we produced an ultrasound-stimulated vibro-acoustic spectrogram of a tuning fork immersed in isopropyl alcohol at two different temperatures. We aimed the focal point of the confocal transducer at a fixed position on one of the tines. The shear viscosity of alcohol changes with temperature, causing a slight, but detectable, shift in the spectrogram (Fig. 2). The shear viscosity η of a liquid is determined by measuring the resonant frequency f_R and the bandwidth δf_R of a tuning fork immersed in this liquid (12)

$$\eta = \frac{\kappa f_R}{\rho}\left(\frac{\delta f_R}{f_R} - \frac{\delta f_{R0}}{f_{R0}}\right)^2 \qquad (3)$$

where f_{R0} and δf_{R0} are the resonant frequency and bandwidth measured in vacuum, respectively, and ρ is the liquid density. The constant κ is determined experimentally. The measured values for f_R and δf_R were 1769 and 5.76 Hz at 15°C and 1765.7 and 4.53 Hz at 30°C. The viscosity of isopropyl alcohol is reported to be 2.89 cP (1 centipoise = 1 mPa·s) at 15°C (*13*). From this value, the constant κ was calculated. The shear viscosity at 30°C was found using Eq. 3 to be η = 1.77 cP, which is the same as the published data (*13*).

We tested the ability of ultrasonically stimulated vibro-acoustic spectrography to image the frequency response of different objects with identical d_r by scanning three tuning forks with different resonant frequencies. A color acoustic spectrogram was obtained by sweeping the frequency of the radiation force, $\Delta\omega$, in a range covering the resonant frequencies of all forks at each beam position. The acoustic emission signal was filtered by three bandpass filters centered at different frequencies. The outputs of these filters were used to form a three-color composite image (Fig. 3). The forks appear with three distinct colors because each fork responds primarily at its own resonant frequency. Because the forks were made from identical materials, other ultrasound imaging methods would not be capable of distinguishing these objects.

We tested the hypothesis that the amplitude of acoustic emission at a single frequency can be used to detect small, highly reflective isolated objects. We scanned a 380-μm-diameter glass bead placed on a thin latex sheet and recorded the amplitude of acoustic emission (Fig. 4). The latex sheet produces only a small change in the incident energy because it is almost transparent to the ultrasound beam. This experiment demonstrated the ability of the method to detect isolated regions of hardness with respect to a soft background.

To test the feasibility of using the technique to image mechanical properties of tissues, we measured the phase and amplitude of acoustic emission from calcified and noncalcified excised human iliac arteries. The arteries were scanned in a plane perpendicular to the ultrasound beam axis.

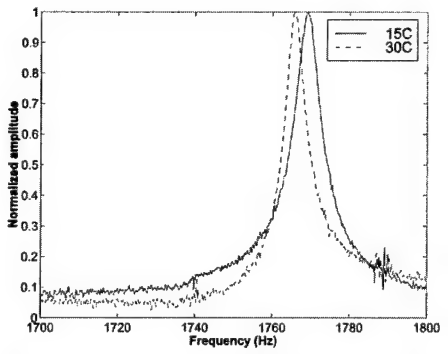

Fig. 2. Vibro-acoustic spectrograms of a tuning fork immersed in isopropyl alcohol at two different temperatures. A point on a tine of the fork was vibrated with the use of the system shown in Fig. 1. The difference frequency was swept from 1600 to 2000 Hz. A change of temperature from 15° to 30°C decreases the shear viscosity of the alcohol, which, in turn, changes the resonance frequency and bandwidth of the tuning fork.

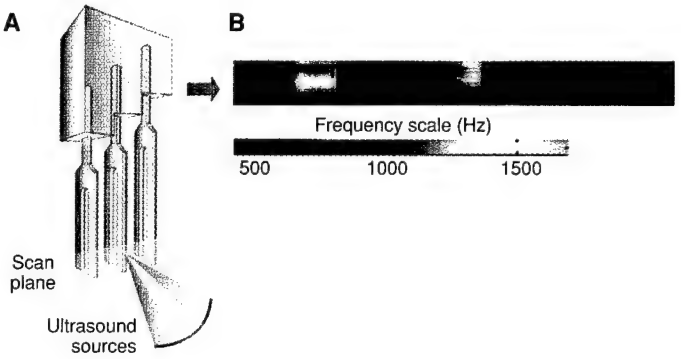

Fig. 3. Vibro-acoustic spectrogram of tuning forks. (**A**) Three tuning forks made from identical material with identical tine cross sections (lengths are different). Resonance frequencies in water are 407 Hz (right), 809 Hz (middle), and 1709 Hz (left). The forks were scanned in a water tank with the use of the system shown in Fig.1. The scanning plane covers the front tines at the bottom part of the forks. At each position, the difference frequency was swept from 250 to 2250 Hz. The ultrasound-stimulated acoustic emission was detected with the hydrophone and filtered by three overlapping bandpass filters with frequencies centered at 500, 1000, and 1500 kHz, respectively. (**B**) Color acoustic spectrogram of the forks. The outputs of the bandpass filters were used to produce the red, green, and blue image components. This image displays two characteristics of the object: shape and frequency response. The color associated with each fork indicates its resonance frequency, which can be deduced from the frequency scale.

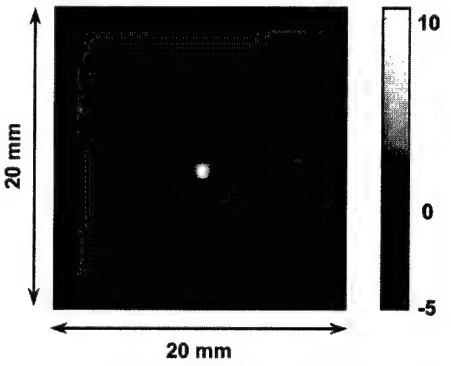

Fig. 4. Image of ultrasonically stimulated acoustic emission amplitude from a 380-μm-diameter glass bead placed on a thin latex sheet. The latex surface was scanned at 0.2-mm increments in each direction. The difference frequency was fixed at 7.3 kHz. The amplitude of the acoustic emission of the bead (in relative units) is shown in gray scale. The latex sheet is almost transparent to the imaging system. The glass bead, however, presents a large acoustic impedance discontinuity, resulting in significant oscillatory radiation force. The magnitude of the radiation force gives rise to large-amplitude acoustic emission, thus yielding a high-contrast image of the bead. The image reveals a system resolution of about 700 μm. The confocal beam geometry leads to a negative-amplitude ring around the bright, positive central spot. This effect produces edge enhancement, as seen on artery walls in Fig. 5.

Calcifications within the arteries produced distinctive amplitude and phase values when compared to the normal arterial walls (Fig. 5). The phase of the oscillation of driven mechanical systems relative to the driving force depends on the ratio of mass to stiffness (*14*). Calcified regions of the diseased artery, identified by an x-ray of the sample, produced phase shifts in acoustic emission completely different from that of the noncalcified, and thus softer or less dense, regions. The amplitude images are highly detailed and exhibit variations in acoustic emission from both calcified and uncalcified regions of the diseased artery. These differences are caused by variations in the product of the reflection properties d_r and the effective mechanical vibration admittance properties $Q(\Delta\omega)$ of the tissue. Thus, vibro-acoustic spectrography is similar to conventional pulse-echo ultrasound imaging, which is sensitive to the ultrasonic parameters of the object, but has the advantage of also being sensitive to the mechanical admittance $Q(\Delta\omega)$ at low frequencies.

Motion induced by ultrasound and measured with ultrasound pulse echo has been used previously to study "hardness" (*15*). However, the sensitivity of ultrasound pulse echo to motion at common ultrasound frequencies is limited to several micrometers. The advantage of ultrasound-stimulated vibro-acoustic emission is its high displacement sensitivity. Cyclic displacement of 100 nm at 10 kHz produces an acoustic intensity of about 3.0×10^{-3} W/cm^2. Hydrophones similar to the one used in these experiments are sensitive to as little as 10^{-15} W/cm^2 and, therefore, can detect very small cyclic displacements. For example, the hydrophone detected an acoustic pressure of about 15×10^{-3} Pa at a distance of 5 cm from the glass bead shown in Fig. 4. Under the assumption of isotropic vibration, this pressure would be produced by a similarly sized sphere vibrating with a displacement amplitude of about 6 nm. The method will be more sensitive for higher frequency sound because acoustic power is proportional to the square of frequency for constant displacement amplitude. The practical upper limits for the difference frequency produced with modern ultrasound transducers is about equal to their bandwidth. For modern transducers, this value is 80% or more of the central frequency of the transducer. For experiments like those we conducted, emission frequency well in excess of 1 MHz could be produced. The lower limit on the frequency of radiation pressure is zero, that is, static pressure.

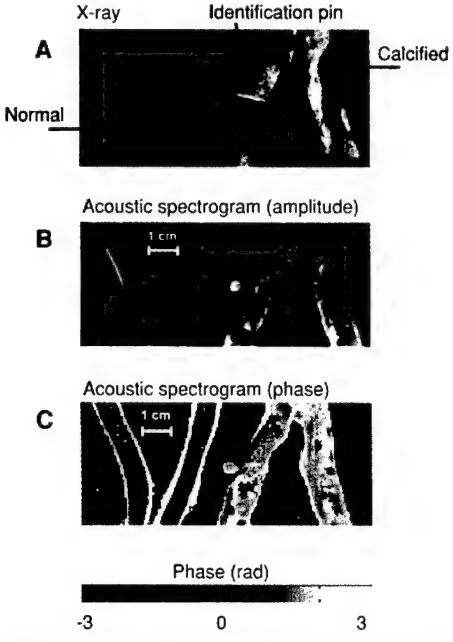

Fig. 5. Vibro-acoustic spectrography of excised human iliac arteries. (**A**) X-ray image of normal (left) and calcified (right) excised human iliac arteries obtained from a 35-year-old woman and a 67-year-old man, respectively. Bright areas indicate calcifications. (**B**) Vibro-acoustic spectrogram amplitude image at a fixed difference frequency of 6 kHz. Calcification details appear bright, whereas the arterial walls are dim. (**C**) Phase image. Calcified regions produce acoustic emission of different phase with respect to regions of the tissue having little calcification, as indicated by the x-ray.

Ultrasound-stimulated vibro-acoustic spectrography has potential applications in at least two general areas. The first is nondestructive evaluation of materials, where material characteristics and structural flaws can be identified by measuring changes in the mechanical response to vibration at a point. The object under test could be remotely vibrated, for instance, by beams propagating and interfering in either water or air, or beams propagating within the object could be used to produce acoustic emission from flaws. For medical imaging and detection, the technique appears particularly suitable for noninvasive detection of hard tissue inclusions, such as the imaging of arteries with calcification, detection of breast microcalcifications, visualization of hard tumors, and detection of foreign objects. The stiffness of soft tissues is related to their composition (for example, relative values of fibrotic content), and its change is often related to pathology or therapy. In conventional palpation, physicians estimate tissue stiffness by feeling with the fingers. Because changes of stiffness alter the vibration frequency response or damping of tissue, the present method can potentially provide a noninvasive, remote, high-resolution "palpation" technique that can reach small abnormalities that are otherwise untouchable by conventional methods.

REFERENCES AND NOTES

1. J. Maynard, *Phys. Today* **49**, 26 (January 1996).
2. R. Muthupillai *et al.*, *Science* **269**, 1854 (1995).
3. For a review of elasticity imaging methods, see L. Gao, K. J. Parker, R. M. Lerner, S. F. Levinson, *Ultrasound Med. Biol.* **22**, 959 (1996).
4. The study of radiation force and radiation pressure dates back nearly one century, to the time of Rayleigh [Lord Rayleigh, *Philos. Mag.* **3**, 338 (1902); *ibid.* **10**, 364 (1905)]. More recent analysis of the theory and explanation of the physical significance of the mathematics can be found in G. R. Torr, *Am. J. Phys.* **52**, 402 (1984). Critical and historical reviews on radiation force and radiation pressure are presented in B-T. Chu and R. E. Apfel, *J. Acoust. Soc. Am.* **72**, 1673 (1982) and R. E. Beyer, *ibid.* **63**, 1025 (1978). Some recent analysis of radiation force and pressure in attenuating medium (which may be applicable to biological tissues) are presented in O. V. Rudenko, A. P. Sarvazyan, S. Y. Emelianov, *J. Acoust. Soc. Am.* **99**, 2791 (1996) and Z.-Y. Jiang and J. F. Greenleaf, *ibid.* **100**, 741 (1996).
5. P. J. Westervelt, *J. Acoust. Soc. Am.* **23**, 312 (1951).
6. The complex drag coefficient due to radiation pressure is defined for unit energy density of the incident wave and can be written as (*5*)

$$d_r = \frac{1}{S}(\Pi_a + \Pi_s - \int\gamma\cos\beta dS) - \frac{j}{S}\int\gamma\sin\beta dS \quad (4)$$

where Π_a and Π_s are the total absorbed and scattered powers, respectively; γ is the scattered intensity (π_a, π_s, and γ are expressed per unit incident intensity); β is the angle between the incident and scattered intensities; s is the projected area of the object; and dS is the area element. The real and imaginary parts represent the components of the force parallel and perpendicular to, respectively, the incident field momentum. In our treatment, we assume a planar object normal to the beam axis; hence, d_r is real, and the force has only a normal component to the object surface.
7. The term "acoustic emission" is used here to describe the acoustic field in response to a cyclic vibration of the object and should not be confused with similar terminology used in the field of nondestructive testing of materials or in opto-acoustic imaging context, where it is used to describe the acoustic field resulting from structural deformation, cracking, or thermal expansion of the object. We note a fundamental difference between the method we present and that of opto-acoustic imaging. In ultrasound-stimulated vibro-acoustic spectrography, the ultrasound energy is converted directly to low-frequency acoustic energy by the object, whereas the opto-acoustic method relies on the conversion of light energy to heat, causing acoustic emission in response to rapid thermal expansion of the object.
8. Modulation of a single beam with the use of a focused transducer driven by an amplitude-modulated signal results in a field that is not spatially confined, producing a radiation force on any object (including the transducer itself) that happens to be in the beam path. The use of two single-frequency beams is advantageous because field modulation occurs only in a confined region, the size of which is controlled by the intersection of the two beams.
9. We define the short-term time average of an arbitrary function of time $f(t)$ around time instance t as

$$\langle f(t)\rangle_T = \frac{1}{T}\int_{-T/2}^{T/2} f(\tau - t)d\tau \quad (5)$$

The long-term time average is obtained when $T \to \infty$. To compute the short-term time average of the acoustic energy density relevant to acoustic emission at $\Delta\omega$, we choose T longer than the ultrasound wave period but much shorter than the acoustic wave period, that is, $2\pi/\omega_2 \ll T \ll 2\pi/\Delta\omega$.
10. In Eq. 2, $H(\Delta\omega)$ can be position-invariant if the geometry of the propagation medium remains unchanged during the scan. In our experiments, we minimized position dependency by fixing the position of the transducer relative to the hydrophone and moving, instead, the object in raster-scanning motion.
11. Changing $\Delta\omega$ by shifting the frequency of the ultrasound

beams does not change the beam amplitude because $\Delta\omega$ is a small fraction of the bandwidth of typical ultrasound transducers. For instance, the bandwidth of the ultrasound transducer may be greater than 1 MHz, whereas $\Delta\omega$ might be around 10 kHz.
12. M. R. Fisch, R. P. Moeller, E. F. Carome, *J. Acoust. Soc. Am.* **60**, 623 (1976).
13. D. R. Lide, Ed., *CRC Handbook of Chemistry and Physics* (CRC Press, Boca Raton, FL, ed. 72, 1991), pp. 6–158.
14. P. M. Morse and K. U. Ingard, *Theoretical Acoustics* (McGraw-Hill, New York, 1968).
15. T. Sugimoto, S. Ueha, K. Itoh, in *1990 IEEE Ultrasonics Symposium Proceedings*, B. R. McAvoy, Ed. (Institute of Electrical and Electronic Engineers, New York, 1990), vol. 3, p. 1377.

10 November 1997; accepted 17 February 1998

BMUS Bulletin (British Medical Ultrasound Society), 8(4), pp 16 and 18, Nov 2000

Imaging and Evaluating the Elastic Properties of Biological Tissues

M Fatemi, JF Greenleaf

Department of Physiology and Biophysics, Mayo Clinic and Mayo Foundation, Rochester, MN, USA

Introduction

A common approach for evaluating some of the characteristics of an object is listening to the sound that object makes. This approach is used for many purposes in our daily life. Evaluating the quality of a crystal glass by tapping a finger on it is a simple example. Plucking a violin string to adjust the tuning is another.

It is well known that changes in elasticity of soft tissues are often related to pathology. Physicians traditionally use sound as a diagnostic tool, for example, by tapping on the patient's body. Vibro-acoustography implements the same concept but in micro-scale, and in a way that can be applied to living tissues. This method uses a small point-like tapping force that vibrates a region within the body, while a sensitive microphone is used to listen to the "sound" of the vibrating region.

In analogy to the sound of the crystal glass, sound from the body carries some information about the structure and the material properties of the region in the body. For example, the loudness of the sound may indicate the hardness of the body region being vibrated. Also, regions with different elasticity may respond differently at different frequencies. Sound from body vibrations can be used to produce an image of the body. To do this, the point-like tapping force is moved across the region of interest in a raster motion, and the sound emitted from each point is used to determine the brightness of the corresponding point on the image display system. The result is a display of elastic properties of the region of interest.

In this paper, we first describe how vibro-acoustography works, then present results of some experiments on biological tissues.

Vibro-acoustography

Vibro-acoustography produces a map of the mechanical response of an object to a dynamic force applied at each point. The method utilizes ultrasound radiation force to remotely exert a localized force (a force that is confined to a small region) at a desired frequency within (or on the surface of) an object, and records the resultant acoustic response[1,2]. This acoustic response, which is normally at low kHz range, is a function of the viscoelastic properties of the object and can be used to produce an image of the object[3].

Before introducing the system, we shall briefly discuss the phenomenon of the radiation force. The phenomenon of acoustic radiation force and radiation pressure has been studied for a century[4,5]. The acoustic radiation force is an example of a universal phenomenon in any wave motion that introduces some type of unidirectional force on absorbing or reflecting targets in the wave path. For example, the radiation force of sunlight pushes the tail of comets away from the sun. Similarly, a sound wave can produce the radiation force on objects it interacts with. Vibro-acoustography utilizes an oscillating radiation force of ultrasound to vibrate the tissue, and consequently, produce an acoustic emission from the object. To produce an oscillating radiation force the intensity of the incident ultrasound must be amplitude modulated at the desired low frequencies. Using a single amplitude modulated beam seems to be the simplest means to attain this purpose. However, such a beam will exert a radiation force on any object that is present along the beam path, producing undesirable acoustic emission. To confine oscillations of the radiation stress to the desired region, vibro-acoustography uses two unmodulated continuous wave beams at slightly different frequencies, propagating along separate paths. The beams are arranged to cross each other at their respective foci, and thus produce a modulated field at a confined, small, cross over region. This beam produces a force, oscillating at the difference frequency, on any object located at the focal region.

Figure (1) illustrates a vibro-acoustography system. The elements of a two-element annular array transducer are driven by two continuous wave signals at frequencies f_1 and f_2. The object to be imaged is placed at the joint focal plane of the transducer elements (the scanning plane). The ultrasound field produces a localized radiation stress at the focal point on the object at frequency $f_2 - f_1$. Depending on the elastic properties of the object, the radiation force may cause a portion of the object, or the entire object, to vibrate at this frequency. The acoustic emission resulting from object vibration is received by a hydrophone (or microphone) that is located nearby. Normally, the wavelength of the vibration is large compared to the object size, hence the acoustic emission field is almost omnidirectional. Therefore, hydrophone position is not a critical parameter in this measurement. The filter is used to eliminate noise and other interfering signals. To form an image, the focal point of the transducer is moved across the scanning plane within the object in a raster pattern. The acoustic emission is received at each position, and an image is formed by displaying the amplitude (or phase) of such signals at corresponding positions on the image plane. The spatial resolution of this imaging method is determined by the ultrasound beamwidth at the focal plane, which is normally comparable to the incident ultrasound wavelength.

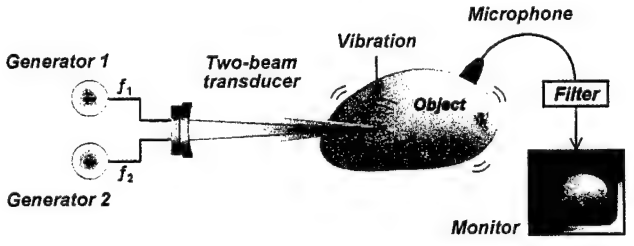

Fig. 1. Vibro-acoustography system. The object is vibrated by the radiation force of the confocal, two-beam transducer. Resulting vibrations are detected by the microphone (or hydrophone) and mapped into the image.

Experiments

In medical applications, one can use vibro-acoustography to obtain images of the human body for diagnostic purposes. To demonstrate the capability of vibro-acoustography, we used this method to image a specimen of human iliac artery that included calcifications. A 3 MHz transducer, with a diameter of 45mm and focal length of 70mm, was used for this experiment. The difference frequency was set at 44 kHz (this is also the frequency of object vibrations). Figure (2a) shows a photo of the artery that is cut open. The areas with calcification are marked

by letter "C". The vibro-acoustic image of the same artery is shown in Fig. (2b). Calcium deposits are formed in large plates, ranging in size from a few mm to a few cm. Such calcium plates, which are much stiffer than the arterial wall, constitute efficient acoustic radiators and can produce a strong acoustic field when vibrated by the radiation force of the incident ultrasound, allowing the calcified regions to stand out in the vibro-acoustography image.

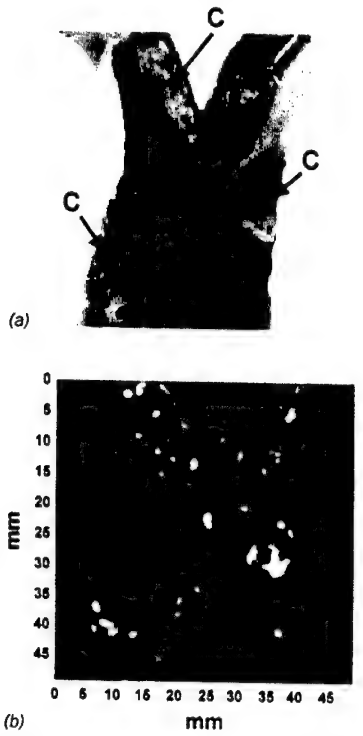

Fig. 2. Vibro-acoustic image of an ex-vivo human iliac artery near the bifurcation. On the left (a) is a photo of the cut-open artery specimen. Calcified areas are marked with letter "C". Vibro-acoustic image of the specimen is shown on the right (b). Calcified areas stand out as bright spots. This image was obtained with a 3 MHz confocal transducer as described in the text. The difference frequency was set at 44 kHz. The gray-level scale is in arbitrary units. (Reproduced with permission from Reference 6)

The next example illustrates detection of micro-calcifications in breast tissue. Figure (3a) shows a photograph of a piece of human breast tissue collected from a 57-year-old subject. Two small sutures are knotted on the tissue for identification purpose. Figure (3b) shows the x-ray mammogram of this tissue piece. The sutures are barely visible in this mammogram. This sample was scanned by a vibro-acoustography system similar to the one used in the previous experiment. The resulting vibro-acoustic image of the tissue at 25 kHz is shown in Fig. (3c). Micro-calcifications can be seen in this image as bright spots. It is interesting to note that the number and position of micro-calcifications matches with the corresponding spots in the x-ray mammogram. Also noticeable is that tissue inhomogeneities appear dim and do not interfere with calcification in the acoustic image. Sutures are also visible in the vibro-acoustic image, apparently because they contain entrapped gas.

The above experimental results show that vibro-acoustography can be used for high-quality imaging. The spatial resolution is comparable to the ultrasound beamwidth at the focal region. For example, for the 3 MHz ultrasound transducer used in the experiments, the spatial resolution is about 700 μm. These results also show that vibro-acoustic images have high signal-to-noise ratio and no speckle. These features allow vibro-acoustography to delineate calcium deposits with high definition and contrast.

In summary, elastic properties of tissue appear to be closely related to tissue pathology. These properties also relate to our perception of how the tissue feels. Therefore, they are readily understandable by the physician. The value of the information on elastic properties of tissue cannot be overemphasized. Methods aimed at imaging or evaluating elastic features of tissue promise a new era in diagnostic imaging.

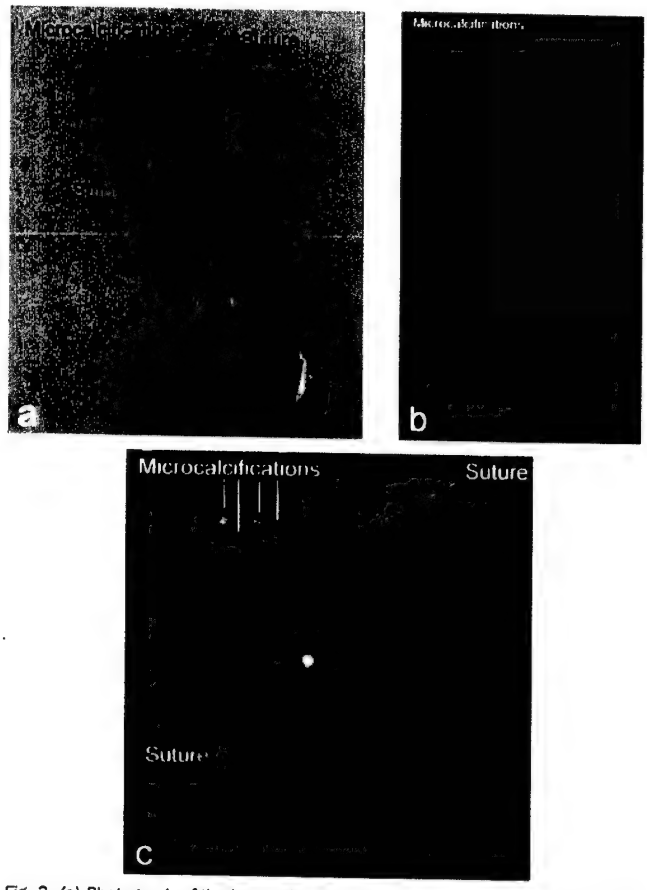

Fig. 3. (a) Photograph of the breast tissue sample. Micro-calcifications are located at the top left corner of the sample (indicated by the arrow). Two sutures are knotted on the tissue as indicators. (b) Tissue x-ray mammogram of the tissue sample. This sample includes four small micro-calcifications at the top left corner. The brightness of the image has been reduced to make the micro-calcifications stand out from the high density tissue at the top left corner of the sample. As a result, most of the tissue is not visible in the x-ray image, except for the calcified region and some bright irregular regions (containing no calcification) at the center. (c) Vibro-acoustic image of the sample in (a) and (b). This image clearly shows four micro-calcifications as bright spots at the top left corner of the tissue sample. The two sutures are also indicated in the image. The location of micro-calcifications shown here matches well with those shown in the x-ray mammogram.

Acknowledgments

This work was supported in part by grant BC971878 from the Army Medical Research and Materiel Command and grant HL 61451 from the National Institutes of Health.

References

1. Fatemi M, Greenleaf JF: Ultrasound-stimulated vibro-acoustic spectrography. Science 1998; 280:82-85.
2. Fatemi M, Greenleaf JF: Vibro-acoustography: An imaging modality based on ultrasound-stimulated acoustic emission. Proc Natl Acad Sci USA (PNAS) 1999; 96:6603-6608.
3. Fatemi M, Greenleaf JF. Probing the dynamics of tissues by the radiation force of ultrasound. Phys Med Biol 2000; 45:1449-1464.
4. Beyer RT: Radiation pressure - the history of a mislabeled tensor. J Acoust Soc Am April 1978; 63(4):1025-1030.
5. Chu B-T, Apfel RE: Acoustic radiation pressure produced by a beam of sound. J Acoust Soc Am 1982; 72(6):1673-1687.
6. Fatemi M, Greenleaf JF: Imaging the viscoelastic properties of tissue: In: M. Fink , J-P Montagner, A. Tourin: Imaging complex Media with Acoustic and Seismic Waves. To be published with the series "Topics in Applied Physics", Springer-Verlag, 1999 (in press).

Imaging the Viscoelastic Properties of Tissue

Mostafa Fatemi and James F. Greenleaf

Department of Physiology and Biophysics, Mayo Clinic and Mayo Foundation, Rochester, Minn. 55905, USA
{fatemi.mostafa,jfg}@mayo.edu

Abstract. Elasticity and viscosity of soft tissues are often related to pathology. These parameters, along with other mechanical parameters, determine the dynamic response of tissue to a force. Tissue mechanical response, therefore, may be used for diagnosis. Measuring and imaging of the mechanical properties of tissues is the aim of a class of techniques generally called elasticity imaging or elastography. The general approach is to measure tissue motion caused by a force or displacement and use it to reconstruct the elastic parameters of the tissue. The excitation stress can be either static or dynamic (vibration). Dynamic excitation is of particular interest because it provides more comprehensive information about tissue properties in a spectrum of frequencies. In one approach an external stress field must pass through the superficial portion of the object before reaching the region of interest within the interior. An alternative strategy is to apply a localized stress directly in the region of interest. One way to accomplish this task is to use the radiation force of ultrasound. This approach offers several benefits, including: (a) safety – acoustic energy is a noninvasive means of exerting force; (b) adaptability – existing ultrasound technology and devices can be readily modified for this purpose; (c) remoteness – radiation force can be generated remotely inside tissue without disturbing its superficial layers; (d) localization – the radiation stress field can be highly localized, thus allowing for precise positioning of the excitation point; and (e) a wide frequency spectrum. Several methods have been developed for tissue probing using the dynamic radiation force of ultrasound, including: (a) transient methods which are based on impulsive radiation force; (b) shear-wave methods which are based on generation of shear-waves; and (c) vibro-acoustography, recently developed by the authors, where a localized oscillating radiation force is applied to the tissue and the acoustic response of the tissue is detected by a hydrophone. Here, we focus on vibro-acoustography and present a detailed description of the theory and the experimental results. We conclude with the capabilities and limitations of these radiation-force methods.

1 Introduction

It is well known that changes in elasticity of soft tissues are often related to pathology. Traditionally, physicians use palpation as a simple method for estimating mechanical properties of tissue. In palpation, a static force is applied and a crude estimation of tissue elasticity is obtained through the sense of touch. The force is applied on the body surface and the result is a collective response of all the tissues below. Clinicians can sense abnormalities if

Fink et al. (Eds.): Imaging of Complex Media with Acoustic and Seismic Waves,
Topics Appl. Phys. **84**, 257–275 (2002)

the response to palpation of the suspicious tissue is sufficiently different from that of normal tissue. However, if the abnormality lies deep in the body, or if it is too small to be resolved by touch, then the palpation method fails. The dynamic response of soft tissue to a force is also valuable in medical diagnosis. For instance, rebound of tissue upon sudden release of pressure exerted by the physician's finger on the skin provides useful diagnostic information about the tissue.

Quantitative measurement of the mechanical properties of tissues and their display in a raster format is the aim of a class of techniques generally called elasticity imaging or elastography [1]. The general approach is to measure tissue motion caused by an external (or, in some methods, internal) force or displacement and use it to reconstruct the elastic parameters of the tissue. The excitation stress can be either static or dynamic (vibration). The dynamic excitation is of particular interest because it provides more comprehensive information about tissue properties in a spectrum of frequencies, or alternatively, the transient behavior of the tissue could be deduced from the measurements. In most elasticity imaging methods ultrasound is used to detect the motion or displacement resulting from the applied stress. Magnetic resonance elastography is a recently developed method [2] that employs a mechanical actuator to vibrate the body surface and then measures the strain waves with phase-sensitive magnetic resonance imaging (MRI). The majority of elasticity imaging methods are based on an external source of force, resulting in a spatially wide stress field distribution. This requires the stress field to pass through the superficial portion of the object before reaching the region of interest within the interior. This requirement can complicate the estimation of stiffness because the stress-field patterns change at different depths. Also, because the stress field is widely distributed, the response of the object is an integral sum of the stress field. An alternative strategy is to apply a localized stress directly in the region of interest. One way to accomplish this is to use the radiation pressure of ultrasound.

Acoustic radiation force is the time-average force exerted by an acoustic field on an object. This force is produced by a change in the energy density of an incident acoustic field [3], for example, due to absorption or reflection. Several benefits may result from using ultrasound radiation force for evaluating tissue properties, including: (a) acoustic (ultrasound) energy is a noninvasive means of exerting force; (b) existing ultrasound technology and devices can be readily modified for this purpose, thus eliminating the need for developing a new technology; (c) radiation force can be generated remotely inside tissue without disturbing its superficial layers; (d) the radiation stress field can be highly localized, thus allowing for precise positioning of the excitation point; and (e) radiation force can be produced in a wide range of frequencies or temporal shapes. These features make radiation-force methods more attractive than other, mostly mechanical, excitation methods used in elasticity imaging.

Tissue probing with the radiation force produced by ultrasound can be accomplished in a variety of techniques, depending on the excitation and detection methods used. We may categorize these methods as follows: (a) transient methods, where an impulsive radiation force is used and the transient response of the tissue is detected by Doppler ultrasound [4]; (b) shear-wave methods, where an oscillating radiation is applied to the tissue and the resulting shear wave is detected by ultrasound or other methods [5,6,7]; and (c) vibro-acoustography, recently developed by the authors, where a localized oscillating radiation force is applied to the tissue and the acoustic response of the tissue is detected by a hydrophone [8,9]. Figure 1 illustrates the relationship between various methods that have been developed for evaluating or imaging the elastic properties of tissue.

Dynamic radiation-force methods seem to be evolving rapidly as a new field in tissue characterization and imaging. The purpose of this chapter is to systematically discuss the features and capabilities that are offered in this group of elasticity measurement techniques. Here, we describe the general approach used in the transient, shear-wave, and vibro-acoustography methods. We pay particular attention to the last method, present its theory, and discuss its features. Finally we discuss the capabilities and limitations of all three methods.

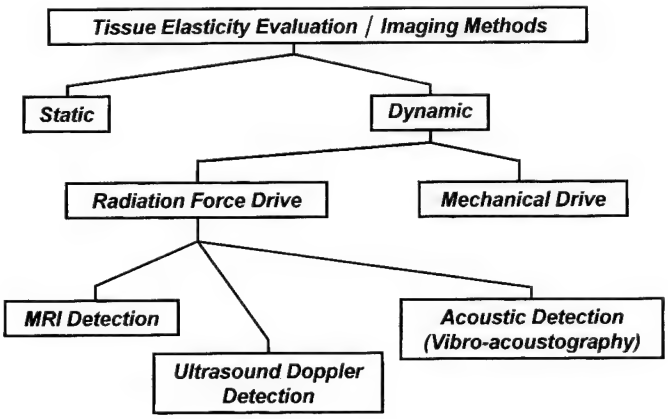

Fig. 1. Tissue elasticity evaluation and imaging methods. These methods can be divided into two general groups. The static group employs a steady force to deform the object. The dynamic group use either a momentary or an oscillating force to vibrate the object and can be divided into two subgroups. Mechanical-drive methods use a mechanical actuator, whereas the radiation-force-drive methods use the radiation force of ultrasound to excite the object. The latter subgroup is divided into three subsubgroups based on the detection method used. Vibro-acoustography uses a hydrophone to detect object response

2 Theory of the Radiation Force

The study of radiation force and radiation pressure dates back nearly one century, to the time of *Rayleigh* [10]. Since then, this subject has been under continuous investigation. A historical review of radiation force and radiation pressure is presented in [11], and a critical review of the subject can be found in [3]. Some recent analyses of radiation force/pressure in an attenuating medium, which may be applicable to biological tissues, are presented in [12] and [13].

The acoustic radiation force is an example of a universal phenomenon in any wave motion that introduces some type of unidirectional force on absorbing or reflecting targets in the wave path. Radiation force in fluids is often studied in the context of radiation pressure. Depending on the boundary conditions, radiation pressure can be defined differently. Simple explanations of these definitions can be presented by considering a sound traveling inside, and along the axis of, a cylindrical container toward the opposite wall [11]. Rayleigh radiation pressure is the excess pressure produced on the opposite wall when the container's side wall is confining the fluid inside. Langevin radiation pressure is the excess pressure on the opposite wall when we remove the confining side wall, so that the fluid is free to move (Fig. 2). Here we will focus on Langevin radiation pressure because the conditions for which this pressure is defined apply to our experimental situation. It can be shown that the Langevin radiation pressure of a plane wave impinging normally on a perfectly absorbing wall is equal to the total energy density $\langle E \rangle$, where $\langle \ldots \rangle$ represents the time average. If the wall is partially reflecting, this pressure would be equal to $(1+R)\langle E \rangle$, where R is the power reflection coefficient [11]. Thus, in general, we can write the radiation force of a normally impinging sound beam on a wall as

$$F = d_r S \langle E \rangle, \tag{1}$$

where F is the force in the beam direction, and d_r is the "radiation-force function" or the drag coefficient. This dimensionless coefficient is defined per unit incident energy density and unit projected area. For a planar object, d_r is numerically equal to the force on the object. Physically, the drag coefficient represents the scattering and absorbing properties of the object [14]. For a perfectly absorbing object $d_r = 1$, and for a perfectly reflecting object $d_r = 2$. In the case of oblique incidence, the radiation force will have a normal as well as a transverse component. A more detailed description of d_r is presented in [14].

To produce a time-varying radiation force, the intensity of the incident beam can be modulated in various ways. For example, a short ultrasound pulse can produce a transient pulsed radiation force, and a sinusoidally modulated beam can result in a sinusoidally varying force.

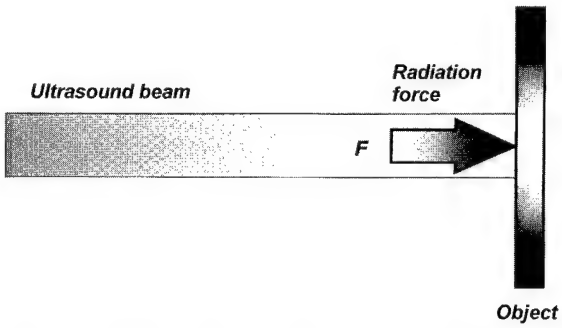

Fig. 2. Radiation force produced by projection of ultrasound on an object. Interaction of an ultrasound beam with an object that scatters and/or absorbs results in a force on the object in the beam direction. The magnitude of this force is proportional to the time-average energy density of the incident beam and a factor that represents the scattering and absorbing properties of the object

3 Radiation-Force Methods

In transient methods the radiation force of ultrasound is used to make a minute deformation in the tissue. The transient recoil of the tissue resulting from this deformation is measured and used for evaluation of tissue elastic properties. A method for measuring tissue hardness, presented by *Sugimoto* et al. [4], uses the radiation force of a single focused ultrasound beam. Ideally, hardness may be represented by the spring constant of the object, which is the ratio of the applied force to the displacement. Principles of the transient methods are presented in Fig. 3.

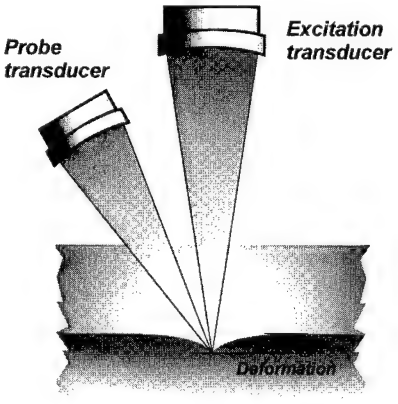

Fig. 3. Principle of the transient method. The excitation transducer produces a momentary radiation force which induces a minute deformation in the object. Doppler methods are used to measure this deformation using the probe transducer

3.1 Transient Method

In this method an ultrasound pulse is used to generate a short-duration radiation force which produces localized deformation of the tissue. Immediately after the force pulse, the resulting transient deformation of the tissue is measured as a function of time with Doppler ultrasound using a separate transducer. The deformation includes an initial rapid squeeze of the tissue, followed by a relaxation and possibly a rebound. The deformation is a function of tissue viscoelastic parameters, as well as the applied force. The authors argue that, because quantitatively measuring the internal radiation force is difficult, it is advantageous to derive a relative quantity that is representative of tissue hardness. To derive a single relative quantity from the deformation data, the relaxation part of the function is approximated by a sum of several exponential curves, and the sum of the first-order derivatives of such exponentials is calculated. *Sugimoto* et al. [4] show that this quantity is correlated to the spring constant of the tissue; thus it may be used as a measure of tissue hardness.

3.2 Shear-Wave Methods

The shear modulus is related to the hardness or elasticity of the material. It is known that the shear moduli of various soft tissues range over several orders of magnitude, while the bulk modulus, a parameter that is associated with the conventional pulse echo ultrasound compressional wave speed, varies significantly less than an order of magnitude [15,16]. These features indicate that the shear modulus may be a better parameter for tissue characterization than bulk modulus. Tissue attenuation of the shear wave is very large, even at low kHz frequencies. One way to induce localized shear waves inside tissue is to use the radiation force of focused ultrasound [5]. In a method called shear-wave elasticity imaging (SWEI) [6], an amplitude-modulated, single-focused ultrasound beam is used to induce a localized radiation stress inside the soft tissue. Localization of the stress field is critical to the success of the method. To achieve a high degree of localization, the method uses a focused ultrasound beam. It is shown that the radiation stress exerted within a dissipative medium peaks about the focal region of the highly focused transducer. Also, it has been suggested that localization can be improved by designing the transducer and selecting the beam parameters such that a nonlinear shock wave is produced in the focal region, increasing the magnitude of the stress field in the vicinity of the focal region, thus augmenting localization of the stress field.

Modulation of the ultrasound beam can be in the form of an oscillating wave or short pulse. The resulting radiation force elicits a shear wave propagating in the radial direction with respect to the beam axis, with particle motion parallel to the beam axis. Shear waves in soft tissue travel at very low speed, typically around a few meters per second; thus the corresponding

wavelength is much shorter than that of the compressional waves for the same frequency. Shear waves are also highly attenuated in soft tissue, with an attenuation coefficient two or three orders of magnitude higher than that of the compressional waves. Because of high attenuation of shear waves, it is possible to induce them in a very limited region in the vicinity of the focal point of the ultrasound beam, hence avoiding the influence of tissue boundaries. Shear parameters of the tissue, such as shear modulus and shear viscosity, can be calculated by measuring the amplitude and the temporal characteristics of this wave. For example, the time required for the wavefront to propagate from one point to another can be used to calculate the shear-wave speed, and consequently the shear-wave modulus μ as

$$\mu = \rho c_t^2 \tag{2}$$

where ρ and c_t are the density and the shear-wave velocity, respectively.

Shear waves may be detected optically. In this method a laser source and a photo detector are used to detect the displacement of particles due to the shear wave in a transparent phantom [6]. Because this method requires a transparent medium, its application in vivo is difficult. Phase-sensitive MRI [2,6] is an alternative method that can be used to measure the 3-dimensional distribution of particle displacement in a given direction versus time in a material. Figure 4 illustrates a simplified system for shear-wave elasticity measurement using MRI. In an experiment presented in [6], an ultrasound pulse of 3.6-ms duration produced by a 70-mm diameter transducer focused at 100 mm was transmitted within a cylindrical rubber phantom. The displacement was measured by 2.0-T MRI system at two different times after the acoustic pulse was applied. The position of the peak displacement at these time points was used to estimate the shear velocity, which was shown to be consistent with the independently measured value. Shear waves can also be detected by Doppler ultrasound [5]. It has been shown [7] that to achieve the appreciable displacement needed for Doppler detection, most soft tissues require high ultrasound intensities which might be beyond the safe limit.

3.3 Vibro-Acoustography

This technique produces a map of the mechanical response of an object to a dynamic force applied at each point. The method utilizes an ultrasound radiation force to remotely exert a localized oscillating stress field at a desired frequency within (or on the surface of) an object, and records the resultant acoustic response [8,9]. Figure 5 illustrates the principle of this method. This acoustic response, which is normally in the low kHz range, is a function of the viscoelastic properties of the object and can be used to produce an image of the object.

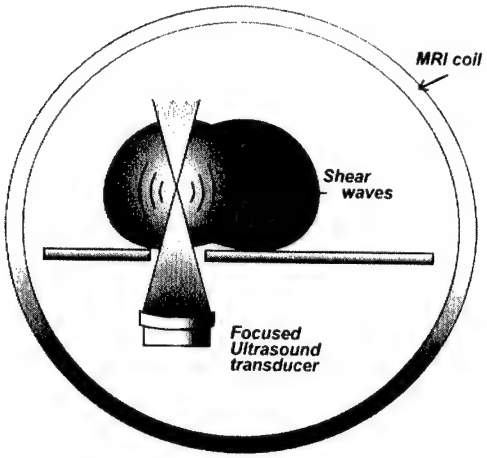

Fig. 4. Principle of shear-wave elastography. The focused ultrasound beam is absorbed by the object, resulting a localized radiation stress, which squeezes the elastic object. This deformation propagates in the form of shear waves through the object. The phase-sensitive MRI machine detects the spatial distribution of the resulting displacement in the object

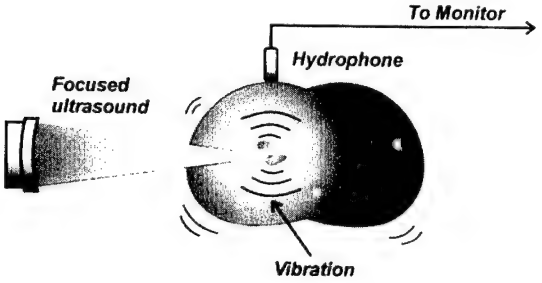

Fig. 5. Principle of vibro-acoustography. The ultrasound beam is used to produce a localized oscillatory radiation stress to vibrate the object. Vibration of the object produces an acoustic emission field in the medium. This field, which is a function of the viscoelastic properties of the object, is detected by a sensitive hydrophone

3.3.1 Method

This method operates on an oscillating radiation force to vibrate the tissue and consequently produce an acoustic emission from the object. To produce an oscillating radiation force the intensity of the incident ultrasound must be amplitude modulated at the desired low frequency. Using a single amplitude-modulated beam seems to be the simplest means to attain this purpose.

However, such a beam could exert a radiation force on any object that is present along the beam path, producing undesirable acoustic emission. To confine the radiation stress to the desired region, we use two unmodulated cw beams at slightly different frequency, propagating along separate paths. The beams are positioned to cross each other at their respective foci, and thus produce a modulated field at a confined, small, cross-sectional region.

3.3.2 Theory

In the beamforming method to be described, the amplitude-modulated field is obtained by the interference of two unmodulated ultrasound beams. The main advantage of this approach is that the interference volume size can be limited to a small region. Radially symmetric interfering beams are obtained when two coaxial, confocal transducers are used [9]. For this purpose, elements of a two-element spherically focused annular array (consisting of a central disc with radius a_1 and an outer ring with the inner radius of a_2' and outer radius of a_2) are excited by separate cw signals at frequencies $\omega_1 = \omega_0 - \Delta\omega/2$ and $\omega_2 = \omega_0 + \Delta\omega/2$, respectively. We assume that the beams are propagating in the $+z$-direction with the joint focal point at $z = 0$, as shown in Fig. 6. The resultant field on the $z = 0$ plane may be written as follows:

$$p(t) = P_1(r)\cos\left[\omega_1 t + \psi_1(r)\right] + P_2(r)\cos\left[\omega_2 t + \psi_2(r)\right] , \tag{3}$$

where $r = \sqrt{x^2 + y^2}$ is the radial distance. The amplitude functions are [17]

$$P_1(r) = \rho c U_{01} \frac{\pi a_1^2}{\lambda_1 z_0} \mathrm{jinc}\left(\frac{r a_1}{\lambda_1 z_0}\right) , \tag{4}$$

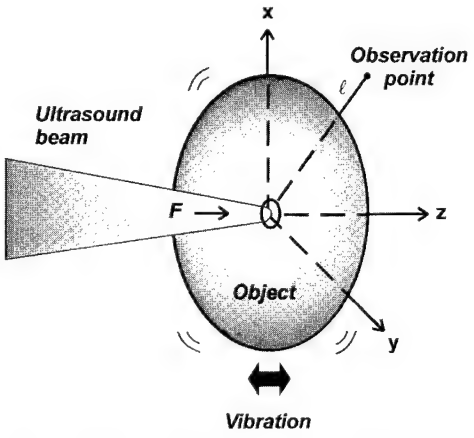

Fig. 6. The coordinate system describing the position of the ultrasound beam and the observation point relative to the object. The beam travels in the z-direction

and

$$P_2(r) = \rho c U_{02} \frac{\pi}{\lambda_2 z_0} \left[a_2^2 \text{jinc}\left(\frac{r a_2}{\lambda_2 z_0}\right) - a_2'^2 \text{jinc}\left(\frac{r a_2'}{\lambda_2 z_0}\right) \right], \tag{5}$$

where U_{0i} is the velocity amplitude at the ith transducer element surface, and $\lambda_i = 2\pi/\omega_i$ for $i = 1, 2$ are the ultrasound wavelengths. The phase functions,

$$\psi_i(r) = -\frac{\pi r^2}{\lambda_i z_0}, \tag{6}$$

for $i = 1, 2$, are conveniently set to be zero at the origin. Also, $\text{jinc}(X) = J_1(2\pi X)/\pi X$, where $J_1(\ldots)$ is the first-order Bessel function of the first kind.

The instantaneous energy is $E = p^2(t)/\rho c^2$. Replacing $p(t)$ from (3), this energy will have a time-independent component, a component at the difference frequency $\Delta\omega = \omega_2 - \omega_1$ which results from the cross-product of the two pressure fields, and high-frequency components at ω_1 and ω_2 and their harmonics. The energy component at the difference frequency is

$$e_{\Delta\omega}(t) = \frac{P_1(r_0) P_2(r_0)}{4\rho c^2} \cos\left[\Delta\omega t - \Delta\psi(r_0)\right], \tag{7}$$

where $\Delta\psi(r_0) = \psi_2(r_0) - \psi_1(r_0)$.

Now, we define a *unit point target* with an area of $\mathrm{d}x\mathrm{d}y$ at position (x_0, y_0) on the focal plane, and with a drag coefficient $d_r(x_0, y_0)$ such that $d_r(x_0, y_0)\mathrm{d}x\mathrm{d}y = 1$ on the target and zero elsewhere. This equation is merely used as a mathematical model. In this case, the projected area can be considered to be $S = \mathrm{d}x\mathrm{d}y$. Therefore, if the projected area is unity, then $d_r(x, y) = 1$, which corresponds to a totally absorptive object.

Referring to (1), and replacing $d_r S$ with unity and $\langle E \rangle$ with $e_{\Delta\omega}(t)$ of (7), we can write the low-frequency component of the radiation force on the unit point target as

$$f_{\Delta\omega}(x_0, y_0; t) = \frac{1}{\rho c^2} P_1(r_0) P_2(r_0) \cos\left[\Delta\omega t + \Delta\psi(r_0)\right], \tag{8}$$

where arguments x_0 and y_0 are added to denote the position of the point target, and $r_0 = \sqrt{x_0^2 + y_0^2}$. Referring to (4) and (5), the complex amplitude of the stress field can be found as

$$\begin{aligned} F_{\Delta\omega}(x_0, y_0) = {} & \rho U_{01} U_{02} \frac{\pi a_1^2}{\lambda_1 z_0} \text{jinc}\left(\frac{r_0 a_1}{\lambda_1 z_0}\right) \\ & \times \left[\frac{\pi a_2^2}{\lambda_2 z_0} \text{jinc}\left(\frac{r_0 a_2}{\lambda_2 z_0}\right) - \frac{\pi a_2'^2}{\lambda_2 z_0} \text{jinc}\left(\frac{r_0 a_2'}{\lambda_2 z_0}\right) \right] \\ & \times \exp\left(-j \frac{r_0^2}{2\Delta\lambda z_0}\right), \end{aligned} \tag{9}$$

where $\Delta\lambda = 2\pi c/\Delta\omega$ is the wavelength associated with $\Delta\omega$. The above equation indicates that the radiation stress is concentrated at the focal point

and decays quickly as $\text{jinc}(\ldots)^2$. It should be noted that because $f_{\Delta\omega}(x_0, y_0; t)$ and $F_{\Delta\omega}(x_0, y_0)$ are defined per unit point target, they have the dimension of force per unit area, or equivalently the unit of stress. As an example, we consider a confocal transducer with dimensions $a_1 = 14.8\,\text{mm}$, $a_2' = 16.8\,\text{mm}$, $a_2 = 22.5\,\text{mm}$, and the focal length 70 mm. Also, we assume that the center frequency is 3 MHz, and the difference frequency is 7.3 kHz. The radiation stress at the focal plane of this transducer is plotted in Fig. 7.

In medical applications the maximum ultrasonic intensity is regulated for safety reasons. It is therefore useful to write the stress field in terms of the peak ultrasonic intensity at the focal point. The long-term average of ultrasonic intensity at the focal point can be written as

$$I(0) = \frac{P_1^2(0) + P_2^2(0)}{2\rho c}, \tag{10}$$

where $P_1(0)$ and $P_2(0)$ can be found from (4) and (5) as

$$I(0) = \frac{\rho c}{2}\left[U_{01}^2\left(\frac{\pi a_1^2}{\lambda_1 z_0}\right)^2 + U_{02}^2\left(\frac{\pi}{\lambda_2 z_0}\right)^2\left(a_2^2 - a_2'^2\right)^2\right]. \tag{11}$$

Assuming $U_{01} = U_{02} = U_0$, we can write the focal plane stress field in terms of $I(0)$:

$$F_{\Delta\omega}(x_0, y_0) = \frac{2I(0)}{c} \times \frac{\frac{\pi a_1^2}{\lambda_1 z_0}}{\left(\frac{\pi a_1^2}{\lambda_1 z_0}\right)^2 + \left(\frac{\pi}{\lambda_2 z_0}\right)^2\left(a_2^2 - a_2'^2\right)^2}$$

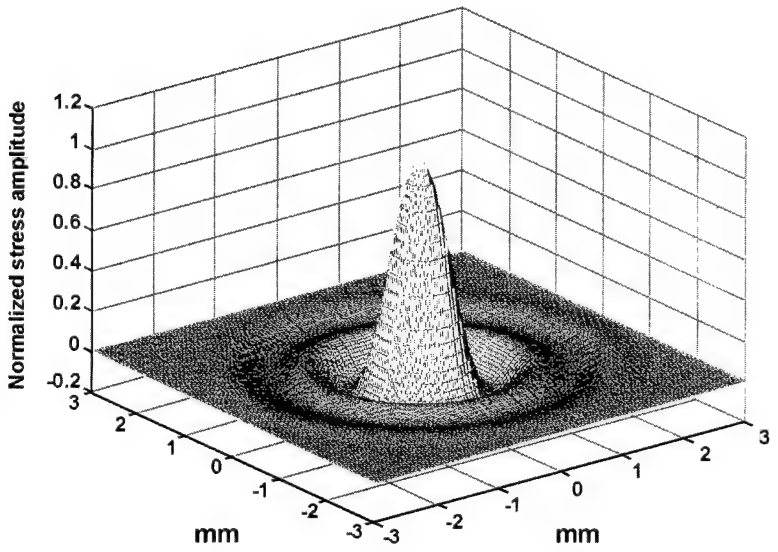

Fig. 7. Normalized stress field of the vibro-acoustography system with a 3-MHz confocal transducer

$$\times \text{jinc}\left(\frac{r_0 a_1}{\lambda_1 z_0}\right)\left[\frac{\pi a_2^2}{\lambda_2 z_0}\text{jinc}\left(\frac{r_0 a_2}{\lambda_2 z_0}\right) - \frac{\pi a_2'^2}{\lambda_2 z_0}\text{jinc}\left(\frac{r_0 a_2'}{\lambda_2 z_0}\right)\right]$$
$$\times \exp\left(-j\frac{r_0^2}{2\Delta\lambda z_0}\right). \tag{12}$$

The first fraction in the above equation represents the static radiation force produced by the two beams on a total absorber, the second fraction is a constant factor, and the rest represents the spatial distribution of the stress field on the focal plane. If $\Delta\omega \ll \omega_2$, then we may replace λ_1 and λ_2 with image spatialλ_0, and simplify the expression for the stress field. Under these conditions, the stress at the focal point is

$$F_{\Delta\omega}(0,0) = \frac{2I(0)}{c}\frac{a_1^2\left(a_2^2 - a_2'^2\right)}{a_1^4 + \left(a_2^2 - a_2'^2\right)^2}. \tag{13}$$

The fraction on the right represents the effect of transducer dimension on the stress field. For the transducer used in the previous example, the value of this fraction is 0.4999. [This fraction can be also calculated for a single-element transducer of the same diameter excited by an amplitude-modulated signal. For this purpose, we may let $a_1 = a_2$ and $a_2' = 0$. For these values, the last fraction in (13) is 0.5.] The resulting radiation stress (assuming $c = 1500\,\text{m/s}$ for water) is $F_{\Delta\omega}(0,0) = 6.67\times10^{-4} I(0)\text{N/m}^2$. Now, letting $I(0) = 7200\,\text{W/m}^2$, which is the intensity suggested by the FDA for safe in vivo applications, the resulting stress at the focal point is $F_{\Delta\omega}(0,0) = 4.80\,\text{N/m}^2$. Referring to Fig. 7, we note that this stress field is applied only in a small region around the focal point to the object.

Acoustic Emission To explain the acoustic emission we consider an "object" within an homogeneous infinite medium. This model allows us to separate the roles played by the parameters of the object and the surrounding medium. Also, this model can be fitted to various applications. When an oscillating stress field is applied to the object, the object vibrates at the frequency of the stress field. Vibrational energy of the object is partly transferred to the surrounding medium, resulting in an acoustic emission field. Here, we calculate the acoustic emission of an object subjected to cyclic radiation stress.

To explain the physics in an analytical form, we consider a flat plate facing the beam. Here, we assume that the vibrating object has a circular cross-section of radius b and uniformly vibrates back and forth like a piston. We also consider an area $S \leq \pi b^2$ of the piston surface to be projected normally to the beam. We can always return to our elementary point object by reducing the area of this disk to $dxdy$. Similar solutions can be carried out for objects of other forms. The theory can be also extended to include arbitrary vibrating-part shapes and nonuniform displacement of the object. The total radiation force on this object, $\overline{F_{\Delta\omega}}$, can be found by integrating the radiation stress over the area of the object. This force vibrates the target

object at frequency $\Delta\omega$. The steady-state normal velocity amplitude of a piston at frequency $\Delta\omega$, $U_{\Delta\omega}$, due to a harmonic force $\overline{F_{\Delta\omega}}$, can be written as

$$U_{\Delta\omega} = \frac{\overline{F_{\Delta\omega}}}{Z_{\Delta\omega}}, \tag{14}$$

where $Z_{\Delta\omega}$ is the mechanical impedance of the object at $\Delta\omega$. The mechanical impedance of the object has two components, one resulting from the inertia, friction, and the elasticity of the object itself, and the other resulting from the loading effect of the surrounding medium on the vibrating object. The mechanical impedance can be interpreted as a measure of object rigidity and how much it yields to the applied force. For example, for a rigid object, $Z_{\Delta\omega}$ is high and hence resisting the force.

Knowing $U_{\Delta\omega}$, we can calculate the pressure field it produces in the medium. We assume that the acoustic emission signal propagates in a free and homogenous medium. The far-field acoustic pressure due to a piston source of radius b set in a planar boundary of infinite extent is given by [17]:

$$P_{\Delta\omega} = -\mathrm{j}\Delta\omega\rho\frac{\exp(\mathrm{j}\Delta\omega l/c)}{4\pi l}\left(\frac{2J_1\left(\frac{\Delta\omega b}{c}\sin\vartheta\right)}{\frac{\Delta\omega b}{c}\sin\vartheta}\times\frac{\cos\vartheta}{\cos\vartheta+\beta_{\mathrm{B}}}\right)\left(2\pi b^2 U_{\Delta\omega}\right), \tag{15}$$

where l is the distance from the observation point to the center of the piston, ϑ is the angle between this line and the piston axis, and β_{B} is the specific acoustic admittance of the boundary surface (the specific acoustic admittance is $\beta_{\mathrm{B}} = \frac{\rho c}{Z_{\mathrm{B}}}$, where Z_{B}, the acoustic impedance of the boundary, represents the ratio between the pressure and normal fluid velocity at a point on the object). The factor two comes from the presence of the boundary wall. It would be replaced by unity if the boundary wall were not present [17].

The acoustic emission field resulting from object vibration can be written in terms of object mechanical impedance by combining (14) and (15) as

$$P_{\Delta\omega} = \rho c^2\left[\mathrm{j}\frac{\Delta\omega}{c^2}\times\frac{\exp(\mathrm{j}\Delta\omega l/c)}{4\pi l}\left(\frac{2J_1\left(\frac{\Delta\omega b}{c}\sin\vartheta\right)}{\frac{\Delta\omega b}{c}\sin\vartheta}\times\frac{\cos\vartheta}{\cos\vartheta+\beta_{\mathrm{B}}}\right)\right]\times\frac{2\pi b^2}{Z_m}\overline{F_{\Delta\omega}}. \tag{16}$$

For wavelengths long compared to the object size, i.e., when $b\Delta\omega/c \to 0$, the term in the paranthesis approaches a constant, hence we may consider the contents of the brackets to be an object-independent function (the specific acoustic admittance β_{B} relates to the surrounding boundary surface). Under these conditions, the bracket contents in the above equation represent the effect of the medium on the acoustic emission field, which we may call the *medium transfer function*, which my be denoted by

$$H_{\Delta\omega}(l) = \mathrm{j}\frac{\Delta\omega}{c^2}\times\frac{\exp(\mathrm{j}\Delta\omega l/c)}{4\pi l}\times\frac{\cos\vartheta}{\cos\vartheta+\beta_{\mathrm{B}}}. \tag{17}$$

The last fraction in (16) includes $\frac{1}{Z_{\Delta\omega}}$, which is the mechanical admittance of the object at the frequency of the acoustic emission ($\Delta\omega$), and we denote this by $Y_{\Delta\omega}$. It is convenient to combine this term with the next term ($2\pi b^2$) in (16), as $Q_{\Delta\omega} = 2\pi b^2 Y_{\Delta\omega} = 2\pi b^2 / Z_{\Delta\omega}$, which is the total acoustic outflow by the object per unit force (acoustic outflow is the volume of the medium, e.g., the fluid, in front of the object surface that is displaced per unit time due to object motion). Function $Q_{\Delta\omega}$ represents the object characteristics at the acoustic frequency. We may thus rewrite (16) in a more compact form as

$$P_{\Delta\omega} = \rho c^2 H_{\Delta\omega}(l) Q_{\Delta\omega} \overline{F_{\Delta\omega}} \,. \tag{18}$$

Equation (18) indicates that the acoustic emission pressure is proportional to the following: (a) the radiation force, which itself is proportional to the square of ultrasound pressure and the ultrasound characteristics of the object, d_r, in the projected area S; (b) the acoustic outflow by this object, $Q_{\Delta\omega}$, representing the object size b and its mechanical admittance at the acoustic frequency, $Y_{\Delta\omega}$; and (c) the transfer function of the medium at the acoustic frequency, $H_{\Delta\omega}(l)$. Note the difference between the projection area S and the vibrating area πb^2. The projection area determines the extent of the force applied to the object (1). The vibrating area, however, influences the total acoustic outflow in the medium caused by object vibration.

3.3.3 Applications

Evaluating the characteristics of an object (or a medium) by listening to its sound is a traditional approach that has been used for many purposes. Qualitative evaluation of a crystal glass by tapping on it is a simple example. Vibro-acoustography implements the same approach but in microscale, and in a way that could be applied to tissues.

Equation (18) presents a general relationship between the mechanical parameters of the objects, surrounding medium, and the acoustic emission field resulting from object vibration. By measuring the acoustic emission field, it would be possible, in principle, to estimate some of the object or medium parameters, either in an absolute or in a relative sense. For example, one can use vibro-acoustography to measure the resonance frequency of an object, and from that information it is possible to estimate some viscoelastic parameters of the object or the medium (Fig. 8). This method has been used to measure the Young's modulus of a metallic rod [18]. In another experiment, by measuring the resonance frequency of a known resonator in a liquid medium, the viscosity of the fluid has been estimated with good accuracy [19]. These applications are not necessarily medical, but the principle could be used for evaluation of soft tissues, blood, bone, etc.

In medical applications, one can use vibro-acoustography to obtain images of the human body for diagnostic purposes. In such applications, the image may not represent a physical quantity, rather it provides a means to visualize

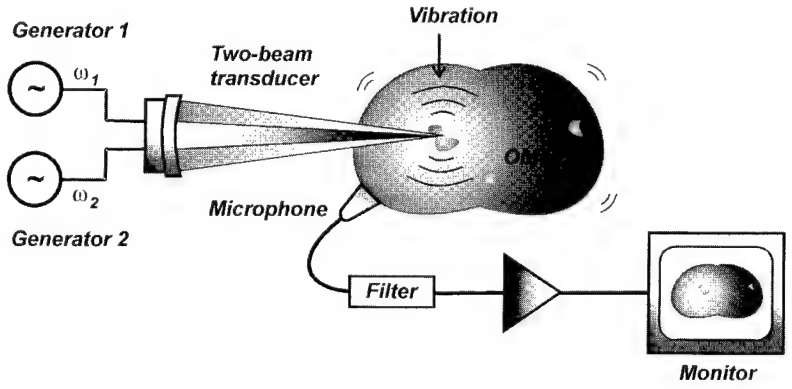

Fig. 8. Vibro-acoustography system. The object is vibrated by the radiation force of the confocal, two-beam transducer. Resulting vibrations are detected by the microphone (or hydrophone) and mapped into the image

object details. To demonstrate the capability of vibro-acoustography, we used this method to image a specimen of the human iliac artery that included calcifications. A 3-MHz confocal transducer with dimensions $a_1 = 14.8\,\text{mm}$, $a_2' = 16.8\,\text{mm}$, and $a_2 = 22.5\,\text{mm}$ and a focal length of 70 mm, was used for this experiment. The difference frequency was set at 44 kHz. Figure 9 shows a photo of the artery that is cut open. The areas with calcification

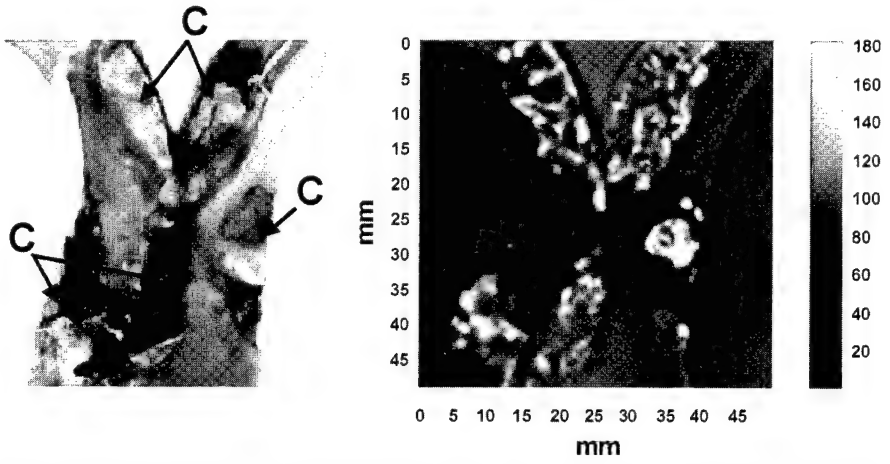

Fig. 9. Vibro-acoustic image of an ex-vivo human iliac artery near the bifurcation. On the left is a photo of the cut-open artery specimen. Calcified areas are marked with letter "C". Vibro-acoustic image of the specimen is shown on the right. Calcified areas stand out as bright spots. This image was obtained with a 3-MHz confocal transducer as described in the text. The difference frequency was set at 44 kHz. The gray-level scale is in arbitrary units

are marked by the letter "C". The vibro-acoustic image of the same artery is shown on the right. Calcium deposits, which are formed in large (a few mm to a few cm long) and stiff (compare to the arterial wall) plates, are efficient acoustic radiators, producing strong acoustic emission when they are exposed to the radiation force of the incident ultrasound. Hence, they stand out in the vibro-acoustography image. The vibro-acoustic image has high resolution, no speckle, and a high signal-to-noise ratio. These features allow vibro-acoustography to delineate calcium deposits with high definition and contrast.

4 Capabilities and Limitations

Although the methods described above tend to estimate the mechanical properties of the object, the quantities they measure are different. The quantity measured in the transient method is somewhat arbitrary, and not a direct measure of any physical quantity. The merit of this method is that tissue hardness is measured from relative displacement values, without the need to measure the applied force. The shear-wave method directly measures a physical parameter of the material in an absolute sense. The acoustic emission field measured in vibro-acoustography is a function of several physical parameters that relate to the object and the surrounding medium. It is possible to measure a single parameter only if one has enough knowledge about other parameters involved. For example, one can measure the shear viscosity of a liquid using a known resonator as an object in the liquid [19], or, for a given the geometry, the Young's modulus of a metallic object can be measured [18] by vibro-acoustography.

Detection sensitivity is critical to the success of any of the above methods. Greater ultrasound intensity would be needed if the detection sensitivity is poor. As a result, the peak ultrasound intensity in the focal area may be limited by the safe in vivo limit. Ultrasound Doppler methods, at conventional ultrasound frequencies, probably can detect displacements on the order of a few micrometers. The sensitivity of the MRI technique is on the order of 100 nm [2]. Vibro-acoustography has been shown to detect motions as small as a few nanometers [8]. The high sensitivity of this method is a result of the fact that small motions of the object can produce an acoustic emission pressure field that is easily detectable by a sensitive hydrophone.

Image spatial resolution is an important parameter when assessing the capability of an imaging method in delineating fine structures in the object. Vibro-acoustography can be used for high-quality imaging. The spatial resolution is proportional to the width of the stress-field main lobe. For example, for the 3-MHz ultrasound transducer presented in Fig. 7, the spatial resolution is about 700μm. Imaging complex objects using the transient or the shear-wave methods has not been fully explored in the literature.

Performance of each method is partly influenced by viscoelastic properties of the material. Both the transient and shear-wave methods work best if the material under test supports the shear wave, has enough attenuation to allow the build-up of enough radiation force, and is compliant enough to allow appreciable displacement. Application of these methods for hard materials, such as bone and calcifications, would be difficult or impractical because (a) stiff materials have low compliance, hence their displacement in response to the force is relatively small and difficult to detect and (b) the shear wave travels at high speed in such materials. In vibro-acoustography hard materials produce structural vibrations which are often stronger than those of soft tissue. Such vibrations result in strong and easily detectable acoustic emissions. The bright appearance of the arterial calcifications in the experiment presented in [8] is a demonstration of this phenomenon. Vibro-acoustography can be used to detect particles in materials that do not support shear waves, for example, detecting gas bubbles in liquids. The acoustic emission resulting from particle vibration includes a compressional-wave component that can travel in the surrounding medium including the liquid. Tissue attenuation for compressional waves at low frequencies is small; hence such waves can be detected by the hydrophone from a distance. Shear waves in a liquid medium decay very rapidly and are difficult to detect by most methods.

The ultimate goal of viscoelastic parameter imaging methods is to measure these parameters in the human body. In vivo application of the transient method is not clear because it requires high ultrasound power to produce a detectable displacement. Application of the shear-wave method in the human body largely depends on the detection method used. Optical methods are not likely to be usable in vivo. MRI detection methods are generally complex, especially when the technique is to be linked to the ultrasound system in the magnetic field. Ultrasound Doppler is a more practical detection method for shear-wave detection; however its sensitivity may not be sufficient for ultrasound intensities within the safe limit [7]. Vibro-acoustography uses a hydrophone for detection which is simple to operate in clinical settings. It however requires an acoustically quiet environment for proper detection. The biological noise spectrum seems to be below 1 kHz, which can be easily filtered out if the operation frequency is above this limit [8].

Before any of the methods discussed here are used in the human body, one must be certain that the ultrasound exposure does not harm the subject. Vibro-acoustography uses either cw or tone-burst ultrasound. Therefore, the continuous ultrasound intensity (spatial peak temporal average intensity) limit must be observed for the safety reasons. This limit according to the FDA is $720\,\mathrm{mW/cm^2}$. However, because of the high sensitivity of hydrophone detectors, it is possible to detect very small levels of the acoustic emission while using low transmittance power. For example, it is shown that a submillimeter object can be detected at ultrasound intensities far below the FDA limit [9]. The shear-wave method presented in [6] uses high-intensity pulsed ultrasound

for excitation and either the optical or MRI methods for detection. It is argued that, although the intensity is high, the total exposure is within the FDA limits. However, in vivo use of such detection methods would be difficult. Using Doppler ultrasound for detection is less sensitive; hence it requires higher peak ultrasound intensity to produce enough radiation force on the tissue. This intensity level may exceed the safe spatial peak pulse average intensity limit.

5 Summary

The radiation force of ultrasound is a noninvasive means for introducing a highly localized vibrating force inside tissue. The three methods described here utilize this tool to evaluate the dynamic viscoelastic properties of tissue. The transient method measures minute transient tissue deformation versus time. The shear-wave method measures the amplitude and velocity of the shear waves resulting from excitation by a radiation force. Finally, vibro-acoustography measures the acoustic field resulting from object vibration at a specified frequency.

Acknowledgements

This work was supported in part by grant BC971878 from the Army Medical Research and Materiel Command and grant HL 61451 from the National Institutes of Health.

References

1. L. Gao, K. J. Parker, R. M. Lerner, S. F. Levinson, Imaging of the elastic properties of tissue -- a review, Ultrasound Med. Biol. **22**, 959–977 (1996)
2. R. Muthupillai, D. J. Lomas, P. J. Rossman, J. F. Greenleaf, A. Manduca, R. L. Ehman, Magnetic resonance elastography by direct visualization of propagating acoustic strain waves, Science **269**, 1854–1857 (1995)
3. B. T. Chu, R. E. Apfel, Acoustic radiation pressure produced by a beam of sound. J. Acoust. Soc. Am. **72**, 1673–1687 (1982)
4. T. Sugimoto, S. Ueha, K. Itoh, Tissue hardness measurement using the radiation force of focused ultrasound, IEEE Ultrasonics Symp. Proc. **3**, 1377–1380 (1990)
5. V. Andreev, V. Dmitriev, O. V. Rudenko, A. Sarvazyan, A remote generation of shear-wave in soft tissue by pulsed radiation pressure, J. Acoust. Soc. Am. **102**, 3155 (1997)
6. A. P. Sarvazyan, O. V. Rudenko, S. D. Swanson, J. B. Fowlkes, S. Y. Emelianov, Shear wave elasticity imaging: a new ultrasonic technology of medical diagnostics, Ultrasound Med. Biol. **24**, 1419–1435 (1998)
7. W. F. Walker, Internal deformation of a uniform elastic solid by acoustic radiation, J. Acoust. Soc. Am. **105**, 2508–2518 (1999)

8. M. Fatemi, J. F. Greenleaf, Ultrasound-stimulated vibro-acoustic spectrography, Science **280**, 82–85 (1998)
9. M. Fatemi, J. F. Greenleaf, Vibro-acoustography: An imaging modality based on ultrasound-stimulated acoustic emission, Proc. Natl. Acad. Sci. USA **96**, 6603–6608 (1999)
10. Lord Raleigh, Philos. Mag. **3**, 338–346 (1902); see also: Lord Raleigh, Philos. Mag. **10**, 364–374 (1905)
11. R. T. Beyer, Radiation pressure – the history of a mislabeled tensor, J. Acoust. Soc. Am. **63**, 1025–1030 (1978)
12. O. V. Rudenko, A. P. Sarvazian, S. Y. Emelionov, Acoustic radiation force and streaming induced by focused nonlinear ultrasound in a dissipative medium, J. Acoust. Soc. Am. **99**, 1–8 (1996)
13. Jiang Z-Y, J. F. Greenleaf, Acoustic radiation pressure in a three-dimensional lossy medium, J. Acoust. Soc. Am. **100**, 741–747 (1996)
14. P. J. Westervelt, The theory of steady force caused by sound waves, J. Acoust. Soc. Am. **23**, 312–315 (1951)
15. S. A. Goss, R. L. Johnston, F. Dunn, Comprehensive compilation of empirical ultrasonic properties of mammalian tissues, J. Acoust. Soc. Am. **64**, 423–457 (1978)
16. L. A. Frizzell, E. L. Carstensen, Shear properties of mammalian tissues at low megahertz frequencies, J. Acoust. Soc. Am. **60**, 1409–1411 (1976)
17. P. M. Morse, K. U. Ingard (Eds.) *Theoretical Acoustics* (McGraw-Hill, New York 1968)
18. M. Fatemi, J. F. Greenleaf, Application of radiation force in noncontact measurement of the elastic parameters, Ultrasonic Imaging **21**, 147–154 (1999)
19. M. Fatemi, J. F. Greenleaf, Remote measurement of shear viscosity with ultrasound-stimulated vibro-acoustic spectrography, Acta Phys. Sin. **8**, S27–S32 (1999)

Appendix 7

Contrast Coherent Imaging (CCI) at low mechanical index was used. On a semiquantitative scale the capability, to s structures and possible modifications of parenchyma during the basal arterial, portal, and late phases using color or power Doppler with and without echocontrast administration, was evaluated. *RESULTS AND CONCLUSIONS:* Color/power Doppler is widely used for the study of focal liver lesions. Its limitations in terms of sensitivity prevents the possibility of showing the microcirculation. This study demostrates that low MI-CCI and contrast enhancement allow the visualization of both macrovascular and parenchymal circulation characteristics.

Breast Masses

Moderators: Brian S. Garra, MD, and Cynthia L. Rapp, BS, RDMS

3205 Comparison of the Sensitivity of Ultrasound for Demonstration of Benign Versus Malignant Disease at the Time of Needle Localization

Copit DS, Stassi J, Wang J, Cavanaugh BC Albert Einstein Medical Center, Philadelphia, PA*

OBJECTIVE: To compare the efficacy of ultrasound (US) in demonstrating benign disease and invasive breast carcinoma after a mammographic abnormality is identified using needle localization and surgical biopsy for confirmation. *METHODS:* During an 18-month period, 220 localizatons for a mammographic abnormality other than calcifications were attempted using US guidance. After placement of the needle with US, position was confirmed mammographically. Cases were considered positive if (1) the needle passed through the mammographic abnormality, and (2) the mammographic lesion was demonstrated in the specimen radiograph. Retrospective review of these cases was performed to determine the number of benign vs. malignant lesions. *RESULTS:* Eighty-four invasive cancers were identified pathologically, of which 73 had a positive US, giving a sensitivity for US of 94.8%. Of the 143 benign cases, 101 had a positive US, giving a sensitivity of 70.6% for benign disease. *CONCLUSIONS:* Although the US characteristics of both benign and malignant disease have been studied, there is little written about the sensitivity of US once a mammographic abnormality is discovered. We have shown that the sensitivity of US for demonstrating confirmed invasive cancer is higher than that for benign disease. Our findings suggest that the overall sensitivity of US for demonstrating invasive cancer once focused on a mammographic finding may be excellent. This has importance in clinical practice in terms of the potential for increasing the positive predictive value of mammography once abnormalities are seen. Further investigation to support these findings will be necessary.

3210 Breast Sonography Complementary to Mammography in the Identification of Malignancy Causing Mammographic Architectural Distortion

Hashimoto BE, Kramer DJ, Picozzi VJ, Lee ME, Morgan G, Sonntag JS, Boswell S Virginia Mason Medical Center, Seattle, WA*

OBJECTIVE: To correlate mammographic architectural distortion with breast sonography, pathology, and clinical followup. *METHODS:* We retrospectively reviewed reports from 51,962 mammograms from 2 consecutive years. Additional mammographic views were recommended in 3162/51,962 reports (6%). One hundred eighty-eight of 3162 (6%) of these additional views were performed because of mammographic architectural distortion. In 41/188 (21%), the architectural distortion was associated with another mammographic abnormality (density, mass, or calcification). In 156/197 (79%), architectural distortion was the sole abnormality. In 45/188 cases (24%), breast sonograms were performed in addition to mammograms. Histologic information was available for 50/188 cases (27%). *RESULTS:* Twenty-three of 50 biopsies (46%) performed for mammographic architectural distortion were malignant. This malignant biopsy rate is higher than the overall malignancy rate of all breast biopsies performed on this population during the same time period (30%). Pathology results, radiographic, and clinical followup of 188 lesions demonstrated that mammographic additional views had a sensitivity 70%, specificity 91%, PPV 50%, NPV 96%. For the 45 lesions which were evaluated by both mammography and sonography, sonography demonstrated better sensitivity (sensivity 91%, specificity 64%, PPV 62%, NPV 97%) compared to mammography (sensitivity 82%, specificity 43%, PPV 38%, NPV 90%). If both modalities are combined, the sensitivity improves (sensitivity 100%, specificity 44%, PPV 37%, NPV 100%). *CONCLUSIONS:* Breast sonography may have better sensitivity in identifying malignancy compared to mammography alone. The improvement in sensitivity when both modalities are combined suggests that these tests provide complementary information, which may improve detection of malignancy in this group of patients.

3212 Imaging Breast Microcalcification by Vibro-Acoustography

Fatemi M, Wold LE, Morton MJ, Greenleaf JF Mayo Clinic/Foundation, Rochester, MN*

OBJECTIVE: Imaging breast microcalcification in excised tissue by vibro-acoustography. *METHOD:* Vibro-acoustography [Science 280:82-5, 1998] is a novel method evaluating tissue mechanical response at low kHz frequencies. This method utilizes the radiation force of ultrasound to induce low-frequency elastic waves in tissue and detects its response. These waves are detected by an audio hydrophone and can be used to construct an image of the object mechanical properties. Microcalcifications that are much stiffer than the surrounding soft tissue produce a stronger response than the tissue, resulting in high contrast appearance in the final image. Excised breast tissues were scanned by a vibro-acoustography system with a 3-MHz transducer. The vibration frequency of the imaging system was typically in the range of 5 to 28 kHz. High-resolution x-ray tissue mammography of the samples was also obtained and used as control images. *RESULTS:* Vibro-acoustic images of tissue samples provided clear and well defined display of microcalcifications. The number and position of the

microcalcifications matched with those seen in mammography. Microcalcifications as small as 100 microns in diameter could be detected by vibro-acoustography. The presence of microcalcifications was validated by histological study of the samples. *CONCLUSIONS:* Vibro-acoustography can be used for imaging small breast microcalcifications. The non-invasive nature of vibro-acoustography promises in vivo applications, especially in cases where mammography cannot be used either because of high breast density or hazards of x-ray to the patient.

3219 Classification of Breast Lesions Using Multifeature Analysis Procedures

Alam SK,[*1] *Lizzi FL,*[1] *Feleppa EJ,*[1] *Liu T,*[2] *and Kalisz A,*[1] [1]*Riverside Research Institute, New York, NY, and* [2]*Department of Radiation Oncology, Columbia University, New York, NY*

OBJECTIVE: Various features in ultrasound gray scale images are used clinically to discriminate benign from malignant breast lesions. These include acoustic features ("echogenicity," "heterogeneity," "shadowing") and morphometric features ("area," "location," "aspect ratio," "border irregularity," "margin definition"). Accordingly, our goal is to develop a family of quantitative descriptors of breast-lesion features to reliably distinguish benign from malignant lesions and thereby reduce the number of unnecessary breast biopsies. These quantitative descriptors are independent of instrument properties and physician expertise, and are applicable to small tumors. *METHODS:* We quantify acoustic features using calibrated spectrum analysis of radio-frequency (RF) echo signals (rather than gray scale images) and we quantify morphometric features using geometric and fractal parameters. RF echo data were acquired during routine ultrasonic examinations prior to biopsy. Gray scale images were generated from RF data, and lesion boundaries and adjacent areas on the images were manually traced. Spectral parameter maps were computed within these areas to derive quantitative measures of acoustic features. Morphometric features were computed by geometric and fractal analysis of manually traced lesion boundaries. *RESULTS AND CONCLUSIONS:* Early results on biopsy-proven cases are promising and show that multifeature analysis may improve discrimination of cancerous and non-cancerous lesions. We have processed data for 119 patients using 8 quantitative features, and produced an ROC-curve area of 0.8727 ± 0.0416. Lesion echogenicity, aspect ratio, a convexity parameter (descriptor of spiculation), and a fractal-dimension measure (descriptor of border irregularity) were the most useful descriptors. Some morphometric features (e.g., the fractal-dimension measure) were particularly effective in lesion classification.

3202 Lactating Adenoma of the Breast: Sonographic Findings

Sonntag JS, Hashimoto BE Virginia Mason Medical Center, Seattle, WA*

DESCRIPTION OF CASES: Case 1 is a 35-year-old woman with a right breast mass. The patient is 9 months postpartum and breast feeding. An ultrasound of the palpable abnormality corresponds to a 19 mm circumscribed, ellipsoid mass of mixed echogenicity in the inner right breast at 7 o'clock with bilateral edge shadowing. Case 2 is a 33-year-old pregnant woman with a palpable mass in the outer left breast at 3 o'clock. Ultrasound demonstrates a 51 mm hypoechoic, ellipsoid mass with well circumscribed margins and equal transmission. Case 3 is a 21-year-old pregnant woman with an enlarging, palpable abnormality in the outer left breast at 2 o'clock which has been present for several months. Sonographic evaluation discovers a 12 mm lobulated shadowing mass of mixed echogenicity with circumscribed margins. Case 4 is a 31-year-old woman who is 2 months postpartum with a palpable lump in the outer right breast at 3 o'clock. Ultrasound reveals a 30-mm gently lobulated, ellipsoid mass of mixed echogenicity with equal transmission. *PROOF OF DIAGNOSIS:* All cases were histologically proven lactating adenomas biopsied between 1998 and 2000. *RELEVANCE:* Although rare, lactating adenomas are important sonographic findings. Lactating adenomas typically present as palpable masses in pregnant or lactating women, so sonography is generally the first test performed to evaluate these lesions. The above cases demonstrate the spectrum of sonographic findings of lactating adenomas.

3203 Detection of Silicone Adenopathy in Silicone Gel Breast Implant Patients

McNamara MP Jr, Punjabi R MetroHealth Medical Center, Cleveland, OH*

DESCRIPTION OF CASES: Over the last 9 years, we have examined nearly 2000 breast implant patients with ultrasound. Early in our experience, we encountered an implant patient who complained of focal supraclavicular pain and requested that the area be scanned at the completion of her breast implant ultrasound examination. At the site of her concern, a small round hyperechoic mass with a "dirty" acoustical shadow was noted. Given the similarity in appearance to silicone granuloma, a supraclavicular node containing silicone was suspected. The mass was needle localized under ultrasound guidance and pathologically proven as silicone lympadenopathy. Subsequently, we began a systematic search of the remainder of the lymph node chains that drain the breast. As a result, in addition to patients with silicone in intramammary and low axillary (Level 1) nodes, we have subsequently identified patients with silicone-containing nodes in retropectoral (Level 2 and 3), Rotter, supraclavicular, and internal mammary chain lymph nodes in patients with intact and ruptured implants. *PROOF OF DIAGNOSIS:* Diagnosis at each anatomic site was proven with pre-operative localization, operative excision, specimen ultrasound, and histology. *RELEVANCE:* Intramammary and low axillary silicone lymphadenopathy has been reported in the peer reviewed literature. Additionally, one case of internal mammary chain involvement identified with CT has been reported. This paper documents that silicone adenopathy can also affect the other lymphatic chains draining the breast. Further, we illustrate the typical sonographic appearance and the techniques employed to demonstrate it. Most patients with silicone adenopathy had polyurethane-coated implants

Phys. Med. Biol. 45 (2000) 1449–1464. Printed in the UK PII: S0031-9155(00)08618-8

Probing the dynamics of tissue at low frequencies with the radiation force of ultrasound

Mostafa Fatemi and James F Greenleaf

Department of Physiology and Biophysics, Mayo Clinic and Mayo Foundation, Rochester, MN 55905, USA

E-mail: fatemi.mostafa@mayo.edu and jfg@mayo.edu

Received 12 October 1999, in final form 21 March 2000

Abstract. Over the past few years there has been an increasing interest in using the radiation force of ultrasound for evaluating, characterizing and imaging biological tissues. Of particular interest are those methods that measure the dynamic properties of tissue at low frequencies. In this paper we present dynamic radiation force methods for probing tissue as a new field, discuss the inter-relationship of several methods within this field and compare their features. The techniques in this field can be categorized into three groups: transient methods, shear-wave measurement methods and a recently developed method called vibro-acoustography. The last method is the focus of this paper. After briefly describing the key concepts of the first two methods, we will present a detailed description of vibro-acoustography. Finally, we will compare the capabilities and limitations of these methods.

1. Introduction

It is well known that changes in the elasticity of soft tissues are often related to pathology. Traditionally, physicians use palpation as a simple method for estimating the mechanical properties of tissue. In this method, a static force is applied and a crude estimation of tissue elasticity is obtained through the sense of touch. In palpation, the force is applied on the body surface and the result is a collective response of all the tissues below. Clinicians can sense abnormalities if the response to palpation of the suspicious tissue is sufficiently different from that of normal tissue. However, if the abnormality lies deep in the body, or if is too small to be resolved by touch, then the palpation method fails. The dynamic response of soft tissue to a force is also valuable in medical diagnosis. For instance, rebound of tissue upon sudden release of pressure exerted by the physician's finger on the skin provides useful diagnostic information about the issue.

Quantitative measurement of the mechanical properties of tissues and their display in a raster format is the aim of a class of techniques generally called elasticity imaging, or elastography. The general approach is to measure tissue motion caused by an external (or, in some methods, internal) force or displacement and use it to reconstruct the elastic parameters of the tissue. The excitation stress can be either static or dynamic (vibration). Dynamic excitation is of particular interest because it provides more comprehensive information about tissue properties in a spectrum of frequencies; alternatively, the transient behaviour of the tissue could be deduced from the measurements. In most elasticity imaging methods, ultrasound is used to detect the motion or displacement resulting from the applied stress. Magnetic resonance

0031-9155/00/061449+16$30.00

elastography is a recently developed method (Muthupillai *et al* 1995) that employs a mechanical actuator to vibrate the body surface and then measures the strain waves with a phase sensitive magnetic resonance imaging (MRI) machine.

The majority of elasticity imaging methods are based on an external source of force. In these methods the object is pressed by a known amount of force or displacement, and the resulting internal deformations are measured by means of pulse-echo ultrasound. The elasticity of the region of interest is then calculated based on the resulting deformation in relation to the magnitude of the applied force (or displacement). Normally, the region of interest rests deep in the body and away from the source of the force. The force that is actually exerted on the region of interest depends on the elastic properties of the tissues located between the source and the region of interest. Hence, the deformation, and the estimated elasticity of the region of interest, are subject to variables of the intervening tissues.

An alternative strategy is to apply a localized stress directly in the region of interest. One way to accomplish this is to use the radiation pressure of ultrasound. Acoustic radiation force is the time average force exerted by an acoustic field on an object. This force is produced by a change in the energy density of an incident acoustic field (Chu and Apfel 1982), for example, due to absorption or reflection. The use of ultrasound radiation force for evaluating tissue properties has several benefits, for example:

(a) Acoustic (ultrasound) energy is a non-invasive means of exerting force.
(b) Existing ultrasound technology and devices can be readily modified for this purpose, thus eliminating the need for developing a new technology.
(c) Radiation force can be generated remotely inside tissue without disturbing its superficial layers.
(d) The radiation stress field can be highly localized, thus allowing for precise positioning of the excitation point.
(e) Radiation force can be produced in a wide range of frequencies or temporal shapes.

These features make radiation force methods more attractive than other, mostly mechanical, excitation methods used in elasticity imaging.

Tissue probing with the radiation force of ultrasound can be accomplished by a variety of techniques, depending on the excitation and detection methods used. As in elasticity imaging methods with mechanical excitation, the radiation force methods can use either a static or dynamic stress.

It is the opinion of the authors that using a dynamic radiation force to remotely probe tissue has certain unique characteristics and capabilities that can open a new chapter in the field of tissue characterization and imaging. We believe that the techniques based on this phenomenon have the potential to provide new information about tissue that has never been available from other methods. We also believe that it is important to recognize and treat this set of techniques as a new field. In particular, it is insightful to set this new field apart from conventional ultrasound tissue characterization/imaging. A major difference being the fact that using the dynamic radiation stress allows one to analyse the object based on its structural vibration properties as opposed to its ultrasonic parameters.

Our intention in writing this paper is to present the dynamic radiation force methods for probing tissue as a new field by discussing the inter-relationship of several methods within this field and comparing their features. To the best of our knowledge, such a discussion has not been presented in the literature before.

The dynamic radiation force methods may be categorized as:

(a) Transient methods, where an impulsive radiation force is used and the transient response of the tissue is detected by Doppler ultrasound (Sugimoto *et al* 1990).

(b) Shear-wave methods, where an impulsive or oscillating radiation is applied to the tissue and the resulting shear wave is detected by ultrasound or other methods (Andreev *et al* 1997, Sarvazyan *et al* 1998, Walker 1999).

(c) Vibro-acoustography, a method recently developed by the authors, where a localized oscillating radiation force is applied to the tissue and the acoustic response of the tissue is detected by a hydrophone or microphone (Fatemi and Greenleaf 1998, 1999a).

In this paper we systematically discuss the features and capabilities that are offered by the dynamic radiation force techniques. We describe the general approach used in the transient, shear-wave and vibro-acoustography methods. We pay particular attention to the last method, present its theory and discuss its features. Then, we compare the capabilities and limitation of all three methods and discuss their possible applications.

2. Radiation force methods

The acoustic radiation force is a time average force exerted by an acoustic field on an object. This force is an example of a universal phenomenon in any wave motion that introduces some type of unidirectional force on absorbing or reflecting targets in the wave path. For a review of this topic the reader may refer to Chu and Apfel (1982).

Consider a plane ultrasound beam interacting with a planar object of zero thickness and arbitrary shape and boundary impedance that scatters and absorbs. The radiation force vector, $\boldsymbol{F}$, arising from this interaction has a component in the beam direction and another transverse to it. The magnitude of this force, is proportional to the average energy density of the incident wave $\langle E \rangle$ at the object, where $\langle\rangle$ represents the time average, and S the area of the projected portion of the object (Westervelt 1951):

$$\boldsymbol{F} = \boldsymbol{d}_r S \langle E \rangle. \tag{1}$$

Here $\boldsymbol{d}_r$ is the vector drag coefficient with a component in the incident beam direction and another transverse to it. The coefficient $\boldsymbol{d}_r$ is defined per unit incident energy density and unit projected area. For a planar object, the magnitude of $\boldsymbol{d}_r$ is numerically equal to the force on the unit area of the object per unit energy density. Physically, the drag coefficient represents the scattering and absorbing properties of the object, and is given by (Westervelt 1951)

$$\boldsymbol{d}_r = \hat{\boldsymbol{p}} \frac{1}{S} \left(\Pi_a + \Pi_s - \int \gamma \cos \alpha_s \, \mathrm{d}S \right) + \hat{\boldsymbol{q}} \frac{1}{S} \int \gamma \sin \alpha_s \, \mathrm{d}S \tag{2}$$

where $\hat{\boldsymbol{p}}$ and $\hat{\boldsymbol{q}}$ are the unit vectors in the beam direction and normal to it respectively. The quantities Π_a and Π_s are the total absorbed and scattered powers respectively, and γ is the scattered intensity, all expressed per unit incident intensity. Also, α_s is the angle between the incident and the scattered intensity and $\mathrm{d}S$ is the scalar area element. The drag coefficient can also be interpreted as the ratio of the radiation force magnitude on a given object to the corresponding value if the object were replaced by a totally absorbing object of similar size. For simplicity, we assume a planar objected oriented perpendicular to the beam axis. In this case, the transverse component vanishes, thus the drag coefficient (force) will have only a component normal to the target surface which we denote by scalar $d_r(F)$.

To produce a time-varying radiation force, the intensity of the incident beam can be shaped in various ways. For example, a short ultrasound pulse can produce a transient pulsed radiation force, and a sinusoidally modulated beam can result in a sinusoidally varying force.

2.1. Transient methods

In the transient methods the radiation force of ultrasound is used to make a minute deformation in the tissue. The transient recoil of the tissue resulting from this deformation is measured and used for the evaluation of tissue elastic properties.

A method for measuring tissue hardness, presented by Sugimoto *et al* (1990), uses the radiation force of a single focused ultrasound beam. Ideally, hardness may be represented by the spring constant of the object, which is the ratio of the applied force to the displacement. This method relies on evaluating the hardness based on changes in relative values. In this method an ultrasound pulse is used to generate a short-duration radiation force which produces localized deformation of the tissue. Immediately after the force pulse, the resulting transient deformation of tissue is measured as a function of time with Doppler ultrasound using a separate transducer. The deformation includes an initial rapid squeeze of the tissue, followed by a relaxation and possibly a rebound. This displacement is a function of tissue viscoelastic parameters, as well as the applied force. Sugimoto *et al* (1990) argue that because measuring the internal radiation force in an absolute sense *in vivo* is difficult, it is advantageous to derive a quantity that is representative of relative tissue hardness. To derive a single relative quantity from the deformation data, the relaxation part of the function is approximated by a sum of several exponential curves, and the sum of the first-order derivatives of such an exponential is calculated. It is shown that this quantity is correlated with the spring constant of the tissue and thus may be used as a measure of tissue hardness.

2.2. Shear-wave methods

Shear modulus is related to the hardness or elasticity of the material. It is known that the shear modulus of various soft tissues ranges over several orders of magnitude, while bulk modulus, a parameter that is associated with the conventional pulse-echo ultrasound compressional wave speed, varies significantly less than an order of magnitude (Goss *et al* 1978, Frizzell and Carstensen 1976). These features indicate that shear modulus may be a better parameter for tissue characterization than bulk modulus. One way to induce localized shear waves inside tissue is to use the radiation force of focused ultrasound (Andreev *et al* 1997). In a method called shear-wave elasticity imaging (SEWI) (Sarvazyan *et al* 1998), an amplitude-modulated single-focused ultrasound beam is used to induce a localized radiation stress inside the soft tissue. Localization of the stress field is the key to success of the method. To achieve a high degree of localization, the method used a focused ultrasound beam. It is shown that the radiation stress exerted within a dissipative medium peaks near the focal region of a highly focused transducer. It has also been suggested that localization can be improved by designing the transducer and selecting the beam parameters such that a nonlinear shock wave is produced in the focal region, increasing the magnitude of the stress field in the vicinity of the focal region, thus augmenting localization of the stress field (Sarvazyan *et al* 1998).

Modulation of the ultrasound beam can be in the form of an oscillating wave or short pulse. The resulting radiation force elicits a shear wave propagating in the radial direction with respect to the beam axis, with particle motion parallel to the beam axis. Shear waves in soft tissue travel at a very low speed, typically around a few metres per second (Frizzell and Carstensen 1976, Sarvazyan *et al* 1998), thus the corresponding wavelength is much shorter than that of compressional waves for the same frequency. Shear waves are also highly attenuated in soft tissue, with an attenuation coefficient two or three orders of magnitude higher than that of compressional waves (Frizzell and Carstensen 1976, Sarvazyan *et al* 1998). Because of the high attenuation of shear waves, it is possible to induce them in a very limited region in

the vicinity of the focal point of the ultrasound beam, hence avoiding the influence of tissue boundaries. In SWEI, a short ultrasound pulse is delivered to the tissue, causing a radial shear oscillation around the beam axis. By measuring the amplitude and the temporal characteristics of this wave, shear parameters of the tissue, such as shear modulus and shear viscosity, can be calculated. For example, the time required for the wave front to propagate from one point to another can be used to calculate the shear-wave speed, and consequently the shear-wave modulus μ, as

$$\mu = \rho c_t^2 \tag{3}$$

where ρ and c_t are the density and the shear-wave velocity respectively.

Shear waves may be detected optically. In this method a laser source and a photodetector are used to detect the displacement of particles due to the shear wave in a transparent phantom (Sarvazyan *et al* 1998). Because this method requires a transparent medium, its application *in vivo* is difficult. Phase-sensitive magnetic resonance imaging (Muthupillai *et al* 1995, Sarvazyan *et al* 1998) is an alternative method that can be used to measure the two-dimensional distribution of particle displacement in a given direction versus time in a material. In an experiment presented by Sarvazyan *et al* (1998), an ultrasound pulse of 3.6 ms duration produced by a 70 mm diameter transducer focused at 100 mm was transmitted within a cylindrical rubber phantom. The displacement was measured by 2.0 T MRI system at two different times after the acoustic pulse was applied. The position of the peak displacement at these time points was used to estimate the shear velocity, which was shown to be consistent with the independently measured value. Shear waves can also be detected by Doppler ultrasound (Andreev *et al* 1997). It has been shown (Walker 1999) that to achieve the appreciable displacement needed for Doppler detection, most soft tissues require high ultrasound intensities which might be beyond the recommended maximum intensity level for diagnostic ultrasound (FDA 1997).

2.3. *Vibro-acoustography*

2.3.1. Method. This technique produces a map of the mechanical response of an object to a dynamic force applied at each point. The method utilizes ultrasound radiation force to remotely exert a localized oscillating stress field at a desired frequency within (or on the surface of) an object and records the resultant acoustic response (Fatemi and Greenleaf 1998, 1999a). This acoustic response, which is normally in the low kHz range, is a function of the viscoelastic properties of the object and can be used to produce an image of the object.

To produce an oscillating radiation force the intensity of the incident ultrasound must be amplitude modulated at the desired low frequency. Using a single amplitude modulated beam seems to be the simplest means to achieve this. However, such a beam will exert a radiation force on any object that is present along the beam path, producing undesirable acoustic emission. To confine the oscillating radiation stress to the desired region, vibro-acoustography uses two unmodulated CW beams at slightly different frequencies, propagating along separate paths. The beams are arranged to cross each other at their respective foci, and thus produce a modulated field at a confined, small cross-sectional region. The single- and double-beam arrangements are illustrated in figure 1.

2.3.2. System diagram and image formation. Figure 2 illustrates a vibro-acoustography system. The elements of the annular array transducer are driven by two CW signals at frequencies $f_1 = \omega_1/2\pi$ and $f_1 + \Delta f = (\omega_1 + \Delta\omega)/2\pi$. The object to be imaged is placed at the joint focal plane of the transducer elements (the scanning plane). The ultrasound field

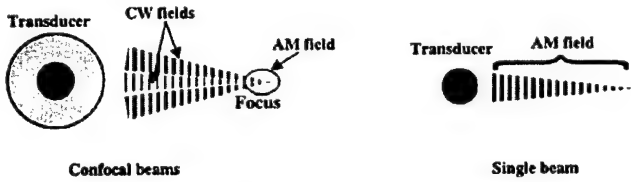

Figure 1. Generation of a modulated ultrasound field by single and confocal beams. The single beam produces a field that is modulated throughout the beam path. This field can produce an oscillating radiation force on any object in the beam path. The confocal annular array transducer generates two CW beams propagating separate paths. These beams interfere near the focal zone, producing a modulated field only in that region. Hence, the oscillating radiation force can only be generated on objects in the beam-crossing region.

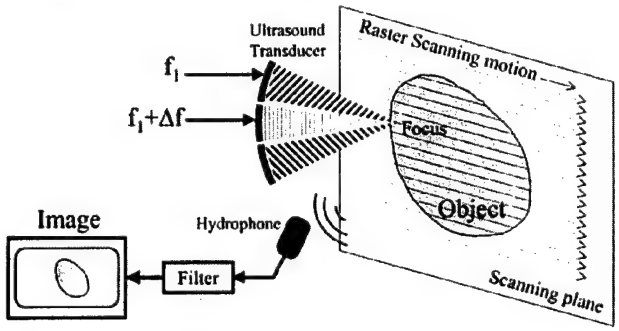

Figure 2. Vibro-acoustography system. The two elements of the confocal annular array are excited by separate CW signals at two different frequencies. The object is placed at the focal plane of the transducer. The ultrasound field produces a radiation force at the difference frequency Δf on the object. This force vibrates the object, which in turn produces a sound field in the medium. This sound field is received by an audio hydrophone placed near the object. To form an image, the beams are scanned in a raster motion across the scanning place, and the resulting acoustic emission is recorded from each point. The brightness of each corresponding point on the image plane is determined by the amplitude (or phase) of the recorded acoustic emission.

produces a localized radiation stress field at the focal point on the object at frequency Δf. Depending on the elastic properties of the object, the radiation force may cause a portion of the object, or the entire object, to vibrate at this frequency. The acoustic emission resulting from object vibration is received by a hydrophone which is located nearby. Normally the wavelength of vibration is large compared with the object size, hence the acoustic emission field is almost omnidirectional. Therefore, hydrophone position is not a critical parameter in this measurement. The filter is used to eliminate noise and other interfering signals. To form an image, the focal point of the transducer is moved across the scanning plane on the object in a raster pattern. The acoustic emission is received at each position, and an image is formed by displaying the amplitude (or phase) of such signals at corresponding positions on the image plane. The spatial resolution of this imaging method is determined by the ultrasound beamwidth at the focal plane, which is normally of the order of the incident ultrasound wavelength.

2.3.3. Theory. In the beam-forming method to be described the amplitude modulated field is obtained by the interference of two unmodulated ultrasound beams. Radially symmetric interfering beams are obtained when two coaxial, confocal transducers are used (Fatemi and

Greenleaf 1999a). For this purpose, elements of a two-element spherically focused annular array (consisting of a central disc with radius a_1 and an outer ring with the inner radius of a_2' and outer radius of a_2 are excited by separate CW signals at frequencies $\omega_1 = \omega_0 - \Delta\omega/2$ and $\omega_2 = \omega_0 + \Delta\omega/2$. We assume that the beams are propagating in the $+z$ direction with the joint focal point at $z = 0$. The resultant field on the $z = 0$ plane may be written as

$$p(t) = P_1(r)\cos(\omega_1 t + \psi_1(r)) + P_2(r)\cos(\omega_2 t + \psi_2(r)) \tag{4}$$

where $r = \sqrt{x^2 + y^2}$ is the radial distance. The amplitude functions are (Morse and Ingard 1968, Kino 1987)

$$P_1(r) = \rho c U_{01} \frac{\pi a_1^2}{\lambda_1 z_0} \operatorname{jinc}\left(\frac{r a_1}{\lambda_1 z_0}\right) \tag{5}$$

and

$$P_2(r) = \rho c U_{02} \frac{\pi}{\lambda_2 z_0}\left[a_2^2 \operatorname{jinc}\left(\frac{r a_2}{\lambda_2 z_0}\right) - a_2'^2 \operatorname{jinc}\left(\frac{r a_2'}{\lambda_2 z_0}\right)\right] \tag{6}$$

where U_{0i} is the velocity amplitude at the ith transducer element surface, and $\lambda_i = 2\pi/\omega_i$ for $i = 1, 2$ are the ultrasound wavelengths. The phase functions

$$\psi_i(r) = -\frac{\pi r^2}{\lambda_i z_0} \tag{7}$$

for $i = 1, 2$, are conveniently set to be zero at the origin. Also, $\operatorname{jinc}(X) = J_1(2\pi X)/\pi X$, where $J_1(.)$ is the first-order Bessel function of the first kind.

The instantaneous energy is $E = p^2(t)/\rho c^2$. Replacing $p(t)$ from equation (4), this energy will have a time-independent component, a component at the difference frequency $\Delta\omega = \omega_2 - \omega_1$ which result from the cross product of the two pressure fields, and high-frequency components at ω_1 and ω_2 and their harmonics. The energy component at the difference frequency is

$$e_{\Delta\omega}(t) = \frac{P_1(r_0)P_2(r_0)}{\rho c^2}\cos(\Delta\omega t + \Delta\psi(r_0)) \tag{8}$$

where $\Delta\psi(r_0) = \psi_2(r_0) - \psi_1(r_0)$.

Now, we define a *unit point target* with an area of $\mathrm{d}x\,\mathrm{d}y$ at position (x_0, y_0) on the focal plane, and with a drag coefficient $d_r(x_0, y_0)$ such that: $d_r(x_0, y_0)\mathrm{d}x\,\mathrm{d}y = 1$ on the target and zero elsewhere. This equation is merely used as a mathematical model. In this case, the projected area can be considered to be $S = \mathrm{d}x\,\mathrm{d}y$. Therefore, if the projected area is unity, then $d_r(x, y) = 1$, which according to equation (2) corresponds to a totally absorptive object.

Referring to equation (1), and replacing $d_r S$ with unity and $\langle E\rangle$ by $e_{\Delta\omega}(t)$ of equation (8), then we can write the low-frequency component of the radiation force on the unit point target as

$$f_{\Delta\omega}(x_0, y_0; t) = \frac{1}{\rho c^2} P_1(r_0)P_2(r_0)\cos(\Delta\omega t + \Delta\psi(r_0)) \tag{9}$$

where arguments x_0 and y_0 are added to denote the position of the point target, and $r_0 = \sqrt{x_0^2 + y_0^2}$. Referring to equations (5) and (6), the complex amplitude of the stress field can be found as:

$$F_{\Delta\omega}(x_0, y_0) = \rho U_{01} U_{02} \frac{\pi a_1^2}{\lambda_1 z_0}\operatorname{jinc}\left(\frac{r_0 a_1}{\lambda_1 z_0}\right)\left[\frac{\pi a_2^2}{\lambda_2 z_0}\operatorname{jinc}\left(\frac{r_0 a_2}{\lambda_2 z_0}\right) - \frac{\pi a_2'^2}{\lambda_2 z_0}\operatorname{jinc}\left(\frac{r_0 a_2'}{\lambda_2 z_0}\right)\right]$$
$$\times \exp\left(-\mathrm{j}\frac{r_0^2}{2\Delta\lambda z_0}\right) \tag{10}$$

where $\Delta\lambda = 2\pi c/\Delta\omega$ is the wavelength associated with $\Delta\omega$. The above equation indicates that the radiation stress is concentrated at the focal point and decays down quickly with distance as jinc(.)^2.

As an example, we consider a confocal transducer with dimensions $a_1 = 14.8$ mm, $a_2' = 16.8$ mm, $a_2 = 22.5$ mm, and focal length 70 mm. Also, we assume that the centre frequency is 3 MHz, and the difference frequency is 7.3 kHz. The radiation stress at the focal plane of this transducer is plotted in figure 3.

In medical applications the maximum ultrasonic intensity is regulated for safety reasons. It is useful, therefore, to write the stress field in terms of the peak ultrasonic intensity at the focal point. The long-term average of ultrasonic intensity at the focal point can be written as

$$I(0) = \frac{P_1^2(0) + P_2^2(0)}{2\rho c} \tag{11}$$

where $P_1(0)$ and $P_2(0)$ can be found from equations (5) and (6) as

$$I(0) = \frac{\rho c}{2}\left[U_{01}^2\left(\frac{\pi a_1^2}{\lambda_1 z_0}\right)^2 + U_{02}^2\left(\frac{\pi}{\lambda_2 z_0}\right)^2 (a_2^2 - a_2'^2)^2\right]. \tag{12}$$

Assuming $U_{01} = U_{02} = U_0$, we can write the focal plane stress field in terms of $I(0)$:

$$F_{\Delta\omega}(x_0, y_0) = \frac{2I(0)}{c}\frac{\pi a_1^2/\lambda_1 z_0}{(\pi a_1^2/\lambda_1 z_0)^2 + (\pi/\lambda_2 z_0)^2(a_2^2 - a_2'^2)^2}\text{jinc}\left(\frac{r_0 a_1}{\lambda_1 z_0}\right)$$
$$\times\left[\frac{\pi a_2^2}{\lambda_2 z_0}\text{jinc}\left(\frac{r_0 a_2}{\lambda_2 z_0}\right) - \frac{\pi a_2'^2}{\lambda_2 z_0}\text{jinc}\left(\frac{r_0 a_2'}{\lambda_2 z_0}\right)\right]\exp\left(-\text{j}\frac{r_0^2}{2\Delta\lambda z_0}\right). \tag{13}$$

The first fraction in the above equation represents the static radiation force produced by the two beams on a total absorber, the second fraction is a constant factor, and the rest represents the spatial distribution of the stress field on the focal plant. If $\Delta\omega \ll \omega_2$, then we may replace λ_1 and λ_2 by λ_0, and simplify the expression for the stress field. Under these conditions, the stress at the focal point is

$$F_{\Delta\omega}(0, 0) = \frac{2I(0)}{c}\frac{a_1^2(a_2^2 - a_2'^2)}{a_1^4 + (a_2^2 - a_2'^2)^2}. \tag{14}$$

The fraction on the right represents the effect of transducer dimension on the stress field. For the transducer used in the previous example, the value of this fraction is 0.4999. (This fraction can be also calculated for a signal-element transducer of the same diameter, excited by an amplitude modulated signal. For this purpose, we may let $a_1 = a_2$ and $a_2' = 0$. For these values, the last fraction in equation (14) is 0.5.) The resulting radiation stress (assuming $c = 1500$ m s^{-1} for water) is $F_{\Delta\omega}(0, 0) = 6.67 \times 10^{-4} I(0)$ N m^{-2}. If we let $I(0) = 7200$ W m^{-2}, which is the maximum spatial peak, time average intensity suggested by the FDA for *in vivo* applications, (FDA 1997), the resulting stress at the focal point is $F_{\Delta\omega}(0, 0) = 4.80$ N m^{-2}. Referring to figure 3, we note that this stress field is applied only in a small region around the focal point to the object.

2.3.4. Acoustic emission. To explain the acoustic emission we consider an 'object' within a homogeneous infinite medium. This model allows us to separate the roles played by the parameters of the object and the surrounding medium, and can be fitted to various applications. When an oscillating stress field is applied to the object, the object vibrates at the frequency of the stress field. Vibrational energy of the object is partly transferred to the surrounding medium, which is called the acoustic emission field. Here, we calculate the acoustic emission of an object resulting from applying the radiation stress.

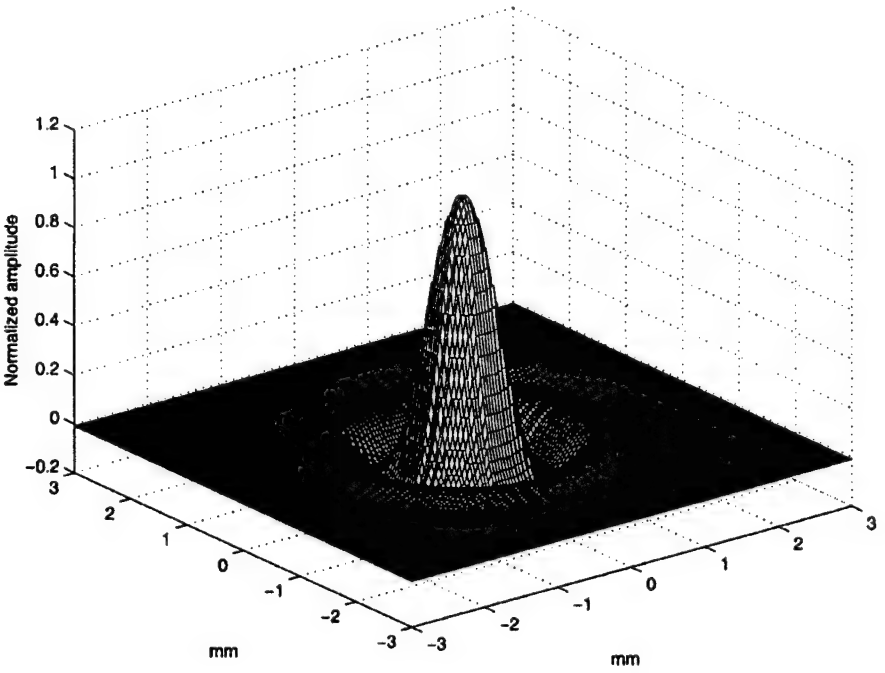

Figure 3. Three-dimensional plot of the stress field amplitude of a confocal annular array transducer at the focal plane at a point in time. Transducer dimensions are: $a_1 = 14.8$ mm, $a_2' = 16.8$ mm, $a_2 = 22.5$ mm, and the focal length is 70 mm. The centre frequency is 3 MHz and the difference frequency is 7.3 kHz.

To explain the physics in more generalized terms, for the moment we consider an object in the form of a flat disc facing the beam. Here, we assume that the vibrating object has a circular cross section of radius b and uniformly vibrates back and forth like a piston. This choice allows us to illustrate the concept in a simple form. We also consider an area $S \leqslant \pi b^2$ of the piston surface to be projected normally by the beam. We can always return to our elementary point object by reducing the area of this disc to $\mathrm{d}x\,\mathrm{d}y$. Similar solutions can be carried out for objects of other forms. The theory can be also extended to include arbitrary vibrating-part shapes and non-uniform displacement of the object. The total radiation force on this object $\overline{F_{\Delta\omega}}$, can be found by integrating the radiation stress over the area of the object. This force vibrates the target object at frequency $\Delta\omega$. The steady-state normal velocity amplitude of a piston at frequency $\Delta\omega$, $U_{\Delta\omega}$, due to a harmonic force $\overline{F_{\Delta\omega}}$, can be written as:

$$U_{\Delta\omega} = \frac{\overline{F_{\Delta\omega}}}{Z_{\Delta\omega}} \tag{15}$$

where $Z_{\Delta\omega}$ is the mechanical impedance of the object at $\Delta\omega$. The mechanical impedance of the object has two components, one resulting from the inertia, friction and elasticity of the object itself, and the other resulting from the loading effect of the surrounding medium on the vibrating object. The mechanical impedance can be interpreted as a measure of object rigidity and how much it yields to the applied force. For example, for a rigid object , $Z_{\Delta\omega}$ is high, and hence the object resist the force.

Knowing $U_{\Delta\omega}$, we can calculate the pressure field it produces in the medium. We assume that the acoustic emission signal propagates in a free and homogeneous medium. The farfield acoustic pressure due to a piston source of radius b set in a planar boundary of infinite extent is given by (Morse and Ingard 1968)

$$P_{\Delta\omega} = -\mathrm{j}\Delta\omega\rho\frac{\exp(\mathrm{j}\Delta\omega l/c)}{4\pi l}\left(\frac{2J_1[(\Delta\omega b/c)\sin\vartheta]}{(\Delta\omega b/c)\sin\vartheta}\frac{\cos\vartheta}{\cos\vartheta+\beta_B}\right)(2\pi b^2 U_{\Delta\omega}) \tag{16}$$

where l is the distance from the observation point to the centre of the piston, ϑ is the angle between this line and the piston axis and β_B is the specific acoustic admittance of the boundary surface. (The specific acoustic admittance is $\beta_B = \rho c/z_B$, where Z_B, the acoustic impedance of the boundary, represents the ratio between the pressure and normal fluid velocity at a point of the object.) The factor of two in the parentheses comes from the presence of the boundary wall. It would be replaced by unity if the boundary wall were not present (Morse and Ingard 1968).

The acoustic emission field resulting from object vibration can be written in terms of object mechanical impedance by combining equations (15) and (16) as

$$P_{\Delta\omega} = \rho c^2\left[\mathrm{j}\frac{\Delta\omega}{c^2}\frac{\exp(\mathrm{j}\Delta\omega l/c)}{4\pi l}\left(\frac{2J_1[(\Delta\omega b/c)\sin\vartheta]}{(\Delta\omega b/c)\sin\vartheta}\frac{\cos\vartheta}{\cos\vartheta+\beta_B}\right)\right]\frac{2\pi b^2}{Z_{\Delta\omega}}\overline{F_{\Delta\omega}}. \tag{17}$$

For wavelengths which are long compared with the object size, i.e. when $b\Delta\omega/c \to 0$, the term in the large round brackets approaches a constant because $2J(X)/X \to 1$ for $X \to 0$. Hence, ignoring the first fraction in the large parentheses, we may consider the contents of the large square brackets to be an object-independent function (the specific acoustic admittance β_B relates to the surrounding boundary surface). Under these conditions, the large square brackets in the above equation represents the effect of the medium on the acoustic emission field, which we may call the *medium transfer function*, and denote it by

$$H_{\Delta\omega}(l) = \mathrm{j}\frac{\Delta\omega}{c^2}\frac{\exp(\mathrm{j}\Delta\omega l/c)}{4\pi l}\frac{\cos\vartheta}{\cos\vartheta+\beta_B}. \tag{18}$$

The last fraction in equation (17) includes $1/Z_{\Delta\omega}$, which is the mechanical admittance of the object at the frequency of the acoustic emission ($\Delta\omega$), and we denote this by $Y_{\Delta\omega}$. It is convenient to combine this term with the next term ($2\pi b^2$) in equation (17), as $Q_{\Delta\omega} = 2\pi b^2 Y_{\Delta\omega} = 2\pi b^2/Z_{\Delta\omega}$, which is the total acoustic outflow by the object per unit force (acoustic outflow is the volume of the medium, e.g. the fluid, in front of the object surface that is displaced per unit time due to object motion). Function $Q_{\Delta\omega}$ represents the object characteristics at the acoustic frequency. We may thus rewrite equation (17) in a more compact form as

$$P_{\Delta\omega} = \rho c^2 H_{\Delta\omega}(l) Q_{\Delta\omega}\overline{F_{\Delta\omega}}. \tag{19}$$

Equation (19) indicates that the acoustic emission pressure is proportional to:

(a) The radiation force, which itself is proportional to the square of ultrasound pressure and the ultrasound characteristics of the object, d_r, and the projected area S.
(b) The acoustic outflow by this object, $Q_{\Delta\omega}$, representing the object size b and its mechanical admittance at the acoustic frequency, $Y_{\Delta\omega}$.
(c) The transfer function of the medium at the acoustic frequency, $H_{\Delta\omega}(l)$.

Note the difference between the projection area S and the vibrating area πb^2. The projection area determines the extent of the force applied to the object (equation (1)). The vibrating area, however, influences the total acoustic outflow in the medium caused by object vibration.

2.3.5. Measuring the acoustic emission. A hydrophone is used to measured the acoustic emission field. Equation (18) indicates that for wavelengths which are long compared with the object size, the acoustic emission field pattern resembles that of a dipole with an angle dependency represented by the last fraction to the right of this equation. This angle dependency is normally weak, and hence the position of the receiving hydrophone is not critical. Also, because the attenuation of low-frequency acoustic waves in tissue and liquids is normally low, one may place the hydrophone at a distance from the object without losing too much intensity. The simplified diagram presented in figure 2 describes how to measure the amplitude of the acoustic emission field. To measure the phase of the acoustic emission, a phase reference needs to be set. One way to accomplish this is to generate a reference signal by electronic down-mixing of the two CW excitation signals to produce a beat signal at the difference frequency Δf. Then, using this reference signal, the phase of the acoustic emission signal (hydrophone output) can be calculated by conventional phase detection methods.

2.3.6. Applications. Evaluation of the characteristics of an object (or a medium) by listening to its sound is a traditional approach that has been used for many purposes. Qualitative evaluation of a crystal glass by tapping on it is a simple example. Vibro-acoustography implements the same approach but on a micro-scale, and in a way that could be applied to tissues.

Equation (19) represents a general relationship between the mechanical parameters of the object, surrounding medium, and the acoustic emission field resulting from object vibration. By measuring the acoustic emission field, it would be possible, in principle, to estimate some of the object or medium parameters, either in an absolute or in a relative sense. For example, one can use vibro-acoustography to measure the resonance frequency of an object, and from that information it is possible to estimate some viscoelastic parameters of the object or the medium. This method has been used to measure the Young's modulus of a metallic rod (Fatemi and Greenleaf 1999b). In another experiment, by measuring the resonance frequency of a known resonator in a liquid medium, the viscosity of the fluid has been estimated with good accuracy (Fatemi and Greenleaf 1999c). These applications are not necessarily medical, but the principle could be used for evaluation of soft tissues, blood, bone, etc.

In medical applications, one can use vibro-acoustography to obtain an image of the object for diagnostic purposes. In such applications, the image may not represent a physical quantity, rather it provides a means to visualize object details.

2.3.7. Experimental results. In the following experiment vibro-acoustography has been used to image excised human carotid arteries that include calcifications. Characteristics of the ultrasound transducer used here are those described in the example presented in section 2.3.3. The object consists of two excised human carotid arteries secured on a thin sheet of latex. This sheet is almost transparent to the ultrasound and x-ray. Figure 4(*a*) shows an x-ray image of these arteries. The left artery is from a young person and shows no calcification. The right artery is from an older person and includes some calcium deposit which can be seen as a bright region near the bifurcation. The arteries were immersed in a water tank for scanning. The difference frequency Δf in this experiment is 7 kHz. The lead number '2' was placed on the latex sheet for identification purposes. Figure 4(*b*) shows the vibro-acoustography image (displaying the amplitude of the acoustic emission signal) of the object. In this image, the calcified region is seen as a bright region, resembling its x-ray image. Calcification, which is formed from stiff (compared with the arterial wall) material, is an efficient acoustic radiator, producing strong acoustic emission when exposed to the radiation force of the incident ultrasound. Hence, it

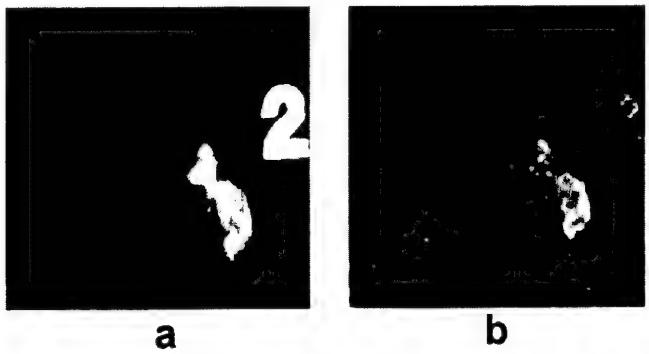

Figure 4. Vibro-acoustography of excised human carotid arteries: (*a*) x-ray image showing a normal (left) and a calcified (right) artery placed on a sheet of latex; (*b*) vibro-acoustography of the arteries in (*a*) measurement at a vibration frequency of 7 kHz. The calcification is seen as a bright region in both x-ray and vibro-acoustography images. Lead number '2' is used for identification.

stands out in the vibro-acoustography image. This image has a high spatial resolution (about 0.7 mm), low speckle and high signal-to-noise ratio. The number '2', which is also made from a hard material, is seen with high contrast. This experiment demonstrates the utility of the method in delineating stiff material against a soft background.

3. Comparisons of the methods

In this paper we have presented three approaches for using a localized ultrasound radiation force to probe biological materials. Here we compare the features and capabilities of the methods.

3.1. Objectives

The transient method estimates a quantity that correlates to the hardness of tissue. While it does not estimate a specific physical parameter, the estimated parameter is quantitative and may be useful for diagnosis.

Shear-wave methods aim specifically at the shear-wave characteristics in soft tissue, in particular, estimating the shear-wave velocity. Shear-wave velocity in soft tissue is very low (typically in the order of a few m s^{-1}), allowing localized measurement of the parameter. Also, because shear-wave attenuation in soft tissue is high, the boundaries of the object have minimal effect on the measurement. This method is not intended for use in hard materials.

Vibro-acoustography has a two-fold objective. In this method, the acoustic emission signal is dependent on both microstructure (local drag coefficient) and macrostructure (the mechanical admittance) of the object. The acoustic emission signal can be analysed to estimate different characteristics of the object. In some applications, both the local parameters and those that are related to the large-scale structure of an object are needed. An instructive example presented in Fatemi and Greenleaf (1999a) demonstrates that vibro-acoustography can be used to produce an image of a tuning fork displaying its detail (microstructure) while measuring its resonance frequency (a parameter related to the macrostructure) represented by colour.

3.2. Excitation method

In the first two methods the radiation force is produced by a single focused transducer which is driven by an amplitude modulated signal, in particular pulse shaped (the shear-wave method can, in principle, operate using a single sinusoidally modulated beam). Vibro-acoustography, however, uses two CW excitation signals (or long tone bursts of CW signals). The major difference in these excitation techniques is the distribution of the radiation stress in the depth direction. A possible drawback of using a single amplitude modulated beam method is that the pulsed ultrasound exerts a radiation stress on all tissue through which it propagates. Also, a shock can be produced on the transducer surface, and then transmitted to the tissue. Such phenomena result in extraneous motion of the object that could introduce errors in the measurements. In vibro-acoustography, the two CW beams pass through separate paths. Outside of their interaction at the focal region, they can only produce a static radiation force on the object, which produces no sound. The beams mix near the focal point to produce a modulated field that can generate an oscillating radiation force only in that location. The resulting acoustic field, therefore, is directly related to the excitation of the object at the focal area. This is an important feature, because the acoustic emission from other parts of the object or the transducer should not be allowed to interfere with the acoustic emission from the focal area.

3.3. Detection method

The transient method and the shear wave method are based on localized detection of displacement of material. This is implemented by using Doppler ultrasound, optical displacement measurement or a more sophisticated method such as MRI. Vibro-acoustography uses an audio hydrophone or microphone for detection, which is a much simpler detection method than Doppler or MRI.

3.4. Sensitivity

Detection sensitivity is critical to the success of any of the above methods. A greater ultrasound intensity would be needed if the detection sensitivity is poor. Ultrasound Doppler methods, at conventional ultrasound frequencies, can probably detect displacements of the order of a few micrometres. The sensitivity of the MRI technique is of the order of 100 nm (Muthupillai *et al* 1995). Vibro-acoustography has been shown to detect motions as small as a few nanometres (Fatemi and Greenleaf 1998). The high sensitivity of this method is a result of the fact that small motions of the object can produce an acoustic emission pressure field that is easily detectable by a sensitive hydrophone.

3.5. Measured quantities

The quantity measured in the transient method is somewhat arbitrary, and not a direct measure of any physical quantity. The merit of this method is that tissue hardness is measured from relative displacement values, without the need to measure the applied force. The shear wave methods directly measure a physical parameter of the material in an absolute sense. The acoustic emission field measured in vibro-acoustography is a function of several physical parameters that relate to the object and the surrounding medium. It is possible to measure a single parameter only if one has enough knowledge about other parameters involved. For example, one can measure the shear viscosity of a liquid using a known resonator as an object

in the liquid (Fatemi and Greenleaf 1999c), or, for a given the geometry, the Young's modulus of a metallic object can be measured (Fatemi and Greenleaf 1999b) by vibro-acoustography.

3.6. Exposure safety

The shear-wave method presented in Sarvazyan *et al* (1998) uses high-intensity pulsed ultrasound for excitation and either the optical or MRI methods for detection. It is argued that, although the intensity is high, the total exposure is within the FDA limits (FDA 1997). These limits are recommended based on possible thermal and mechanical effects of ultrasound on tissue. However, *in vivo* use of such detection methods would be difficult. Using Doppler ultrasound for detection is less sensitive, and hence requires a high peak ultrasound intensity to produce enough displacement of the tissue. This intensity level may exceed the recommended spatial peak pulse average intensity limit.

Vibro-acoustography uses either CW or tone burst ultrasound. Therefore, the continuous ultrasound intensity (spatial peak time average intensity) limit must be observed. This limit, according to the FDA, is 720 mW cm^{-2} (FDA 1997). However, because of the high sensitivity of the hydrophone detector, it is possible to detect very small levels of acoustic emission while using low transmit power. For example, it has been shown that a submillimetre object can be detected at ultrasound intensities far below the FDA limit (Fatemi and Greenleaf 1999a).

3.7. In vivo applicability

In vivo application of the transient method is not likely because it requires high ultrasound power to produce a detectable displacement. Application of the shear-wave method in the human body largely depends on the detection method used. Optical methods are probably not usable *in vivo*. MRI detection methods are generally complex, especially when the operation is to be linked to the ultrasound system in the magnetic field. Ultrasound Doppler is a more practical detection method for shear-wave detection; however, its sensitivity may not be sufficient for ultrasound intensities within the recommended maximum level (Walker 1999). Vibro-acoustography uses a hydrophone for detection, which is simple to operate in clinical settings. It, however, requires an acoustically quiet environment for proper detection. The biological noise spectrum seems to be below 1 kHz, which can be easily filtered out if the operation frequency is above this limit (Fatemi and Greenleaf 1999a).

3.8. Image resolution

Imaging complex objects using the transient or the shear-wave methods has not been fully explored in the literature. Vibro-acoustography can be used for high-quality imaging. The spatial resolution is proportional to the width of the main lobe of the stress field. For example, for the 3 MHz ultrasound transducer presented in figure 3, the spatial resolution is about 700 μm.

3.9. Material properties

Both the transient and shear-wave methods are based on local deformation of soft tissue in the beam direction. These methods work best if the material under test supports the shear wave, has enough attenuation to allow the build-up of enough radiation force, and is compliant enough to allow appreciable displacement. Application of these methods for hard material, such as bone and calcifications, would be difficult or impractical because (a) stiff materials have low compliance, hence, their displacement in response to the force is relatively small

and difficult to detect and (b) the shear wave travels at high speed in such material. In vibro-acoustography hard materials produce structural vibrations which are often stronger than those of soft tissue. Such vibrations result in strong and easily detectable acoustic emissions. The bright appearance of the arterial calcifications in the experiment presented in figure 4 is a demonstration of this phenomenon.

In contrast to the other two methods, vibro-acoustography can be used to detect particles in materials that do not support shear waves, for example detecting gas bubbles in liquids. The acoustic emission resulting from particle vibration includes a compressional wave component that can travel in the surrounding medium including the liquid. Tissue attenuation for compressional waves at low frequencies is small, hence such waves can be detected by the hydrophone from a distance. Shear waves in a liquid medium decay very rapidly and are difficult to detect by most methods.

4. Summary

Recent progress on techniques for evaluation of dynamic viscoelastic parameters of tissue, based on the radiation force of ultrasound, has prompted us to view these techniques as an emerging new field. We recognize the capabilities and potentials of this new field as unique and distinguishable from those of conventional elasticity or ultrasound imaging techniques.

Three methods for probing biological tissue using the dynamic radiation force of ultrasound were presented. The transient method measures a minute transient tissue deformation versus time. The shear-wave method also uses a transient excitation, but measures the resulting shear-wave amplitude and velocity. The last method, vibro-acoustography, measures the acoustic field resulting from the vibration of an object at a specified frequency. Capabilities and limitation of these methods for probing different materials and their potentials for *in vivo* application were discussed.

Acknowledgments

This work was supported in part by grant DAMD17-98-1-8121 from the Army Medical Research and Materiel Command and grant HL 61451 from the National Institutes of Health.

References

Andreev V, Dmitriev V, Rudenko O V and Sarvazyan A 1997 Remote generation of shear wave in soft tissue by pulsed radiation pressure *J. Acoust. Soc. Am.* **102** 3155

Chu B-T and Apfel R E 1982 Acoustic radiation pressure produced by a beam of sound *J. Acoust. Soc. Am.* **72** 1673–87

Fatemi M and Greenleaf J F 1998 Ultrasound-stimulated vibro-acoustic spectrography *Science* **280** 82–5

——1999a Vibro-acoustography: An imaging modality based on ultrasound-stimulated acoustic emission *Proc. Natl. Acad. Sci. USA* **96** 6603–8

——1999b Application of radiation force in noncontact measurement of the elastic parameters *Ultrason. Imaging* **21** 147–54

——1999c Remote measurement of shear viscosity with ultrasound-stimulated vibro-acoustic spectrography *Acta Phys. Sinica* **8** S27–32

FDA 1997 Information for manufacturers seeking marketing clearance of diagnostic ultrasound systems and transducers *US Department of Health and Human Services Food and Drug Administration Report* (Rockville, MD: FDA)

Frizzell L A and Cartensen E L 1976 Shear properties of mammalian tissues at low megahertz frequencies *J. Acoust. Soc. Am.* **60** 1409–11

Goss S A, Johnston R L, Dunn F 1978 Comprehensive compilation of empirical ultrasonic properties of mammalian tissues *J. Acoust. Soc. Am.* **64** 423–57

Kino G S 1987 *Acoustics Waves: Devices, Imaging, and Analog Signal Processing* (Englewood Cliffs, NJ: Prentice-Hall)

Morse P M and Ingard K U 1968 *Theoretical Acoustics* (New York: McGraw-Hill)

Muthupillai R, Lomas D J, Rossman P J, Greenleaf J F, Manduca A and Ehman R L 1995 Magnetic resonance elastography by direct visualization of propagating acoustic strain waves *Science* **269** 1854–7

Sarvazyan A P, Rudenko O V, Swanson S D, Fowlkes, J B and Emelianov S Y 1998 Shear wave elasticity imaging: a new ultrasonic technology of medical diagnostics *Ultrasound Med. Biol.* **24** 1419–35

Sugimoto T, Ueha S and Itoh K 1990 Tissue hardness measurement using the radiation force of focused ultrasound *IEEE Ultrason. Symp. Proc.* **3** 1377–80

Walker W F 1999 Internal deformation of a uniform elastic solid by acoustic radiation force *J. Acoust. Soc. Am.* **105** 2508–18

Westervelt P J 1951 The theory of steady force caused by sound waves *J. Acoust. Soc. Am.* **23** 312–15

SHEAR PROPERTY CHARACTERIZATION OF VISCOELASTIC MEDIA USING VIBRATIONS INDUCED BY ULTRASOUD RADIATION FORCE

A Thesis
Submitted to the Faculty of
the Mayo Graduate School

By

Shigao Chen

in partial fulfillment of the requirements for the
degree of
Doctor of Philosophy in Biomedical Sciences -
Biomedical Imaging

May 2002

Acknowledgements

I would like to express my heartfelt thanks to my advisor Dr. James F. Greenleaf who has been a great mentor and resource. His insight inspiration, encouragement, and patience have been the driving force for the successful completion of my research and thesis. I am also very grateful for the support and guidance of other members of my thesis committee: Dr. Kai-Nan An, Dr. Mostafa Fatemi, Dr. Armando Manduca, and Dr. Erik L. Ritman. Their critique of my work has been tremendous helps to me. Special thanks to Dr. Fatemi for his helpful comments on the project and the writing of the thesis, and Dr. An for his helps on the DMA measurement of shear elasticity.

I appreciate the assistance from Randall R. Kinnick on experiments. Dr. Tao Wu helped validate the shear modulus measurement with MRE. I'd like to thank all the people in the ultrasound lab who helped me directly and indirectly during the past years: Tom Kinter, Elaine Quave, Dr. Xiaohui Hao, Dr. Travis Oliphant, Dr. Todd Pitts, Dr. Cristina Pislaru, Dr. Marek Belohlavek, Dr. Xianoming Zhang, Dr. Azra Alizad, Mohammad Zeraati, and Glauber Tomaz.

I am blessed with an incredibly loving family. Without them I would not have accomplish anything. I would like to dedicate this thesis to them. Finally, I'd like to thank Mayo Graduate School for providing me this cherishable opportunity to pursue advanced education here in USA.

Contents

Chapter 1

Introduction

1.1 General background

Predicting and understanding the behavior of material when they are subject to mechanical forces is the basis for many modern engineering practices, from material science to the design of solid propellant rockets [Timoshenko et al. 1970]. In the early development of the field of mechanics, it often involved applying loads to the system until the system failed, and then the failure mechanism was studied and used to infer the behavior of the material prior to failure. Then, as the technology advanced, it became possible to study the behavior of complex material systems using non-destructive testing procedures, e.g. X-ray analysis, acoustic behavior and photo-elastic behavior. The results of experimental study have contributed to the understanding of material properties and to development of mathematical models that help predict the behavior of more complex material systems [Cheney 1997].

In recent years, this concept has been introduced into medical diagnosis and produced significant amounts of research interest. The primary motivation for imaging tissue mechanical properties stems from the following two important facts.

First, it is well known that changes in tissue mechanical properties such as the elastic modulus can be sensitive indicators of pathology. Palpation, the routine physical examination process used by physicians to distinguish between normal and abnormal tissues is a method for qualitative estimation of tissue elasticity. The clinical success of palpation as a diagnostic tool is evident from the fact that the American Cancer Society recommends breast self-examination as a screening tool for early detection of breast cancer [Holleb et al. 1991]. In some series, 30% of breast cancers are detected by palpation only and not by mammography [Chapuis and Hessler]. Changes in mechanical properties may also indicate the physiologic state of the tissue, e.g., relaxed and contracted states of muscle [Levinson et al. 1995; Duck 1990].

Second, it is also known that the elastic modulus can vary by several orders of magnitude between various tissues. This is in marked contrast with parameters provided by other existing imaging modalities. For example, the ability of conventional B-mode ultrasound imaging to differentiate various tissues depends principally on the acoustic impedance, which in turn depends upon the bulk modulus of the tissue under examination. Figure 1.1 is a summery of material properties for various biological tissues from the literature [Sarvazyan et al. 1998]. It shows that for soft tissues, the range of variation of bulk modulus is very small compared to that of the shear modulus. In X-ray imaging, the variation in X-ray attenuation coefficients of soft tissues is less than

a factor of five and in MR imaging, the variation in the tissue relaxation parameters spans barely an order of magnitude [Muthupillai 1997].

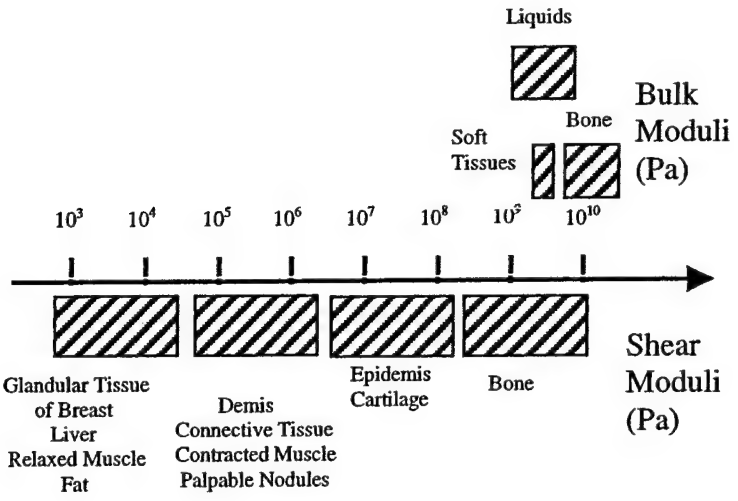

Figure 1.1 Summary of data from the literature concerning the variation of the shear and bulk moduli for various materials and body tissues After Sarvazyan *et al.* (1998).

For the two reasons described above, imaging techniques that exploit the shear modulus, or stiffness, of an object have great potential in medical application. This also explains why elasticity imaging [Gao *et al.* 1996; Ophir et al. 1996, 1999], a general material characterization method under extensive investigation in recent years, has been primarily aimed for tissue characterization. While substantial variations exist in how the details are implemented, all elasticity imaging methods share the following basic elements:

- a mechanical force is applied,
- material motions are measured,
- some derived-quantity is reported.

Elasticity imaging methods can be classified according to how these three elements are implemented. Mechanical force can be applied in a quasi-static, or dynamic fashion. In addition, forces can be either endogenous (naturally

occurring) or exogenous (artificially applied). Exogenous methods can be further distinguished based on whether the force is applied at the surface of the material or deep within the object using radiation force. Material motions can be measured using acoustic, ultrasonic, optical, or nuclear magnetic resonance methods. Furthermore, there are several quantities that can be usefully derived and reported from the measured motion including vibration amplitude and phase, strain, modulus, and apparent phase-velocity (wave-speed). Figure 1.2 is a summary of this classification scheme.

Most elasticity imaging methods use distribution of motion within the object as display. However, it is only a semi-quantitative mapping of the true mechanical properties of the underlying material. When the object being imaged is very complex, the interpretation of the strain distribution image is not straightforward and various artifacts can result [Ophir *et al.* 1996]. Various efforts were made to reconstruct the true elastic modulus of the object, as will be described in Chapter 2. But this generally requires knowledge of stress distribution within the object, which is difficult to obtain. Some methods (i.e. MRE) cleverly use estimation of local shear wave speed to solve for local shear modulus. Since the shear wave speed is also related to shear viscosity, stiffness obtained with such methods is not truly elastic modulus.

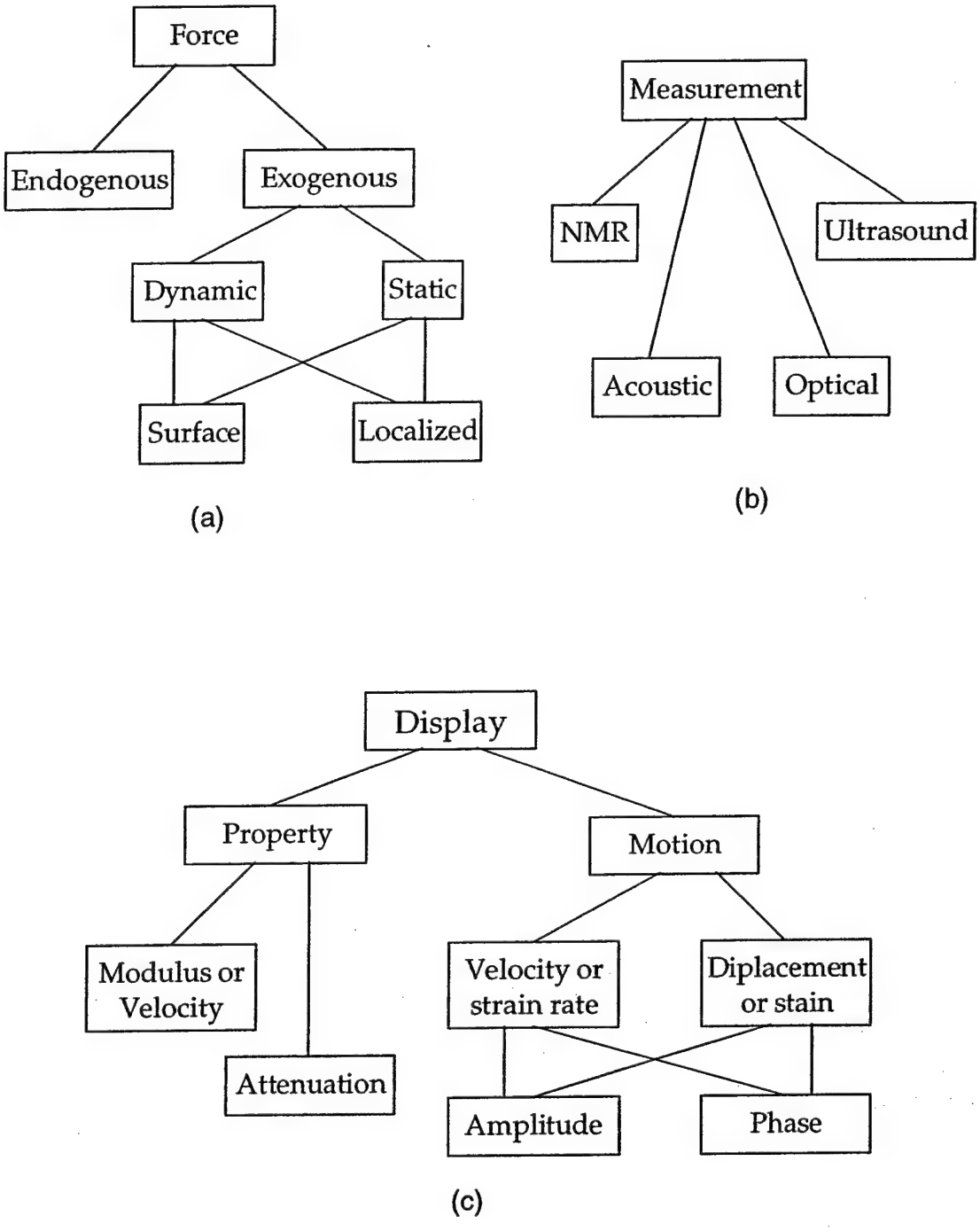

Figure 2.2 Various mechanisms used in elastography for (a) application of force, (b) measurement of motion, and (c) display.

Vibro-acoustography [Fatem and Greenleaf, 1999] is a new elasticity imaging method, which images the acoustic response of a material to localized harmonic excitation produced by radiation force of two interfering ultrasound beams. The details about this promising imaging method and its beneficial features will be described in Chapter 2. However, the acoustic emission at each scanning point is actually a combined response of the reflectivity, stiffness, and object emittance at that particular location. Therefore, the vibro-acoustic image is not a direct presentation of a single mechanical property, but only a semi-quantitative mapping of the "stiffness" distribution of the object. As explained above, truly quantitative techniques are more preferable.

In this thesis work, we want to explore the possibility of using vibro-acoustography for quantitative characterization. The hypothesis of this thesis is that it is possible to derive mechanical properties, such as the complex shear modulus, of an object by evaluating the response of the object to many excitation frequencies. For this purpose, a quantitative model is proposed for a spherical target embedded in a viscoelastic homogenous medium. The goal is to estimate the mechanical properties of the medium by evaluating the displacement-frequency response of an embedded spherical target.

1.2 Summary of chapters

A brief summary of the contents of each of the following chapters is given below.

Chapter 2 consists of a conceptual introduction to mechanical property measurement and a review of the currently available elasticity imaging methods.

Then vibro-acoustography is introduced as a new method to imaging the mechanical properties of the object. The advantages and disadvantages of this imaging method are also analyzed. Finally the motivation and specific aims of this thesis work are presented.

Chapter 3 presents the theoretical model of a sphere in water. The dynamic radiation force on the sphere due to interference of two ultrasound beams is derived. This driving force is used with the radiation impedance and the mechanical impedance of the sphere to calculate the vibrating velocity of the sphere, from which the acoustic emission by the sphere is also solved. Results of experiments are reported, where the velocity and acoustic emission of several spheres are measured versus vibration frequency. The results agree with the prediction of theory.

Chapter 4 extends the model of Chapter 3 to viscoelastic medium. The formulae of radiation force and radiation impedance are modified to consider the effects of shear wave and attenuation. Theory shows that the resonance of the sphere's vibration magnitude versus oscillating frequency is related to the shear properties of the medium around the sphere. Experimental measurements on spheres in gel phantoms confirm the theory. The velocity profiles are used to estimate the shear modulus of the gel, which are also verified by independent measurement methods.

Chapter 5 is the verification of the theory in viscous fluid. The velocity profile of the sphere shows no resonance, just like the case in water. The slope of the curve is related to the viscosity of the fluid. Experiments are performed in viscous standard fluids with known viscosity. The shear viscosity estimation derived from theory agrees with the certificated value of the test fluid. This

method is also used to measure the viscosity changes of glycerin solutions versus temperature.

Chapter 6 demonstrates the feasibility of measuring vibration velocity of a target by the ultrasound Doppler method. In the previous chapters, the vibrations of spheres are measured by a laser vibrometer, which is limited to applications in transparent medium. Results shown in this chapter eliminate this restriction. An analytical expression of the echo from a harmonically vibrating target is provided, from which a demodulation scheme is proposed. Experimental results in gel phantom are compared to measurements from the laser vibrometer, which is used as a gold standard. A number of possible improvements upon this ultrasound Doppler method are also discussed.

Chapter 7 summarizes the thesis work presented in this dissertation and provides a discussion of a few related issues. A future perspective of this work is also presented.

1.3 Reference

1. Carlson AB: Communications Systems. McGraw-Hill, New York, pp221-227, 1968.

2. Chapuis L and Hessler C: Breast cancer before 36 years of age. Helvetica Chirurgica Acta. 55(6):895-902, 1989.

3. Cheney M: Inverse boundary-value problems. Am. Scientist. 85: 448-455, 1997.

4. Duck FA: Physical properties of tissue- A comprehensive reference book. Sixth edition. Academic Press. 225-248, 1990.

5. Holleb AI, Fink DJ, and Murphy GP: American cancer society textbook of clinical oncology. 1991, The American Cancer Society, Inc., Atlanta, GA.

6. Levinson SF, Shinagawa M, and Sato T: Sonoelastic determination of human skeletal muscle elasticity. Journal of Biomechanics. 28(10): 1145-1154, 1995.

7. Muthupillai R: Magnetic resonance elastography. Ph.D. thesis, Mayo Graduate School, 1997.

8. Ophir J, Cespedes I, Garra B, Ponnekanti H, Huang Y, and Maklad N: Elastography: ultrasonic imaging of tissue strain and elastic modulus in vivo. European Journal of Ultrasound. 3: 49-70, 1996.

9. Ophir J, Alam SK, Carra B, Kallel F, Konofagou E, Krouskop T, and Varghese T: Elastography: ultrasonic estimation and imaging of the elastic properties of tissues. Proc. Instn. Mech. Engrs. 213(H): 203-233, 1999.

10. Sarvazyan AP, Redenko OV, Swanson SD, Fowlkers JB, Emelianov SY: Shear wave elasticity imaging: a new ultrasonic technology of medical diagnostics. Ultrason. Med. Biol. 24:1419-1435, 1998.

11. Timoshenko SP and Goodier JN: Theory of elasticity. McGraw-Hill, New York. pp403-409, 1970.